Crack propagation mechanisms in human cortical bone on different paired anatomical locations : biomechanical, tomographic and biochemical approaches

Rémy Gauthier

N°d'ordre NNT :2017LYSE1179

THESE de DOCTORAT DE L'UNIVERSITE DE LYON

opérée au sein de

l'Université Claude Bernard Lyon 1

Ecole Doctorale N° 162

Mécanique – Energétique - Génie civil - Acoustique

Spécialité de doctorat : Biomécanique

Soutenue publiquement le 25 septembre 2017, par :

Rémy Gauthier

Crack propagation mechanisms in human cortical bone on different paired anatomical locations: biomechanical, tomographic and biochemical approaches

---

Devant le jury composé de :

M. Pascal LAUGIER	Directeur de Recherche, CNRS, Paris	Examinateur
Mme. Anne-Sophie BONNET	Maitre de Conférences, Université de Lorraine	Rapporteure
M. Harry van LENTHE	Professeur, Université de Louvain	Rapporteur
M. David ROUSSEAU	Professeur des Universités, Université Claude Bernard Lyon 1	Examinateur
Mme. Françoise PEYRIN	Directrice de Recherche, INSERM, Lyon	Co-directrice de thèse
M. David MITTON	Directeur de Recherche, IFSTTAR, Lyon	Directeur de thèse
Mme. Hélène FOLLET	Chargée de Recherche, INSERM, Lyon	Invitée
M. Max LANGER	Chargé de Recherche, CNRS, Lyon	Invité

UNIVERSITE CLAUDE BERNARD - LYON 1

Président de l'Université	**M. le Professeur Frédéric FLEURY**
Président du Conseil Académique	M. le Professeur Hamda BEN HADID
Vice-président du Conseil d'Administration	M. le Professeur Didier REVEL
Vice-président du Conseil Formation et Vie Universitaire	M. le Professeur Philippe CHEVALIER
Vice-président de la Commission Recherche	M. Fabrice VALLÉE
Directrice Générale des Services	Mme Dominique MARCHAND

COMPOSANTES SANTE

Faculté de Médecine Lyon Est – Claude Bernard	Directeur : M. le Professeur G.RODE
Faculté de Médecine et de Maïeutique Lyon Sud – Charles Mérieux	Directeur : Mme la Professeure C. BURILLON
Faculté d'Odontologie	Directeur : M. le Professeur D. BOURGEOIS
Institut des Sciences Pharmaceutiques et Biologiques	Directeur : Mme la Professeure C. VINCIGUERRA
Institut des Sciences et Techniques de la Réadaptation	Directeur : M. X. PERROT
Département de formation et Centre de Recherche en Biologie Humaine	Directeur : Mme la Professeure A-M. SCHOTT

COMPOSANTES ET DEPARTEMENTS DE SCIENCES ET TECHNOLOGIE

Faculté des Sciences et Technologies	Directeur : M. F. DE MARCHI
Département Biologie	Directeur : M. le Professeur F. THEVENARD
Département Chimie Biochimie	Directeur : Mme C. FELIX
Département GEP	Directeur : M. Hassan HAMMOURI
Département Informatique	Directeur : M. le Professeur S. AKKOUCHE
Département Mathématiques	Directeur : M. le Professeur G. TOMANOV
Département Mécanique	Directeur : M. le Professeur H. BEN HADID
Département Physique	Directeur : M. le Professeur J-C PLENET
UFR Sciences et Techniques des Activités Physiques et Sportives	Directeur : M. Y.VANPOULLE
Observatoire des Sciences de l'Univers de Lyon	Directeur : M. B. GUIDERDONI
Polytech Lyon	Directeur : M. le Professeur E.PERRIN
Ecole Supérieure de Chimie Physique Electronique	Directeur : M. G. PIGNAULT
Institut Universitaire de Technologie de Lyon 1	Directeur : M. le Professeur C. VITON
Ecole Supérieure du Professorat et de l'Education	Directeur : M. le Professeur A. MOUGNIOTTE
Institut de Science Financière et d'Assurances	Directeur : M. N. LEBOISNE

Remerciements

Tout d'abord je tiens à remercier toute mon équipe d'encadrement. Merci Max pour tes conseils scientifiques concernant le traitement de toutes ces images synchrotron, j'espère qu'on aura l'occasion de jouer un peu de musique ensemble l'an prochain. Merci Hélène pour ta gentillesse et ta bonne humeur tout au long de ces trois ans, merci d'être venue me voir en concert et merci pour tes gentils mots le jour de ma soutenance qui m'ont énormément ému. Merci Françoise pour la confiance que tu m'as accordé tout au long de ce projet, et même pour la suite. J'ai eu énormément de plaisir à discuter avec toi tant sur le plan scientifique que pour le reste. Et merci David pour ta gentillesse, ta disponibilité, ta rigueur, tes conseils et tout ce qui va avec. J'ai beaucoup appris de toi pendant cette thèse, et il me reste encore beaucoup à apprendre, merci !

Je souhaite également remercier les membres du jury, David Rousseau, Pascal Laugier, Harry van Lenthe et Anne-Sophie Bonnet. Merci d'avoir accepté d'évaluer mon investissement dans ce projet.

Merci aussi à Philippe Vezin, à l'époque directeur du LBMC, pour m'avoir accueilli au sein du labo pour y effectuer ce projet de thèse.

Evidemment, il faut que je remercie Leila Ben Boubaker qui est probablement la personne avec qui j'ai passé le plus de temps durant ce projet. Merci de m'avoir épaulé dans ces longs moments de découpes et d'expérimentations, et toujours avec le sourire en plus, ce qui n'était pas forcément mon cas. Ce fut un réel plaisir de passer ces moments avec toi, à parler de tout et n'importe quoi (mais surtout pas de la thèse !!).

Je tiens également à dire merci à toutes les autres personnes qui m'ont aidé dans ces travaux de thèse, je pense à Cécile, Pierre-Jean (du côté de Grenoble), Yves, Richard, Jean-Luc, Stéphane (au LBMC), Ilias Aguili (MATEIS), Philippe et Julien (LamCos) et probablement d'autres que j'oublie.

Je remercie tout le personnel du LBMC qui ont participés au fait que je me sente bien au labo, et qui ont tolérer toutes les conneries que j'ai pu dire pendant ces trois ans.

Faut pas que j'oublie mes potes doctorants (ou docteurs) sinon je vais me faire taper dessus. Merci à Papascal pour ce qu'il est, c'est-à-dire un papa ! On ira bientôt se faire un tour en bécane. Merci à Karim, pour sa générosité que tout le monde connait. Je ne sais plus quels sont les comptes au niveau des parties de puissance 4… Tout ce que je sais c'est que je suis plus fort que toi au billard. Merci Anicet pour m'avoir appris à engueuler mon ordi quand il ne marchait pas, pour m'avoir épaulé dans les moments durs de la rédaction (hum hum), et pour tout le reste. Merci d'ailleurs à vous trois pour m'avoir gardé comme ami même si je n'étais qu'un étudiant…Merci Léo, mon ex-pote-stagiaire. Je suis sûr que tu vas tout défoncer pour ta fin de thèse, et qu'après tu feras un énorme kiff' en allant bosser entre Bourges et Vierzon. Merci aux autres, Romain, Romain (un autre), Edison, Julia, Ilias, Tomas…

Je remercie aussi Ines et Alice, les deux étudiantes que j'ai eu la chance d'encadrer, avec qui j'ai eu beaucoup de plaisir à travailler.

Je remercie bien sur tous mes potes normands, qui, même s'ils ne le savent pas, ont contribué à mon bien être tout au long de ces 3 ans, donc merci Tinmar, Guitoune, Georgy, Papy, Hortie, Dianette, Marin, Mae, Flo, Nico, Clémence, Yves, Aurel, Gallon, Paulo, la Nauls, Arty, Jeanne, Margot, Jaja, Tristan, la Dut's, Odran, Siriane, Yo, Bozo, Cécile, Richaud, Colson, Arnaud… ça en fait des potes !

Ma famille a aussi joué un rôle important, me soutenant quand ça n'allait pas (surtout Charlotte) ! Merci Môman, merci Pôpa, Quentin, Alice et Charlotte, mon p'tit n'veu préféré Arthur, et mes nièces adorables Evie et Léa, et évidemment merci Milla et Xav' !

Pour finir je voudrais dire merci à ma p'tite Juju qui a fait le plus dur de tous les travaux qu'il y avait à faire pendant cette thèse : me supporter. Ca a dû être dur pour toi, mais tu l'as fait. Je te décerne donc ton diplôme de docteur en tolérance et en patience ! Merci pour tout.

Ah non, pour finir je vais remercier mon chat, évidemment. Merci Mingus !

Table of contents

Introduction 11

Chapter I State of the art 13

1. Bone anatomy 14
2. Cortical bone: a multi-scale material 17
3. Cortical bone microstructure 18
   i. Micrometric scale 18
   ii. Sub-micrometric scale 19
   iii. Nanometer scale 19
4. Cortical bone porosity: a multi-scale network 21
   i. Blood vessels 21
   i. Micro-cracks 22
   ii. The lacuno-canalicular network 22
5. Bone remodelling 23
   i. Bone remodelling process 23
   ii. Osteoporosis 24
6. Characterization of cortical bone 25
   i. Imaging 25
      - Histomorphometry 25
      - X-ray imaging 26
   ii. Biomechanics 32
      - Continuum mechanics 32
      - Fracture mechanics 33
      - Non-linear fracture mechanics 36
      - How to measure fracture toughness? 37
7. Crack propagation in cortical bone 40
   i. Cortical bone toughness 40
   ii. Cortical bone architecture as a barrier against crack propagation 44
      - Hundreds of micrometers scale 44
      - Micrometer scale 45
      - Nanometer scale 47
8. Conclusion 48

Chapter II Strain rate influence on human cortical bone toughness: a comparative study on three paired anatomical sites* 49

1. Introduction 50
2. Materials and Methods 51

i. Sample preparation 51
ii. Biomechanical experiments 52
- Fracture toughness measurement 52
- R-curve 54
iii. Statistical tests 57
3. Results 57
i. Linear elastic fracture toughness 58
ii. Non-linear fracture toughness 59
iii. R-curves 59
4. Discussion 62
5. Conclusions 66
Chapter III Synchrotron radiation micro-CT imaging of paired human femoral diaphysis, femoral neck and radial diaphysis 67
1. Introduction 68
2. Materials and methods 70
i. Sample preparation 70
ii. Synchrotron radiation micro-computed tomography (SR-μCT) 71
- Absorption coefficient 73
- Bone and canals masks 74
- Segmentation of lacunae 74
- Morphometric parameters on lacunae and micro-cracks 75
- Osteocytes and micro-cracks separation 76
- Lacunae and cracks analysis 78
- Haversian canal analysis 74
iii. Statistical analysis 80
3. Results 80
i. Osteocyte lacunae 81
ii. Micro-cracks 82
i. Haversian canals 82
ii. Influence of mechanical loading 83
iii. Correlations 89
4. Discussion 91
5. Conclusion 98
Chapter IV On the relationships between human cortical bone toughness and collagen cross-links maturation 99
1. Introduction 100
2. Materials and methods 101

i. Bone samples 101
ii. Biomechanical measurements 101
- Sample preparations 101
- Biomechanical experiment 102
- Fracture toughness measurement 102
iii. Biochemical measurements 103
- Sample preparation 103
- Cross-links measurements 104
iv. Statistical tests 105
3. Results 105
i. Biomechanical experiments 105
- Linear elastic strain energy release rate 106
- Non-linear elastic strain energy release rate 107
ii. Biochemical measurements 108
iii. Relationships between age, mechanical and biochemical properties 110
4. Discussion 113
5. Conclusion 118
Chapter V What is the influence of strain rate on human cortical bone crack propagation mechanisms? 119
1. Introduction 120
2. Materials and methods 121
i. Biomechanical measurements 122
ii. Morphometric measurement 122
iii. Biochemical measurements 123
iv. Statistical tests 123
3. Results 123
4. Discussion 128
5. Conclusion 131
Conclusion 133
Perspectives 137
Bibliography 144
Annex 168

Introduction

Osteoporosis remains today a major health problem. An osteoporotic fracture is indeed estimated every three seconds in the world, leading to an increased risk of impairment or even mortality due to clinical complication and a high economic burden (Cooper et al., 1993; Hernlund et al., 2013; Johnell and Kanis, 2006; Leibson et al., 2002). In the clinic osteoporosis diagnosis is based on the evaluation of bone mineral density using Dual X-ray Absorptiometry (DXA, (Genant et al., 1996)). This technique, which has been established as the gold standard method used by clinicians, presents nevertheless some limitations to accurately predict fracture risk. Almost 50 % of the patients diagnosed as "not at risk" will still suffer from a bone fracture (Siris et al., 2004). If bone density is a good predictor of bone strength under quasi-static loading conditions on *ex vivo* experiments (Louis et al., 1995), bone fracture *in vivo* involves more complex loading configurations (Robinovitch et al., 1991; Tan et al., 2006; Verhulp et al., 2008).

In 1991, Hayes et al. defined the fracture risk as the ratio between the load applied to the bone and the bone strength (Hayes et al., 1991). With the recent development of high resolution imaging methods usable in clinics, numerical models have been developed to better estimate the bone strength (Pistoia et al., 2003, 2002; Varga et al., 2009). Bone fractures generally occur after a fall from a standing position (Dubousset, 2014; Gryfe et al., 1977; World Health Organization, 2007), thus involving higher loading rates that in standard experimental conditions (Foldhazy, 2005). In most cases of finite element model for the prediction of fracture, the loads considered are not representative of what actually occur during a fall (van Rietbergen and Ito, 2015). To accurately predict the fracture risk, bone strength should be assessed in the fall configuration.

At the macroscale, bone is made of two different structures: the trabecular bone that presents a sponge-like macrostructural porosity and lies within the organ; and cortical bone that is compact, peripheral, and constitutes the characteristic cylindrical shape of long bones. While both types of bone play a role in the fracture process, cortical bone has been shown to be more determinant in diaphyseal bone fractures (Bala et al., 2015; Holzer et al., 2009).

The fracture process in human cortical bone is a complex problem that involves the overall organization of the tissue (Seeman and Delmas, 2006). Toughness appears to be a good candidate to improve biomechanical knowledge on cortical bone fracture mechanisms, since it determines how much energy is needed to propagate a crack through the tissue microstructure (Ritchie, 1988). Numerous toughening mechanisms have been investigated in the past, involving the complex microstructure of human cortical bone (Zimmermann and Ritchie, 2015). While these so-called

toughening mechanisms have been largely studied and are well known under quasi-static loading condition, only few studies have considered representative loading conditions representative of a fall despite human cortical bone toughness significantly depends on the loading rate (Shannahan et al., 2015; Zimmermann et al., 2014). Moreover, the influence of the bone location is also little discussed in the literature (Brown et al., 2000) despite bone microstructure may be different from a location to another (Wolff, 1892).

Therefore, the aim of this study is to investigate the human cortical bone toughness dependence on the loading conditions: quasi-static and fall-like, and in several sites: femoral diaphysis, femoral neck, tibial diaphysis and radial diaphysis, all extracted from a same donors. This means comparisons of morphometric measurements on paired anatomical locations could be performed to assess bone microstructural parameters at several length scales before and after fracture, using synchrotron radiation micro-computed tomography imaging. Further, biochemical measurement were be performed to assess bone collagen characteristics. An overall characterization of the human cortical bone fracture process can thus be performed and provides new knowledge concerning crack propagation mechanisms under fall-like loading condition.

This study was conducted at the Laboratoire de Biomécanique et Mécanique des Chocs (UMR T_9406, IFSTTAR-UCBL) in collaboration with the laboratory Creatis (UMR 5220, CNRS-INSERM U1206-UCBL-INSA de Lyon), expert of imaging technology, the LYOS (UMR 1033, INSERM-UCBL) expert of bone biology and the laboratory MATEIS (UMR 5510, CNRS-UCBL-INSA de Lyon) expert in material characterization.

Chapter I State of the art

Abstract: The aim of this first chapter is to introduce the complex architecture of cortical bone and its related fracture mechanisms. A brief review of the human skeleton is first given in order to outline why we choose to focus on cortical bone. The overall organization of the cortical bone is then presented, from a scale of hundreds of micrometers to the nanoscale. Bone matrix and porosity network are distinguished in this chapter. The pore network observed within cortical bone plays a specific role for the tissue mechanical behavior. Another aim for this chapter is to introduce different methods of characterization of human cortical bone fracture process. X-rays imaging has largely been used to investigate bone microstructure down to the nanometer. Synchrotron radiation for X-ray micro-tomography appears to be an interesting method to assess cortical bone structural parameters. Biomechanical elastic properties of human cortical bone can be evaluated in order to characterize its ultimate behavior. Investigating its toughness allow to understand crack propagation within the tissue. The association between X-rays micro-CT imaging and toughness analyses allows a better comprehension of human cortical bone fracture mechanisms.

1. Bone anatomy

The vertebrate skeleton fills several functions in the organism. Beyond its main function of providing structural support for the body, organs and muscles, it also has a protective role, mainly of the internal organs. It further provides metabolic storage and supply of calcium in the form of bone mineral.

An adult body is composed of more than 200 bones (Figure 1). There are four different types of bone determined by their geometric characteristics and particularly their aspect ratio which describes the proportional relation between their height and width:

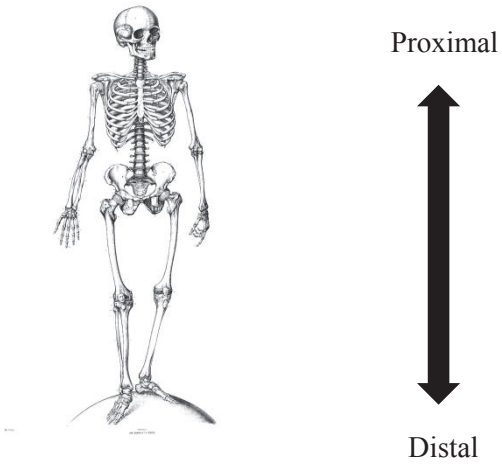

Figure 1: the skeleton is composed of different type of bones which each has a specific function - explications

- Short bones have an aspect ratio close to 1. Their length is nearly the same as their width. They are mainly located at the joints, thus facilitating a greater freedom of movement. For example, the bones of the wrist and ankle are short bones.
- Long or diaphyseal bones have a high aspect ratio. They are located in the limbs, have a nearly cylindrical shape and have their long axis closely aligned with the limb axis. They provide stability of the limb and support for the limb's muscles, which drive the mobility of the limb. Diaphyseal bones can be divided into two categories: weight bearing bones of the lower limbs, such as the femur and tibia, which support the body weight when upright; and non-weight bearing bones in the upper limbs, such as the radius, which do not continuously support body weight.
- Flat bones have a plate like shape. Their main function is protection of internal organs, e.g.,

the skull bone that protects the brain, and the ribs which protect the heart and lungs.

- Irregular bones have a complex geometry that does not fit in the above categories. Macroscopic and microscopic properties of the different bones of the human body depend on their function (Chamay and Tschantz, 1972; Wolff, 1892). Wolf's law states that the shape of each bone depends on the mechanical solicitation it receives while developing. The organ adapts itself to its mechanical environment in order to ensure optimally its function. For example, the femur plays a structural role within human body. That is why it has a pillar shape to ensure the support of one's weight (Figure 2).

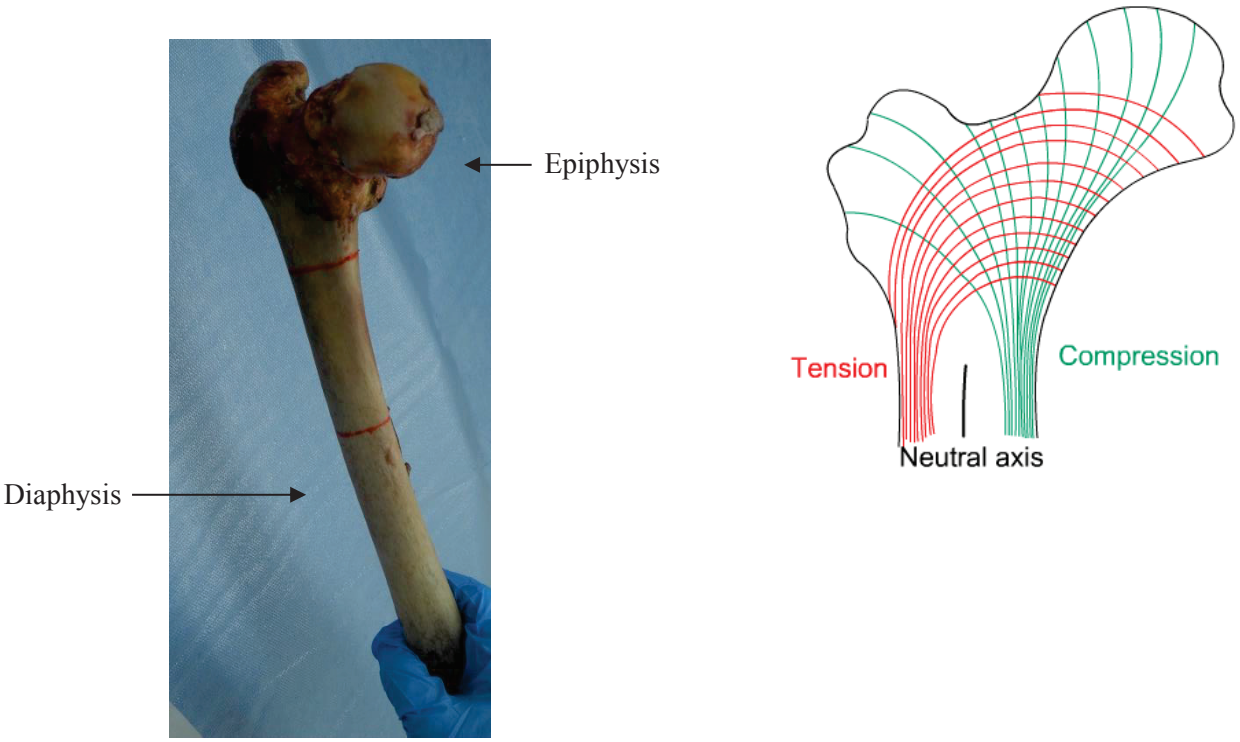

Figure 2 a) Human femoral diaphysis and proximal epiphysis b) stress line (Diagram showing computed lines of constant stress from the analysis of various transverse sections https://www.doitpoms.ac.uk/tlplib/bones/printall.php)

Being more than a simple cylinder, the various shapes betray its various functions. Like all long bones, the femur is composed of a long and cylindrical shaft, called the diaphysis, terminated at each extremity by a more irregular shape called the epiphysis (Figure 2). The internal organization of these two parts is different and adapted to their functions.

At the material scale, we can thus find two different organizations: cortical bone, and trabecular bone. Cortical bone (from Latin *cortex*; cork) is present on the peripheral region of the organ. It consists of a compact material, with approximately 15 - 20% of macro-porosity (Rho et al., 1998; Sedlin and Hirsch, 1966). Trabecular bone (from Latin *trabecula*; small beam) is located at the interior of the organ. It has a spongy appearance where the bone itself is organised into relatively thin struts. This yields an organ level porosity that can be over 80% of the tissue volume (de Vernejoul et al., 1981; Nuzzo et al., 2002; Revell, 1983). The compact part of the diaphysis of long bones is mainly constituted of cortical bone whereas the epiphyses are composed mainly of trabecular bone.

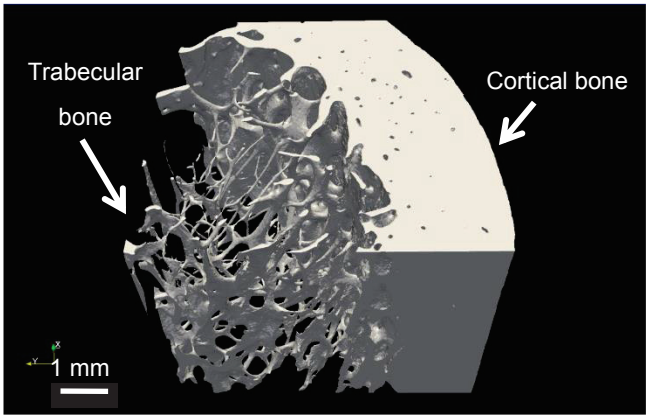

Figure 3 Volume rendering of the section of a radius diaphysis (courtesy of Y. Bala, UMR 1033, Lyon, France)

Both cortical and trabecular bone are known to contribute to the organ fracture behavior (Lotz et al., 1995; Manske et al., 2009; Spadaro et al., 1994). Some studies showed that the contribution of cortical bone to the long bone, as in femoral neck, strength is higher than that of trabecular bone (Bala et al., 2015; Holzer et al., 2009). Further, at least 80% of osteoporotic fractures involve the limbs that comprises the long bones (Kanis et al., 2001). Finally, during a fall, it has been shown that the tensile stresses, that are more critical than the compressive ones both for trabecular and cortical bone (Keaveny et al., 1994; Reilly and Burstein, 1975), are concentrated in the cortical region of femoral neck (Lotz et al., 1995; Verhulp et al., 2008). For these different reasons, we will focus here on the study of cortical bone.

2. Cortical bone: a multi-scale material

As every biological material, cortical bone is constituted of cells and extracellular matrix. The extracellular matrix in bone is a composite material, since it is composed of an organic and a mineral phase. The organic phase is mainly type I collagen fibres, albeit other proteins can also be found. The mineral phase consists of polycrystalline plates of hydroxyapatite (HAP, $Ca_{10}(PO_4)_6(OH)_2$) Human bone mineral is a non-stoichiometric and poorly crystallized apatite. Bone apatitestructure is hexagonal with space group P63/*m,* with lattice parameters a=9.42Å and c=6.88Å. It is a calcium (Ca)-deficient apatite analog, contains major elements like calcium, [Ca2+ (40 wt%)], phosphate [PO43-(18 wt %)], carbonates [CO32- (6-7 wt %)], minor elements such as magnesium (Mg2+) or sodium (Na2+), and trace elements (Farlay and Boivin, 2012; LeGeros et al., 1983). Some water can also be found (Stevens and Lowe, 2006). The mineral phase represents about 70 % of the total weight of bone tissue, whereas organic phase and water represent 20% and 10% respectively, with a notable variability inter-species and inter-anatomical locations (Currey, 1979; Stankeiwicz et al., 1989).

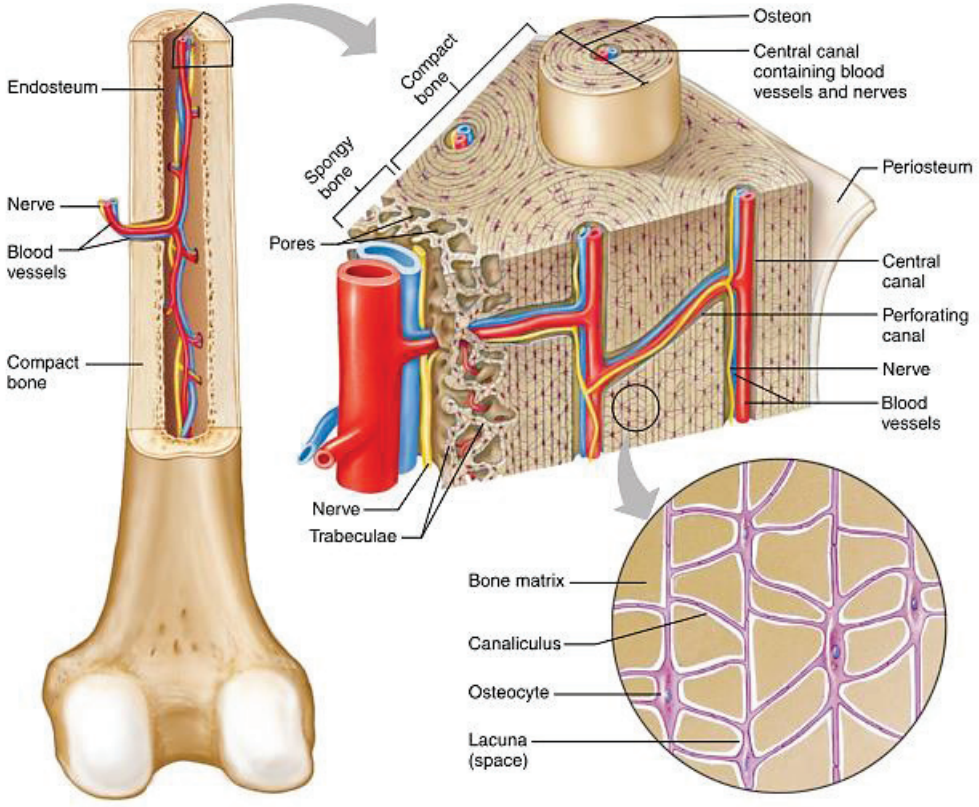

Figure 4 Cortical bone is a complex multi-scale material (Shier et al., 1974)

3. Cortical bone microstructure

i. Micrometric scale

In certain areas within cortical bone tissue, lamellar bone is organized concentrically around canals containing blood vessels and nerves, called Haversian canals, forming the main bone porosity at this scale. This particular concentric arrangement of cylindrical shape oriented mainly along the diaphysis axis, is called an osteon (Ascenzi and Fabry, 1959; Jowsey, 1966; Jowsey et al., 1953; Rho et al., 1998).

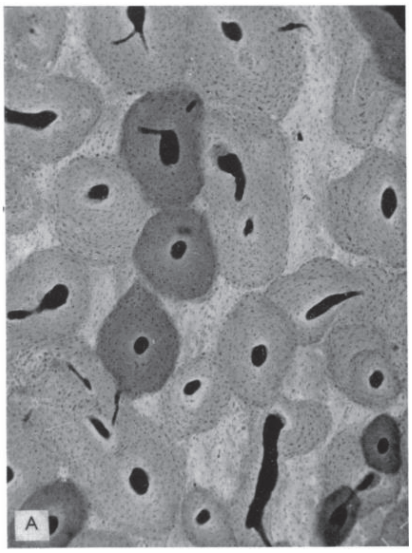

Figure 5 Micro-radiography of femoral cortical bone of a 23 y.o. woman. The osteons are the quasi-circular black areas. They are parallel to the diaphysis axis (Jowsey, 1966)

Osteons are separated by interstitial tissue, the white areas separating osteons on Figure 5. The difference of grey level that can be observed on Figure 5 comes from the difference of degree of mineralization. Bone tissue gets more mineralized with time. The Haversian canals are preferential sites for the secretion of new bone, due to the proximity to circulating blood in the vessels. Osteonal bone is younger than the interstitial tissue, it is thus less mineralized. The interface between osteonal and interstitial tissue, a layer of material roughly 1 µm thick, is called cement line and appears to play a major role in mechanical behavior of cortical bone (Akkus and Rimnac, 2001; Burr et al., 1988; O'Brien et al., 2005a; Wagermaier et al., 2015; Yeni and Norman, 2000a). However, the exact composition and deposition of the cement line is currently not known.

Osteonal density and geometry vary with age and anatomical location. Osteonal density tends to increase with age. Some studies showed that there are more and bigger osteons in the femoral

diaphysis than in the tibial diaphysis (Evans and Bang, 1967; Norman and Wang, 1997; N. J. Wachter et al., 2001; Yeni et al., 1997; Zimmermann et al., 2011).

ii. Sub-micrometric scale

At the sub-micrometric scale, diaphyseal cortical bone is constituted by collagen fibres that are stacked in lamellar structures (Kazanci et al., 2007; Langer et al., 2012; Schrof et al., 2014; Varga et al., 2013) which is called lamellar bone. Lamellae are composed of staggered collagen fibrils forming a thin layer 5-7 µm thick (Ascenzi and Bonucci, 1967; Reznikov et al., 2014; Rho et al., 1998). Each lamella has a specific internal collagen fibre organization. This makes cortical bone a complex material at the sub-micrometric scale (Giraud-Guille, 1988; Schrof et al., 2014; Varga et al., 2013).

iii. Nanometer scale

At this level, the basic element of type I collagen is an arrangement of three polypeptide chains organized in a triple helix structure of approximately 67 nm length, named tropocollagen. A so called "collagen molecule" is a stack of tropocollagen helices making a chain of about 300 nm length and 1.6 nm diameter (Myllyharju and Kivirikko, 2004; Sherman et al., 2015; van der Rest and Garrone, 1991; Viguet-Carrin et al., 2006). These molecules are bound together to form collagen fibrils of 20 to 80 nm diameter (Fleischmajer et al., 1981). At a larger scale, collagen fibrils are arranged in fibres a few micrometers diameter (Rho et al., 1998; Ushiki, 2002). During collagen development, mineral particles of HAP are precipitated in the gap between each collagen molecule (inter-fibrillar), and also on the surface of each collagen fibril (inter-fibrillar) (Rho et al., 1998; Sherman et al., 2015) (Figure 6).

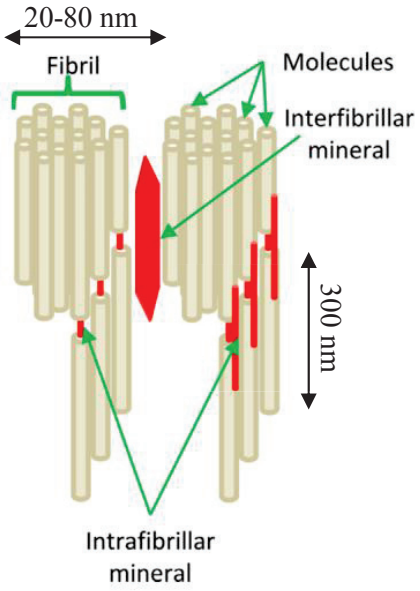

Figure 6 Arrangement of mineral within and around collagen fibril, adapted from (Sherman et al., 2015)

At this scale, the collagen chains are held together by non-collagenous proteins called inter-molecular cross-links (Gineyts et al., 2010; Paschalis et al., 2001; Saito and Marumo, 2010; Yamauchi et al., 1988). Once collagen fibrils are secreted by bone cells, cross-links are formed between two collagen molecules by an enzymatic reaction. These newly formed molecules are called immature enzymatic cross-links. Hydroxylysinonorleucine (HLNL) and dihydroxylysinonorleucine (DHLNL) are two examples of divalent cross-links, meaning that a molecule is bounded to two collagen chains. With maturation of the tissue, new forms of cross-links appear. The immature cross-links evolve into mature cross-links that bind three collagen molecules together. Pyridinoline (PYD) and deoxypyridinoline (DPD) are two examples of trivalent enzymatic cross-links. Non-enzymatic cross-links, such as pentosidine (PEN) are also secreted between collagen molecules. These mature cross-links are markers of the ageing of cortical bone tissue (Saito and Marumo, 2010).

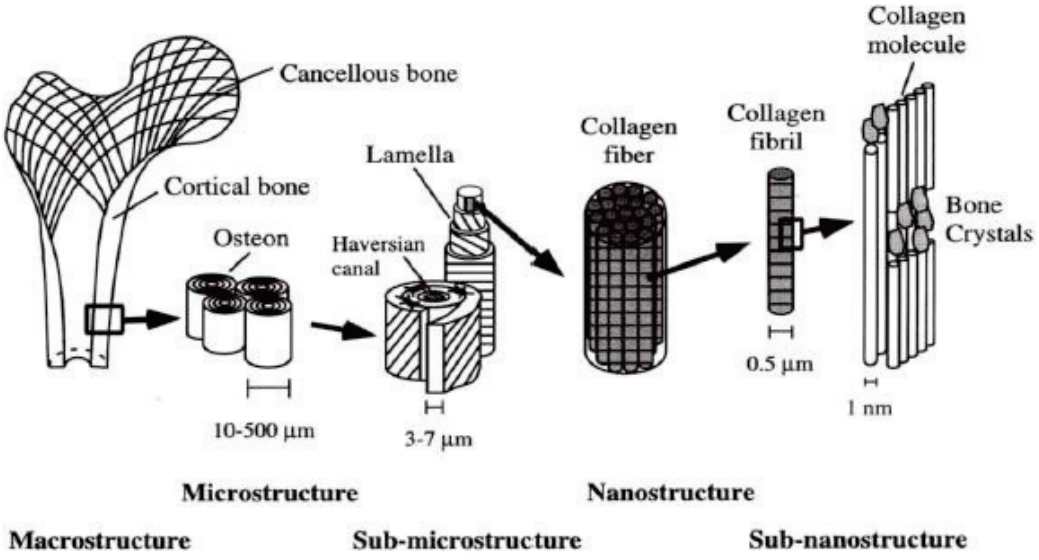

Figure 7 Bone architecture from macro to nano-scale (Rho et al., 1998)

4. Cortical bone porosity: a multi-scale network

Although cortical bone can be considered as a compact material at the organ scale, it exhibits a complex porosity network that can be observed within the tissue at different length scales. This network appears to be essential to the material mechanical behavior (Abraham et al., 2015; Bala et al., 2016; Dong and Guo, 2004; Granke et al., 2011; Perilli et al., 2015; Tang and Vashishth, 2011).

i. Blood vessels

At a higher scale, cortical bone presents cylindrical porosities contain vessels of about 50 µm diameter that provide blood to bone's cells. Two kind of these porosities can be distinguished (Shier et al., 1974; Stevens and Lowe, 2006):

- Haversian canals that are roughly parallel to the main axis of the diaphysis
- Volkmann canals that are roughly perpendicular to the main axis of the diaphysis.

These canals are connected together, showing a complex architecture within the tissue, that may have an influence on its mechanical behavior (Cooper et al., 2007).

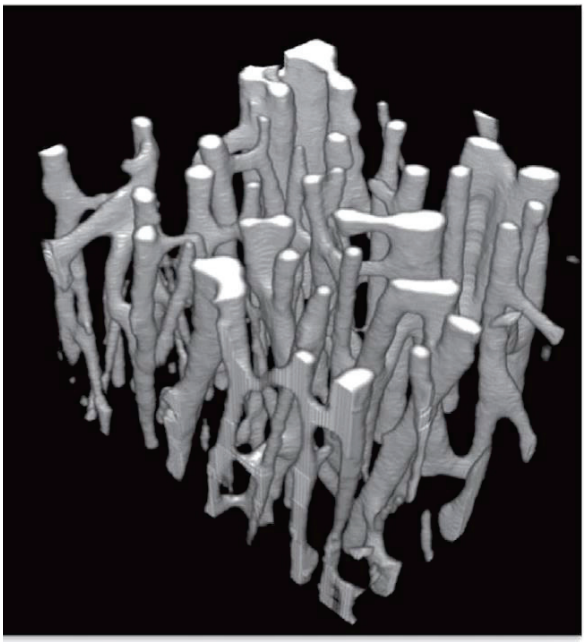

Figure 8 µCT volume rendering of haversian network observed from a 80 y.o. female's fibula. Haversian and Volkman's canals form a complex architectural network within cortical bone tissue (Bala et al., 2016)**.**

i. Micro-cracks

Presence of micro-cracks within the tissue is a sign of mechanical fatigue of the material. When the material cannot sustain more mechanical loading, the formation of microdamages can dissipate a part of mechanical energy in order to relax the tissue. Some authors assume that these porosities cut the lacuno-canalicular network, thus initiating the remodeling process (Lanyon et al., 1982; Lee et al., 2002). If the presence of micro-cracks appear to be essential for bone turnover, it has been observed that a too high density of these porosities can weaken the tissue by coalescing and creating a major crack (Danova et al., 2003; Ritchie et al., 2006; Zimmermann et al., 2011).

ii. The lacuno-canalicular network

Osteocytes, that are considered as bone mechanosensors cells, are embedded in bone matrix in small mineralized holes called lacunae (Bonewald, 2011; Dooley et al., 2012; Qiu et al., 2005; Verborgt et al., 2000). This micro-porosity can be observed in cortical bone as roughly lenticular drop-shaped of average size about $20x10x5\mu m^3$ in human femoral bone (Marotti, 1979). It has been estimated that lacunae density can exceed 20000 mm^{-3} (Dong et al., 2014). Therefore, the volume represented by these osteocyte lacunae is about 2% of the total volume of the tissue (Buenzli and Sims, 2015).

Canaliculi permitting to link the osteocytes together can also be observed within the mineral tissue as small mineralized canals hundreds of nano-meter in diameter (Langer and Peyrin, 2015; Schneider et al., 2011; Varga et al., 2014).

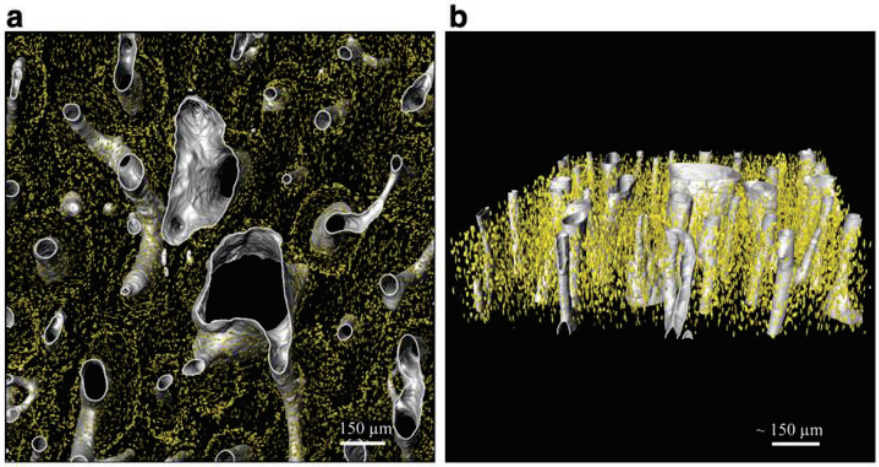

Figure 9 SR-µCT 3D rendering of segmented image. (a) is the top view of the volume, and (b) the side view. The Haversian canal (in white) are surrounded by osteocyte lacunae (yellow) (Dong et al., 2014)

5. Bone remodelling

Cortical bone is subject to a regular replacement during life, in order to replace old and altered tissue with a new and healthy one (Hadjidakis and Androulakis, 2006; Stevens and Lowe, 2006; Verborgt et al., 2000). As mentioned previously, the bone remodelling process is particularly active around Haversian canals. New tissue is formed around these canals. In this manner, 5% of cortical bone can be remodelled each year (Hadjidakis and Androulakis, 2006).

i. Bone remodelling process

The bone modelling process is driven by different bone cells called osteocytes, osteoblasts and osteoclasts (Bonewald, 2011; Gray, 1918; Stevens and Lowe, 2006). During life, the body normally maintains equilibrium of resorption of old bone tissue and secretion of a new. Osteoclast cells initiate the process of bone resorption, whereas osteoblasts create new tissue.

The global process of bone remodelling is driven by the osteocytes. These cells, all linked together by long processes which are embedded in thin canals called canaliculi, and form a mechanosensitive network that can detect tissue damages and thus initiate the remodelling process (Bonewald, 2011; Ebacher et al., 2012; Seeman and Delmas, 2006; Verborgt et al., 2000; Weinbaum et al., 1994).

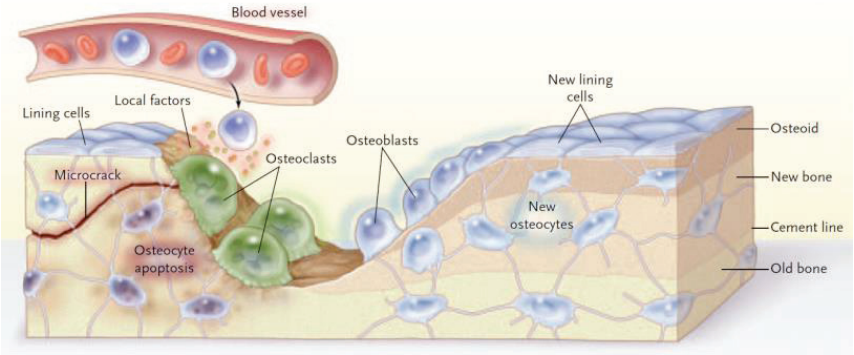

Figure 10 Bone remodelling is a cellular process: Osteoclasts resorb damaged tissues while osteoblasts create new bone. This whole process is governed by the osteocytes (Seeman and Delmas, 2006)

ii. Osteoporosis

Osteoporosis is an example of a disease that is due to imbalance in the remodelling process, inducing a weakening of the tissue mechanical properties (Kimmel et al., 1990; Nanes and Kallen, 2014; Poole et al., 2012; Verhulp et al., 2008; Zimmermann et al., 2016).

Diagnostic methods used in the clinic are based on the measurement of bone mineral density (BMD). If the measured BMD is too low, compared to mean population values, the patient is considered as affected by osteoporosis (Genant et al., 1999, 1996; Nanes and Kallen, 2014). This method, considered the gold standard for osteoporosis diagnosis, presents some limitations (Kanis et al., 2001). Measurement of BMD in human bone might not accurately assess the overall capacity to resist fractures, since osteoporosis also alters the quality of the tissue, thought to influence bone strength as well (Bala et al., 2016; Cohen et al., 2010; Saito and Marumo, 2010; Van Lenthe and Müller, 2008). Bone quality is defined as a number of bone properties that have an influence on fracture (Wallach et al., 1992). Bone quality involves bone mineral density, but also other parameters, such as architecture and biochemical composition. In order to develop an accurate diagnostic method for bone disease, it is likely necessary to consider several or all properties that constitute bone quality.

6. Characterization of cortical bone

There are many techniques of material characterization used for cortical bone. We focus here on the techniques used in this project to investigate relationships between human cortical bone quality and its fracture behavior.

i. Imaging

In order to investigate the complex bone architecture at every length scale, several imaging methods and protocols have been developed, using different types of electromagnetic radiation, allowing observing cortical bone from the millimeter to the nanometer scale.

- ***Histomorphometry***

Histomorphometry was one of the first methods used to investigate bone microstructure, (Beck and Nordin, 1960; Bordier and Chot, 1972; Meunier et al., 1980; Wakamatsu and Sissions, 1969). In order to investigate structural parameters, they decided to look through histological sections of a studied anatomical location (Beck and Nordin, 1960; Revell, 1983; Wakamatsu and Sissions, 1969). Scientists were able to bring to light specific structural parameters (Bordier and Chot, 1972; Lips et al., 1978; Revell, 1983).

If this method can only provide a two-dimensional analysis, it is the basis of today's method of structural investigations of cortical bone (Blue et al., 2015; Duboeuf et al., 2015; Shapiro et al., 2017; Slyfield et al., 2012). Particularly, the general nomenclature for cortical bone morphometric analysis was introduced with this method (Dempster et al., 2013; Parfitt et al., 1987).

a. b.

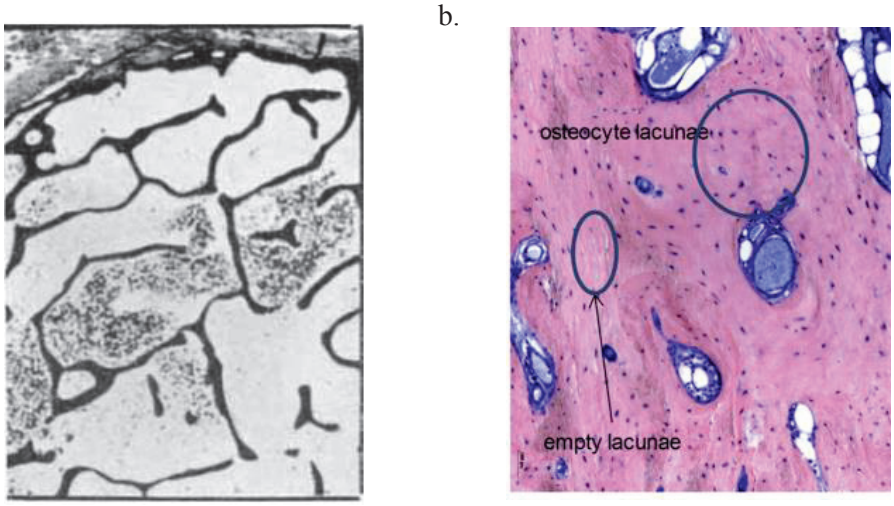

Figure 11 Histomorphometry is the basis for the analysis of human cortical bone, it is still widely used. a. is a section of the iliac crest (Beck and Nordin, 1960) **; b. is a section of an ear ossicle showing lacunae osteocytes** (Duboeuf et al., 2015)**.**

- ***X-ray imaging***

An electromagnetic wave is characterized by several parameters such as its intensity or its wavelength. Electromagnetic waves are usually classified based on their wavelength. For example, light visible to the human eye is electromagnetic radiation with wavelengths roughly in the range between 350 nm (blue light) to 750 nm (red light). Electromagnetic radiation outside this range cannot be seen by human eye. Examples are infrared radiation with wavelengths that are longer than visible light, in the range between 750 nm to 1 mm; and ultraviolet radiation with wavelengths shorter than visible light, in the range 350 nm to 10 nm. X-radiation lies in the range of wavelengths shorter than ultraviolet radiation, in the range between 0.01 to 10 nm.

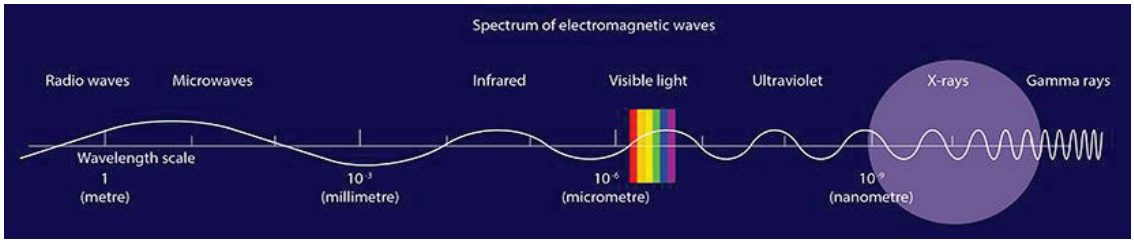

Figure 12 The electromagnetic spectrum comparing the size of the object that can be studied with various techniques (source: www.esrf.eu)

This highly energetic radiation's wave lengths are ranged between 10 nm and 0.01 nm. These wave lengths are directly related to the energy of the wave by the following relation:

$$E = \frac{hc}{\lambda} \tag{I.1}$$

where E (eV) is the energy, and λ (m) the wave length, c=3.0 $.10^8$ $m.s^{-1}$ is the velocity of light in vacuum condition, and h= 4.1343359 .10-15 eV. s is the Planck constant.

Like all electromagnetic radiation, X-rays interact with matter in various ways. In this wavelength range, the interactions are mainly with the electrons in the atom shells. A brief description of the effects on the X-ray when interacting with matter follows.

X-rays of wavelength λ can be described by the wavenumber k:

$$k = \frac{2\pi}{\lambda} \tag{I.2}$$

When the wave propagates in a material with index of refraction n, the wave evolves accordingly, thus the wavenumber changes as the product with the refractive index:

$$k' = kn \tag{I.3}$$

For our purpose, the interaction between a material and X-rays can be modelled by its complex index of refraction N (Dresselhaus, 1966):

$$N = n + i\mu \tag{I.4}$$

where n is the index of refraction, and μ is the attenuation coefficient. Thus, for the simplified case of a plane wave u propagating in the direction z and of intensity I_0:

$$u_z = I_0 e^{ik\prime z} = I_0 e^{iNkz} = I_0 e^{iknz} e^{-k\mu z} \tag{I.5}$$

In this relation, we can see that, when passing through matter, the wave is attenuated because of the attenuation coefficient μ, and it is also phase shifted due to the index of refraction n. With this relation we can thus specify which parameter we want to measure to characterize a material:

- The attenuation contrast, which is related to the attenuation coefficient

- The phase contrast, which is related to the phase shift of the beam, in turn related to the refractive index n.

Synchrotron radiation is a specific case of emission when relativistic moving charged particles are accelerated perpendicularly to their velocity by a magnetic field (Mobilio et al., 2015; Walker, 1992; Woodyard, 1948). This kind of radiation, which can occur naturally, can be generated artificially in a device called a synchrotron (Elder et al., 1947), where charged particles are accelerated in a closed loop path by magnetic fields varying in time, synchronised to the kinetic energy of the particles. Synchrotrons yield a very bright, wide bandwidth X-ray source with a very small emission area. At synchrotron light sources, the track where the particles are kept circulating is called a storage ring.

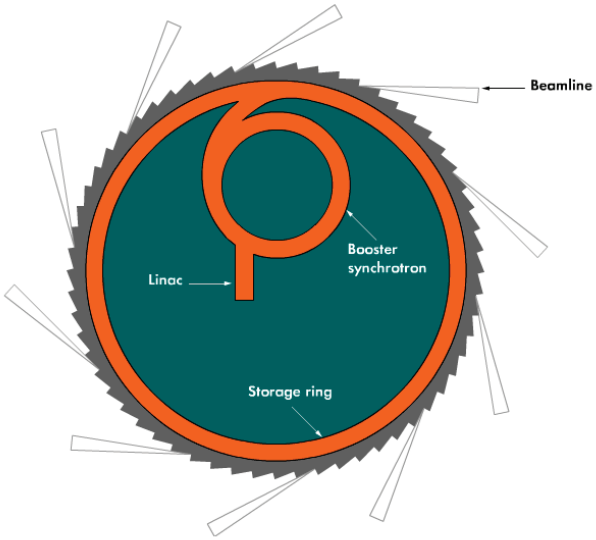

Figure 13 Schematic of the ESRF (source: www.esrf.eu)

Figure 13 shows a schematic of the European Synchrotron Radiation Facilities (ESRF). In this device, electrons that are produced in the linear accelerator (linac) are sent to the booster synchrotron in order to be accelerated to reach energy of about 6 GeV. They are then injected into the storage ring synchrotron that keeps them circulating, maintaining kinetic energy and spatial localisation of the particle beam, creating good conditions for emission of X-rays. X-rays are produced in the storage ring by bending magnets or insertion devices, directed through straight-line tracks called beamlines to the experimental stations where the X-ray experiments are realized (www.ESRF.eu, (Mobilio et al., 2015)).

Synchrotron radiation is interesting for X-ray Computed Tomography (CT) because it has the property to provide a monochromatic, or quasi-monochromatic beam couple with a high flux of

particles. This property allows lowering the artefact of beam hardening due to the variation of energy between photons within the beam without lower acquisition time (Salomé et al., 1999). Other reasons come from the quasi parallel nature of the beam that simplifies tomographic reconstruction and provide exact reconstruction or the high coherence of the beam which permits to implement x-ray phase contrast imaging (Chappard et al., 2006; Mobilio et al., 2015; Nuzzo et al., 2002; Salomé et al., 1999). This is why synchrotron radiations have outstanding properties for CT.

Data acquisition in X-ray computed tomography typically consists in rotating the X-ray source and detector around the studied objects (Hounsfield, 1973). For each X-ray path D, meanings for each straight line between the source and the detector, by knowing the incident intensity I_0 and by measuring the transmitted one I, we can estimate a projection value obtained as the following line integral (Figure 14, a):

$$\int_D \mu(x,y)ds = ln\left(\frac{I_0}{I}\right) \tag{I.6}$$

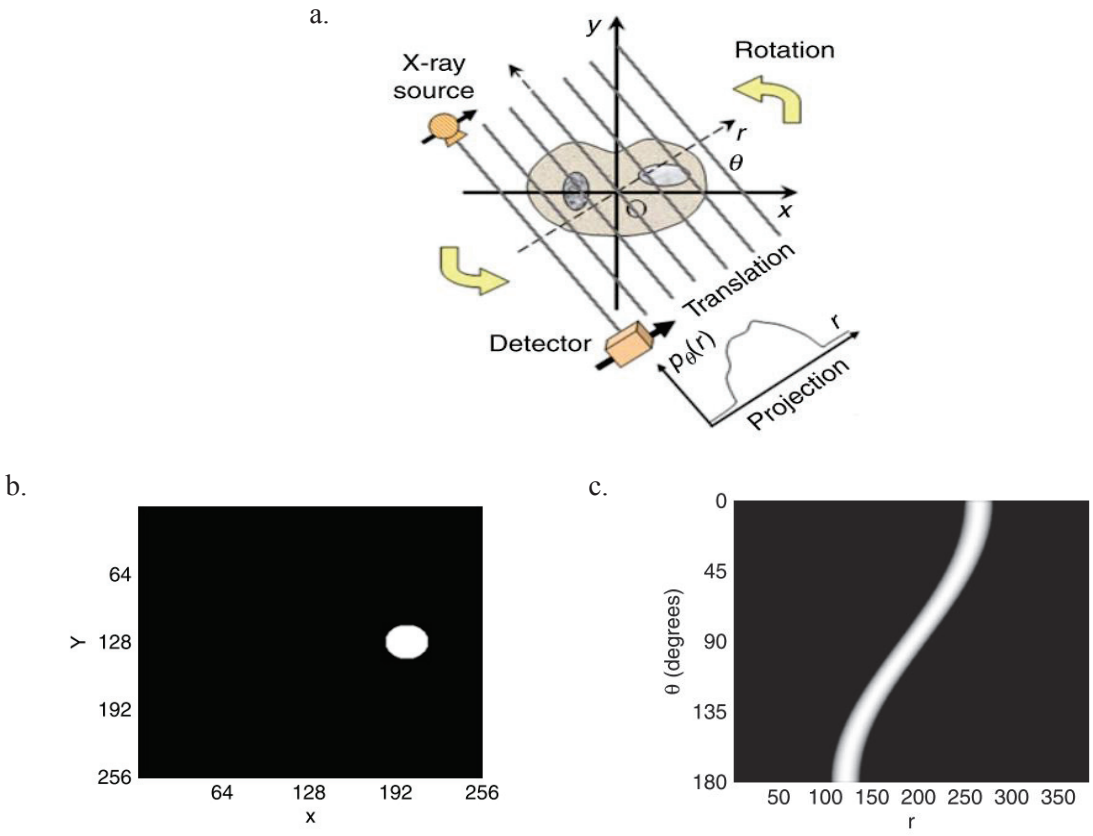

Figure 14 a. During data acquisition, the attenuations of an X-ray beam on parallel X-ray paths are measured on a detector, providing one projection. The X-ray source is then sequentially rotated and new measurements are collected; b./c. the image and its corresponding sinogram (Peyrin and Engelke, 2012)

This relation can be extrapolated to each angle θ and detector position r as:

$$p_\theta(r) = \int_{-\infty}^{+\infty} \mu(rcos\theta - rsin\theta, rcos\theta + rsin\theta)ds \quad \text{(I.6)}$$

which gives the parallel projection $p_\theta(r)$. The set of these parallel projections for θ varying from 0 to π is called the sinogram, a simple example can be seen on Figure 14 (Radon, 1917).

The image can be reconstructed from the set of its projection when θ varies from 0 to π. The theory of image reconstruction relies on the Fourier slice theorem stating that the 1D Fourier transform of the parallel projection of angle θ is a slice of the 2D Fourier transform of the image along a straight line in the direction θ. The most popular reconstruction method is known as the filtered back projection method (Herman, 1980). From a geometrical point of view, the back projection of one projection spreads the values of the projection along the projection direction (Figure 15).

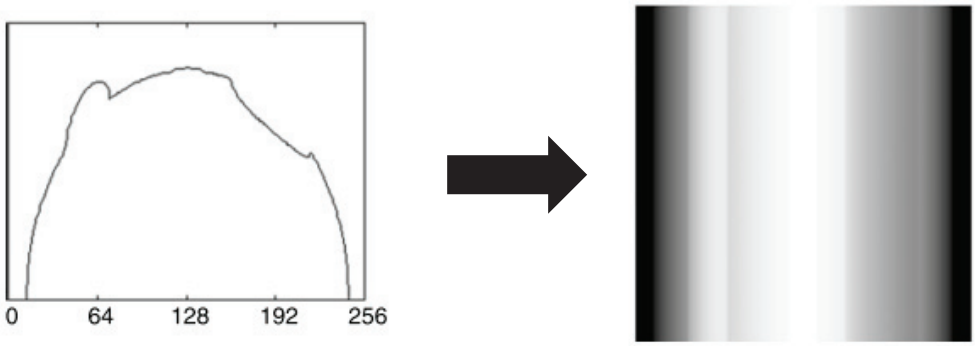

Figure 15 Illustration of the backprojection of one single projection: projection for angle θ = 0 and its backprojection (Peyrin and Engelke, 2012)

The sum of all the backprojections after filtering each projection with a suited kernel provides a reconstruction of the initial image (see Figure 16).

a.

b.

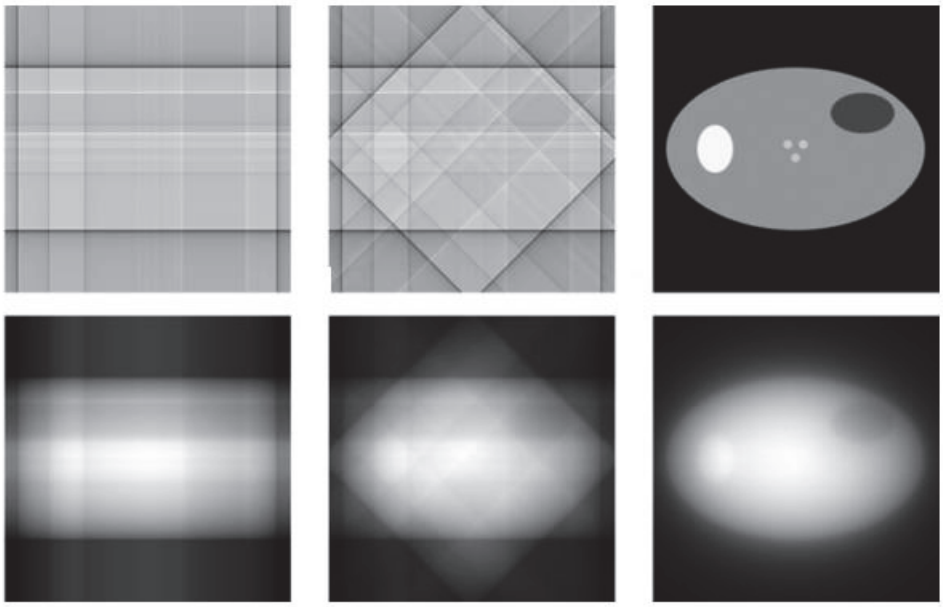

Figure 16 From left to right: a. filtered backprojection after summing, 2, 4 and all projections; b. backprojections without filtering after summing, 2, 4, and all projections (Peyrin and Engelke, 2012)**.**

ii. Biomechanics

The major role of bone within the organism is to hold and support the whole body and muscles. It seems pertinent to study its mechanical behavior.

- ***Continuum mechanics***

A material mechanical behavior is often characterized by the relation between the stress applied to the material and its resultant strain.

The stress, σ (Pa), depends on the applied loading F (N) and the section S (m²) of the material. Thus, for a simple tensile loading, and with the hypothesis of a homogeneous and isotropic material:

$$\sigma = \frac{F}{S} \tag{I.6}$$

The strain, ε (no unit), can be defined by the relative elongation/shrinking of the material. Considering l_0 (m) the initial length of the sample and l_1 its length after the tensile loading:

$$\varepsilon = \frac{l_1 - l_0}{l_0} = \frac{\Delta l}{l_0} \tag{I.7}$$

For elastic material, meaning material that regains its initial shape when unloading, these two parameters are linearly proportional, with a proportionality coefficient that is a material property. The so called elastic modulus, or Young's modulus, E (Pa) is independent of the geometry and characteristic of intrinsic material properties and is expressed as:

$$E = \frac{\sigma}{\varepsilon} \tag{I.8}$$

Some materials have the capacity to undergo irreversible deformation, or plastic deformation when loading above a specific strength. This critical loading is characterized by another material constant called yield stress (σ_Y).

Once the yield stress is reached, the material begins to deform plastically until it cannot handle more stress. The ultimate stress (σ_{ult}), or strength of the material, is then reached and the material breaks.

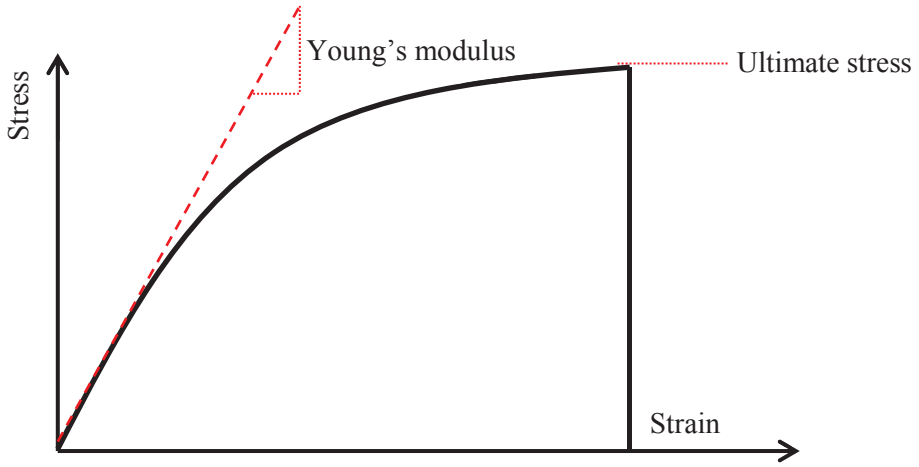

Figure 17 Example of a stress-strain curve, definition of the different parameters

- ***Fracture mechanics***

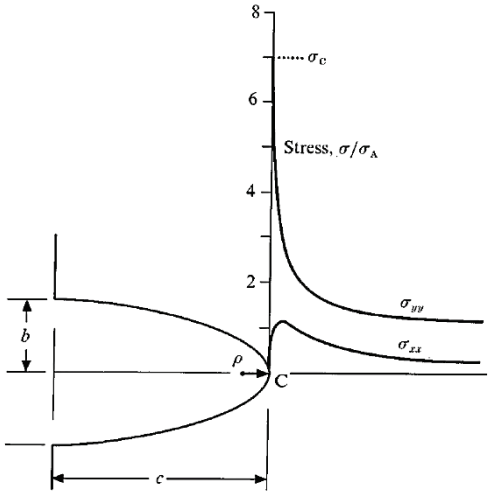

Figure 18 Stress measured in the neighbourhood of a defect (Lawn, 1993)

To understand the phenomena of crack propagation in material science, Griffith model a static crack as a thermodynamic system, in order to solve the problem in term of energy (Griffith, 1921):

$$U = U_M + U_S \tag{I.11}$$

where U is the total energy of the system; $U_M = U_A + U_E$ is the mechanical energy defined as the sum of the potential energy of the outer applied loading U_A, and the strain potential energy U_E; and U_S is the energy needed to create new surfaces. By balancing the mechanical and surface energy

terms over a virtual crack extension dc, Griffith enounced his energy balance concept giving the equilibrium requirement:

$$\frac{dU}{dc} = 0 \tag{I.12}$$

Considering a simple case of uniform tension in the elastic domain, a material behaves as spring, and in accordance with Hooke's law:

$$u_0 = \lambda P \tag{I.13}$$

where u_0 is the displacement under loading P and λ is the elastic compliance. In that case, the strain energy system is equal to the work performed by the elastic loading:

$$U_E = \int_0^{u_0} P du = \frac{1}{2} P u_0 \tag{I.14}$$

and by derivation:

$$dU_E = \frac{1}{2} P du_0 \tag{I.15}$$

We can also calculate the work done by the outer applied loading:

$$dU_A = -P du_0 \tag{I.16}$$

We can see that dU_A=-2dU_E. Thus we have the relation:

$$dU_M = -\frac{1}{2} P du_0 \tag{I.17}$$

G, the strain energy release rate defines the energy needed to propagate the crack from a distance dc:

$$G = -\frac{dU_M}{dc} = -\frac{dU_E}{dc} \tag{I.18}$$

This parameter is highly used to treat of material fracture behavior in the elastic domain.

In order to define mechanically what's happening near a defect, Irwin introduced a parameter describing the mechanisms of stress concentration (Irwin, 1957). He defined this stress intensity factor K (Pa.$m^{0.5}$) as following:

$$\sigma = \frac{K}{\sqrt{2\pi r}} f(\theta) \tag{I.19}$$

where σ is the stress near the tip, r and θ are the polar coordinate.

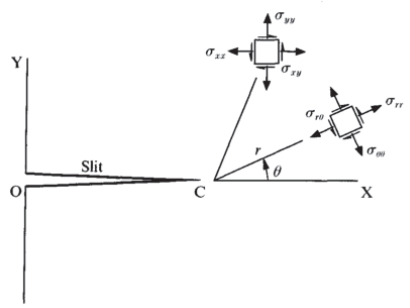

Figure 19 Stress field near the crack tip (Lawn, 1993)

Irwin also defined the toughness parameter as the critical stress intensity factor at which a crack will initiate from the initial defect. Irwin distinguished three fracture modes depending on the nature of the applied loading.

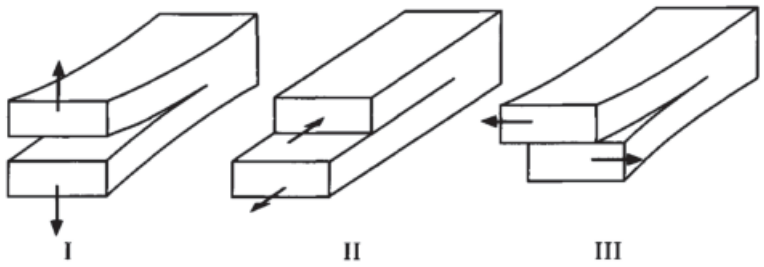

Figure 20 There are three different fracture modes (Lawn, 1993) **Mode I corresponds to an opening mode, mode II to a shear mode by sliding, and mode III to a shear mode by tearing.**

Mode I fracture mode, meaning the opening mode, is known to be the most critical for material. Considering this particular mode, one deal with the mode I critical stress intensity factor K_{Ic}.

Strain energy release rate and stress intensity factor, that describe the same material behavior, can be linked using the following relationship:

$$G = \frac{{K_{Ic}}^2}{E'} \tag{I.20}$$

where E' = E/(1-ν²) is a corrected elastic modulus in the case of plane strain condition (ν is the Poisson's ratio).

- ***Non-linear fracture mechanics***

The hypothesis of an infinite stress at the crack is theoretically impossible. Irwin thus theorized that a small process zone is developed near the defect's tip modifying the stress field. The size of this area is defined as:

$$r_p = \frac{1}{2\pi}\left(\frac{K}{\sigma}\right)^2 \tag{I.21}$$

where r_p is the radius of the process zone, K is the stress intensity factor and σ, the applied stress (Irwin, 1960).

The parameters defined previously are true if we consider a small r_p, that is the case for elastic material as ceramic.

There are therefore some materials, such as polymer materials, that undergo non-linear deformation. In that case, the hypothesis of a small plastic zone is no more respected. One should then introduce non-linear mechanics in the analysis. In 1968, Rice raised the problem, and introduced a new method to measure strain energy release rate considering both linear and non-linear behavior. As the problem stems in the hypothesis of a small plastic area, the idea is to measure a parameter that does not depend on the area of measurement. He thus introduces the path independent J-integral (Rice, 1968).

Considering the mechanical energy U_M:

$$U_M = U_E + U_A = \int_A W dA + \int_\Gamma T.u d\Gamma \tag{I.22}$$

where

$$W = \int_0^\varepsilon \sigma d\varepsilon \tag{I.23}$$

is the strain energy density, A is the surface of the considered area, T is the traction vector perpendicular to the path Γ, and u is the displacement vector.

By derivation, we can define J, and as the crack grows in the x direction (meaning dc = dx):

$$J = -\frac{dU_M}{dc} = \int_\Gamma \left(W dy - T\frac{du}{dx} d\Gamma\right) \tag{I.24}$$

With this relation, it is possible to take a high enough path Γ in order to consider the process zone developed at the notch tip. In the particular case where Γ only follows the edge of the defect, that is stress free, we find:

$$J = -\frac{dU_M}{dc} = \int_{\Gamma} W dy = -\frac{dU_E}{dc} = G \tag{I.25}$$

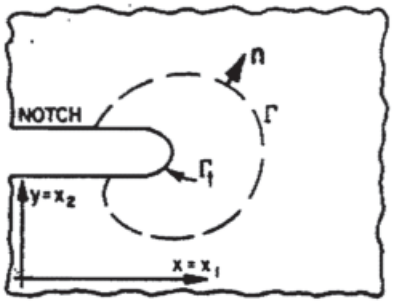

Figure 21 Definition of the path Γ surrounding the notch tip (Rice, 1968)

- ***How to measure fracture toughness?***

There are standardized experimental tests used to specifically measure toughness. The ASTM E-1820 gives the steps to follow in order to measure fracture toughness on ductile material such as metals (ASTM International, 2003). The particularity of these tests is that an initial notch is realized in the sample so that one can control where the crack will initiate. Here is the method SENB (Single Edge Notched Bending) using three-point bending mechanical test:

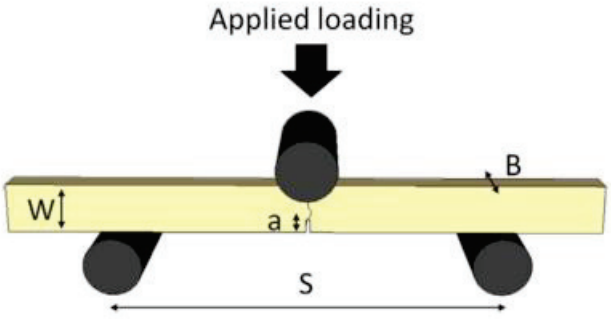

Figure 22 Three-point bending toughness test. The different geometrical parameters are defined on the drawing

The method allows the measurement of both G and non-linear J (N.m^{-1}):

$$J = J_{el} + J_{pl} = G + J_{pl} = \frac{{K_{Ic}}^2}{E'} + J_{pl} \quad \text{(I.26)}$$

As enounced before E' (Pa) = E/(1-ν²) is a corrected elastic modulus used in the case of plane strain condition and ν is the Poisson's ratio. In the case of a three-point bending tests the linear elastic fracture mechanics based toughness, or initiation toughness, is expressed as:

$$K_{Ic} = \frac{PS}{BW^{\frac{3}{2}}} f(\frac{a}{W}) \quad \text{(I.27)}$$

where P (N) is the yield load defined as the intersection between the load-displacement curve and the secant line with a slope of 95 % of the initial curve's slope (Figure 23), S (m) is the distance between the inferior rolls of the apparatus, B (m) and W (m) are respectively the thickness and the height of the sample and a is the initial length of the notch. f(a/W) is a geometrical polynomial function giving by the standard:

$$f\left(\frac{a}{W}\right) = \frac{3\sqrt{\frac{a}{W}}\left[1.99 - \frac{a}{W}\left(1 - \frac{a}{W}\right) * \left(2.15 - 3.93\frac{a}{W} + 2.7\left(\frac{a}{W}\right)^2\right)\right]}{2\left(1 + 2\frac{a}{W}\right)\left(1 - \frac{a}{W}\right)^2} \quad \text{(I.28)}$$

J_{pl} (N.m^{-1}) is the energy needed to propagate the crack once it is initiated:

$$J_{pl} = \frac{\eta A_{pl}}{B(W - a)} \quad \text{(I.29)}$$

where η = 1.9 is a geometrical factor for SENB specimen, A_{pl} (N.m) is the area under the plastic contribution of the load-displacement curve (Figure 23).

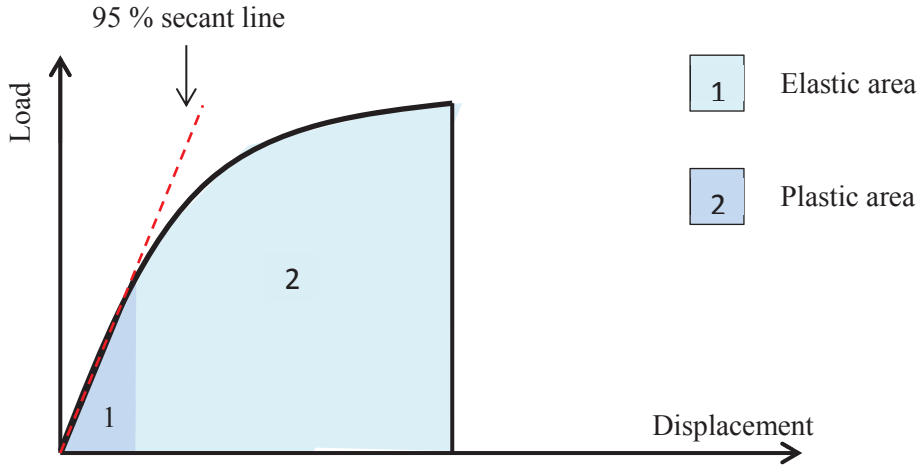

Figure 23 Typical load-displacement curve. A_{pl} is defined as the area 2.

One can then determine the non-linear mechanics based toughness K_{Jc} (Pa.m$^{0.5}$):

$$K_{Jc} = \sqrt{E'J} \tag{I.30}$$

- R-curve

All these previous relations can be adapted in order to assess the resistance curve, or R-curve. This tool allows the measurement of the evolution of the toughness in function of the crack growth. Because of the activation of some toughening mechanisms, that will be discussed later, the energy needed to initiate and propagate a crack evolves with the crack advancement.

To assess the property, we have to use relations given in the ASTM E-1820 and use it incrementally with crack growth a_i:

$$J_{(i)} = J_{el(i)} + J_{pl(i)} \tag{I31}$$

$$K_{Ic(i)} = \frac{P_{(i)}S}{BW^{\frac{3}{2}}} f\left(\frac{a_{(i)}}{W}\right) \tag{I.32}$$

$$f\left(\frac{a_{(i)}}{W}\right) = \frac{3\sqrt{\frac{a_{(i)}}{W}}\left[1.99 - \frac{a_{(i)}}{W}\left(1 - \frac{a_{(i)}}{W}\right) * \left(2.15 - 3.93\frac{a_{(i)}}{W} + 2.7\left(\frac{a_{(i)}}{W}\right)^2\right)\right]}{2\left(1 + 2\frac{a_{(i)}}{W}\right)\left(1 - \frac{a_{(i)}}{W}\right)^2} \tag{I.33}$$

$$J_{pl(i)} = \frac{\eta A_{pl(i)}}{B(W-a)} \tag{I.34}$$

$$K_{Jc(i)} = \sqrt{E' J_{(i)}} \tag{I.35}$$

7. Crack propagation in cortical bone

Cortical bone toughness has been largely studied in the past. It appears that this material can undergo toughening mechanisms that make it more difficult to the crack to propagate within the tissue. We will see in this section an overview of results about cortical bone toughness and toughening mechanisms.

i. Cortical bone toughness

A summary of the results (type of bone and origin of bone ie: animal/ human) will be found in Table 2 and Table 1.

First results on cortical bone toughness emerged in the 1970's (Bonfield and Datta, 1976; Evans, 1973; Pope and Outwater, 1972; Robertson and Barrett, 1978). These first results showed that it is easier for a crack to propagate in the longitudinal direction of the diaphysis, meaning parallel to the osteonal structures (Evans, 1973). In the transverse direction, crack propagates following weak interfaces that represent the cement lines and lamellae (Pope and Outwater, 1972). It had also been shown that density can be related to the initiation toughness K_{Ic}: it appears to be more difficult to initiate a crack in a denser tissue (Behiri, 1990). Others authors have shown that the radius of curvature of the initial notch does not influence the fracture behavior of the material (Bonfield, 1987; Robertson and Barrett, 1978).

Nowadays, cortical bone toughness is still of a great interest for the scientific community (Carriero et al., 2014; Cook et al., 2010; Diez-Perez et al., 2010; Hazenberg et al., 2006; Katsamenis et al., 2015, 2013, 2012, Kulin et al., 2011a, 2011b; Launey et al., 2010; Lee et al., 2003; McCormack et al., 2012; Mischinski and Ural, 2011; Nalla et al., 2006, 2005a; O'Brien et al., 2005a; Olvera et al., 2012; Phelps et al., 2000; Ritchie et al., 2009, 2008; Taylor, 2006; Taylor et al., 2009; Ural et al., 2011; Woodside and Willett, 2016; Yamaguchi et al., 2011; Yang et al., 2006a; Zimmermann et al., 2016, 2009; Zimmermann and Ritchie, 2015; Zioupos, 1998; Zioupos et al., 2008). With the development of new technology, scientists discovered that the tissue response to crack propagation is complex. A lot of toughening mechanisms play a major role in slow down and arrest crack

propagation in cortical bone. But most of the studies consider only the linear elastic behavior of cortical bone whereas its non-linear contribution cannot be neglected (Barth et al., 2010; Granke et al., 2015; Yang et al., 2006b; Zimmermann et al., 2014).

Moreover, few results concerning the influence of bone anatomical locations can be found in the literature (Brown et al., 2000). Studies are generally performed on the femur or tibial diaphyses as their large thickness allow easiest sample preparation. But fractures are mostly located on the femoral neck or on the radius, that exhibit a very thin layer of cortical bone (Chappard et al., 2013; Chen et al., 2010; González-Agüero et al., 2013; Kilappa et al., 2011; Rubinacci et al., 2012; Treece et al., 2010). As these different anatomical locations are not subjected to the same mechanical environment during life, their structural organization may not be the same (Wolff, 1892). We will see later that this can have an influence on the tissue behavior versus crack propagation.

Finally, there is a lack of knowledge concerning the effect of strain rate on cortical bone toughness. Only few studies discuss about it whereas bone fracture mainly occur after a fall involving high loading rate (Foldhazy, 2005; Kulin et al., 2011a; Shannahan et al., 2015; Zimmermann et al., 2014).

Improving our biomechanical knowledge on human cortical bone toughness can be of a great interest to well understand crack propagation mechanisms to help the development of clinical diagnosis and treatment against bone diseases. The aim is thus to understand how cortical bone architecture operates in slow down and arrest of crack propagation.

Table 1 Summary of human cortical bone toughness values found in the literature

Reference	Bone	n (modality)	Method	Loading rate ($mm.min^{-1}$)	K_{Ic} ($MPa.m^{0.5}$)	K_{Jc} ($MPa.m^{0.5}$)
(Akkus et al., 2000)	Femur	3 (long) / 4 (trans)	CT	0.09	1.7 / 3.5	-
(Nalla et al., 2004b)	Humerus	6 (long)	CT	0.9	2.1	-
(Nalla et al., 2004a)	Humerus	7 (youngs) / 5 (mid-aged) / 5 (aged) (long)	CT	0.9	2.1 / 2.0 / 1.3	-
(Nalla et al., 2005b)	Humerus	7 (long)	CT	0.9	2.0	-
(Nalla et al., 2005a)	Humerus	7 (long) / 6 (trans)	DN4PB	0.6	3.5 / 5.3	-
(Koester et al., 2008)	Humerus	17	SENB	-	5.0	-
(Barth et al., 2010)	Femur	7 (initial) / 7 (0.05Gy) / 7(70Gy) / 7 (210Gy) (long)	SENB	0.6	1.8 / 1.1 / 0.9 / 0.7	13.3 / 10.5 / 7.4 / 2.7
(Zimmermann et al., 2014)	Femur	4 (quasi-static) / 5 (middle) / 4 (fast)	SENB	-	-	12.5 / 10.5 / 7.5
(Granke et al., 2015)	Femur	62	SENB	0.6	-	12.0

long: longitudinal; tran: transverse

Table 2 Summary of animals cortical bone toughness values found in the literature

Reference	Species	Bone	n (modality)	Method	Loading rate ($mm.min^{-1}$)	K_{Ic} ($MPa.m^{0.5}$)	K_{Jc} ($MPa.m^{0.5}$)
(Melvin and Evans, 1973)	Bovine	Femur	-	SENB	-	3.2	-
(Bonfield and Datta, 1976)	Bovine	Tibia	-	SENB	-	4.6	-
(Robertson and Barrett, 1978)	Bovine	Femur	7 (not notched) / 7 (notched)	SENB	-	4.8/5.1	-
(Behiri and Bonfield, 1984)	Bovine	Tibia	-	CT	0.01-50	2.8-2.0	-
(Lucksanasombool et al., 2001)	Bovine	Femur	10 (Saline) / 10 (Alcohol) / 9 (Alcohol + Saline)	SENB	15	3.5 / 5.1 / 3.4	-
(Yeni and Fyhrie, 2002)	Bovine	Tibia	9 (long)	SENB	0.18	2.6	-
(Vashishth, 2004)	Bovine	Tibia	5	CT	0.05	4.5	-
(Yan, 2005)	Bovine/ Lamantin	Femur	10 / 10	4PB	0.3	5.8 / 4.5	-
(Yan et al., 2007)	Bovine	Femur	10 (long) / 10 (trans)	SENB	1	2.6 / 5.1	6.2 / 10.5
(Mullins et al., 2007)	Ovine	Tibia	432	Indentation	$1.7.10^{-4}$	2.3	-
(Ritchie et al., 2008)	Murine	Femur	15	SENB	0.06	2.9	-
(Thurner et al., 2010)	Murine	Femur	9 / 9 (OPN deficient)	SENB	0.001	5.6 / 3.9	-
(An et al., 2011)	Bovine	Femur	-	CT	0.01	2.6 (long) / 6.3 (trans)	-
(Kulin et al., 2011a)	Equine	Femur	11 (quasi-static) / 13 (dynamic)	DN4PB	0.005 / pulse	4.8 / 3.4	-
(McCormack et al., 2012)	Equine	Femur	14	DN4PB	0.05	3.4	-

long: longitudinal; tran: transverse

ii. Cortical bone architecture as a barrier against crack propagation

Crack propagation through cortical bone architecture is controlled by different mechanisms spreading the overall hierarchical structure of the tissue and depending on the tissue organization and composition.

- ***Hundreds of micrometers scale***

Osteon is the main mechanical unit that composed cortical bone, they are called Bone Structural Unit (Ascenzi and Bonucci, 1967; Ascenzi and Fabry, 1959). Dealing with crack propagation mechanisms, osteon, and particularly its weak interface with interstitial bone, plays a major role. Probably because osteons and interstitial tissue have different mechanical properties, coming from their different amount of mineralization, when a crack encounters the cement line, this one may not be able to pass through the interface, thus leading to a deflection of its initial path (Burr et al., 1988; He and Hutchinson, 1989; Mischinski and Ural, 2011; O'Brien et al., 2005b; Olvera et al., 2012; Wagermaier et al., 2015; Yeni and Norman, 2000a; Zimmermann et al., 2009). Their density, increasing with age and also between anatomical locations, is negative for fracture toughness (Yeni et al., 1997; Zimmermann et al., 2012).

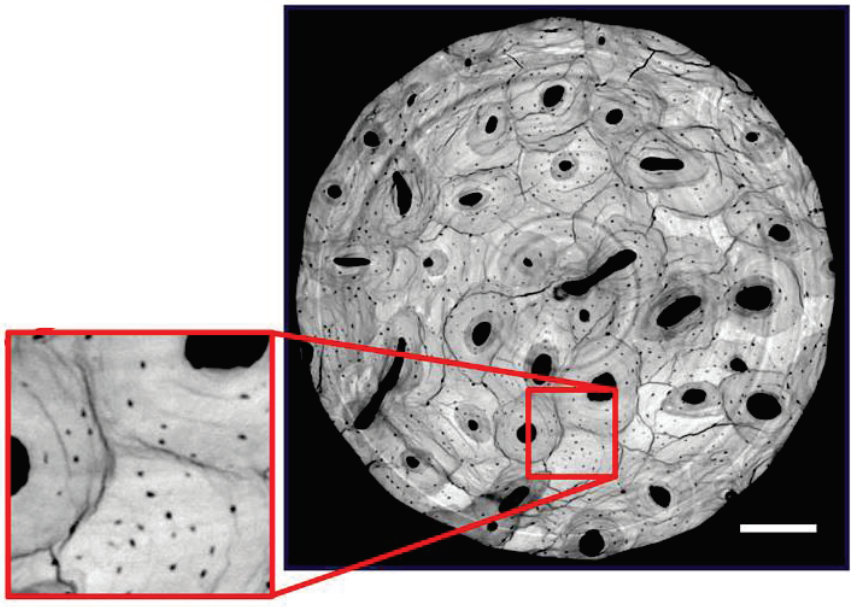

Figure 24 SR µCT image of human cortical bone sample subjected to compression loading (Wolfram et al., 2016)

When loaded at a higher rate, cortical bone toughness decreases. As osteon is the major unit of the

tissue, one may think that its role may differ in function of the loading rate. A recent study used the framework described by He and Hutchison explaining that when a crack encounters an interface between two materials, it will pass through it if the mismatch between mechanical properties (fracture and elastic properties) of the two materials satisfies a particular condition. They assume that under a higher loading rate, the conditions are satisfied thus the crack can pass from a material to the other (He and Hutchinson, 1989; Zimmermann et al., 2014).

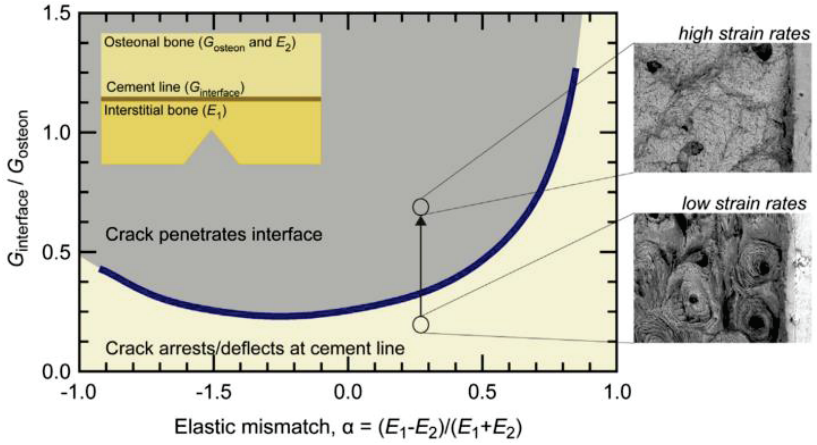

Figure 25 He and Hutchinson condition for a crack to pass through an interface (He and Hutchinson, 1989; Zimmermann et al., 2014)

- ***Micrometer scale***

At a higher scale, the presence of micro-cracks is related to cortical bone resistance to crack propagation. These defects form when the stress within the tissue is too high. By forming they dissipate mechanical energy and then change the mechanical environment around them (Ritchie, 1999). Micro-cracks can be found in cortical bone during life, formed because of a constant mechanical loading that damaged the tissue (Diab and Vashishth, 2005; Haupert et al., 2014; Larrue et al., 2011; Lee et al., 2002; O'Brien et al., 2000; Turnbull et al., 2014). When a major crack propagates within the tissue, its tip represents a highly constrained area involving thus an important formation of micro-cracks (Nalla et al., 2004b; Ritchie, 1988). Cortical bone can create micro-cracks which could be of a great interest when dealing with its fracture behavior.

When a crack propagates in the transverse direction, micro-cracks will form perpendicularly to the main crack path. By dissipating mechanical energy; the driving force for crack growth is reduced involving a blunting of the crack tip. As the material is still loaded, the main crack has to take another path where it needs less driving force, generally along the osteon cement line, leading to a

crack deflection (Koester et al., 2008; Wolfram et al., 2016; Zioupos, 1998). Therefore, a too high accumulation of these defects within cortical bone tissue may lead to their coalescence and thus the formation of a macrocrack (Danova et al., 2003; Zioupos, 1998). Osteocyte lacunae may also play a role in this toughening mechanism as they dictate the path taken by the micro-cracks (Voide et al., 2009). Some results showed that the amount of micro-cracks present in cortical bone increases with age (Norman and Wang, 1997).

With an increase of the loading rate, fewer micro-cracks are formed in the loaded tissue (Hansen et al., 2008; Kulin et al., 2011a; Zioupos et al., 2008). This point is in accordance with the fact that the dissipating mechanism at the collagen molecule scale is mainly a stretching mechanism when loaded faster. Thus fibers are not sliding between each other limiting the breakage at the interfibrillar interface.

Whereas the formation of micro-cracks appear to slightly soften the material, another toughening mechanisms appear to stiffen it by creating bridges between collagen fibrils involving the formation of an un-cracked ligament (Nalla et al., 2004b; Ritchie, 1999, 1988). This ligament can handle a high amount of stress that would have been used to grow the crack.

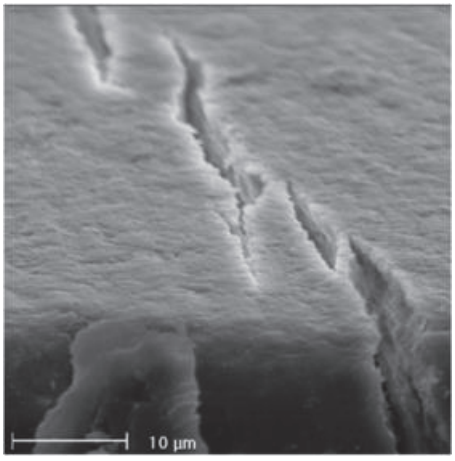

Figure 26 Scanning electron micrograph illustrating crack bridging in cortical bone (Kulin et al., 2011a)

- ***Nanometer scale***

At this molecular scale, collagen chains are involved in crack propagation mechanisms both in cortical bone linear and non-linear behavior.

When subjected to a tensile loading, collagen molecules first dissipate energy by stretching (Bala and Seeman, 2015; Gupta et al., 2006, 2005; Silver et al., 2001; Ural and Vashishth, 2014; Zimmermann and Ritchie, 2015). A good collagen quality, directly related to its stiffness, leads to an effective load transfer between collagen molecules and mineral platelets thus preventing crack nucleation(Lee et al., 2003). A stiffer collagen matrix is less able to dissipate energy and thus transfers a higher level of load to the mineral platelets (Gupta et al., 2006, 2005).

Figure 27 At the nanoscale, elastic behavior of cortical bone is governed by collagen molecules uncoiling (Zimmermann and Ritchie, 2015)

Once collagen chains cannot handle more stretching, the matrix has to develop other mechanisms to dissipate mechanical energy. This energy dissipation mechanism thus occurs by the mean of a sliding between collagen fibrils (Gupta et al., 2013, 2005; Zimmermann et al., 2012). In this mechanism, the non-collagenous proteins that bound collagen molecules together play a major role (Abraham et al., 2015; Berteau et al., 2015; Currey, 2001; Fantner et al., 2005; Farlay et al., 2016; Granke et al., 2015; Hansma et al., 2005; Lieou et al., 2013; Poundarik et al., 2015; Saito and Marumo, 2010; Silver et al., 2001; Tang and Vashishth, 2011; Willett et al., 2013). It has been shown that, with maturity of cortical bone organic matrix, the tissue is less able to dissipate mechanical energy with non-linear mechanisms (Berteau et al., 2015; Saito and Marumo, 2010; Tang and Vashishth, 2011; Willett et al., 2013). By becoming stiffer with age, these molecules cannot allow a large inter-fibrillar sliding involving a higher strain in each fibrils leading to the nucleation of cracks within the tissue.

Loading rate has an influence on cortical bone organic matrix mechanical properties (Hansen et al., 2008; Johnson et al., 2010; Kasapi and Gosline, 1996; Zimmermann et al., 2014). It appears that, when loaded faster, collagen fibrils stretching becomes more important, whereas non-linear energy dissipation mechanisms, such as inter-fibrillar sliding, is less effective (Zimmermann et al., 2014).

8. Conclusion

In this chapter we have seen that human cortical bone is a complex material that spread over different length scale. This multiscale arrangement provides to cortical bone a high toughness under quasi-static loading condition. From the osteon to the collagen molecule, the overall organization of the tissue operates to slow down crack propagation.

There is therefore a lack of knowledge considering the bone capacity crack propagation at higher strain rate. As bone fractures mainly occur after a fall from a standing height, higher loading rate have to be considered to improve this knowledge.

Using different characterization methods, we aim to provide new results about cortical bone toughness under fall-like loading condition. Relationships with the tissue microstructure will also be analyzed to help understanding the mechanisms under crack propagation in human cortical bone.

Chapter II Strain rate influence on human cortical bone toughness: a comparative study on three paired anatomical sites*

*This chapter was published in the Journal of the Mechanical Behavior of Biomedical Materials (Gauthier et al., 2017)

Abstract: Bone fracture is a major health issue worldwide and consequently there have been extensive investigations into the fracture behavior of human cortical bone. However, the fracture properties of human cortical bone under fall-like loading conditions remains poorly documented. Further, most published research has been performed on femoral diaphyseal bone, whereas it is known that the femoral neck and the radius are the most vulnerable sites to fracture. Hence, the aim of this study is to provide information on human cortical bone fracture behavior by comparing different anatomical sites including the radius and the femoral neck acquired from 32 elderly subjects (50 – 98 y.o.). In order to investigate the intrinsic fracture behavior of human cortical bone, toughness experiments were performed at two different strain rates: standard quasi-static conditions, and a higher strain rate representative of a fall from a standing position. The tests were performed on paired femoral neck, femoral, tibial and radius diaphyseal samples. Linear elastic fracture toughness and the non-linear J-integral method were used to take into account both the elastic and non-elastic behavior of cortical bone. Under quasi-static conditions, the radius presents a significantly higher toughness than the other sites. At the higher strain rate, all sites showed a significantly lower toughness. Also, at the high strain rate, there is no significant difference in fracture properties between the four anatomical sites. These results suggest that regardless of the anatomical site (femur, femoral neck, tibia and radius), the bone has the same fracture properties under fall loading conditions. This should be considered in biomechanical models under fall-like loading conditions.

1. Introduction

The aging of human biological tissues is often synonymous with increased vulnerability to traumatic injuries. In the elderly, a fall from a standing position may cause a hip fracture (Court-Brown and Caesar, 2006; Gryfe et al., 1977; World Health Organization, 2007), leading to important disability and sometimes increased risk of mortality (Johnell and Kanis, 2006). From results presented in the literature, this increased vulnerability might be due to a change in structural properties such as increased porosity (Perilli et al., 2015).

Measurements of bone mineral density is currently the gold standard clinical diagnostic method for osteoporosis (Genant et al., 1999, 1996). It has been shown that bone mineral density decreases in osteoporosis (Nanes and Kallen, 2014), and that this loss of bone mass is correlated with its structural strength (Ammann and Rizzoli, 2003; Duchemin et al., 2008).

It appears, however, that the assessment of this single parameter cannot fully discriminate whether a given patient presents an increased fracture risk (Siris et al., 2014, 2004). Other structural and mechanical parameters have to be considered in order to describe the overall fracture behavior of human bone (Griffith et al., 2010). Subject-specific finite element models are under development in order to improve fracture risk prediction (Pistoia et al., 2002). Even if these methods can give good estimations of bone structural strength, the fracture risk still remains difficult to predict precisely (van Rietbergen and Ito, 2015). It is assumed that the loading conditions may be a major determinant, but in most of the studies the loading conditions are not representative of what occurs in real cases of fall injuries (van Rietbergen and Ito, 2015). Moreover, mechanical properties integrated in the models are mostly obtained from quasi-static tests, whereas rate might have an influence on these properties (Ural et al., 2011). When studying such traumatic injuries, particular loading conditions have to be considered, implying a specific loading rate that had been measured at 2 $m.s^{-1}$ corresponding to a strain rate of 10^{-1} s^{-1} (Foldhazy, 2005; Nankaku et al., 2005). In the following, we refer to such strain rates as fall-like loading conditions.

In order to study bone behavior at the material scale, we choose to study the specific fracture properties of human cortical bone, as it is more involved in fracture mechanisms than cancellous bone (Holzer et al., 2009). Particularly, fracture toughness parameters can provide information about human cortical bone fracture mechanisms. The influence of strain rate on human cortical bone fracture toughness has been relatively little studied. In the literature, only measurements on femoral diaphysis (Sanborn et al., 2016; Zimmermann et al., 2014) have been reported. It was shown that when loaded at a higher rate, cortical bone toughness decreases. This means that bone is more able to resist crack propagation at low strain rates (Zimmermann et al., 2014). Albeit of great interest,

that finding was based on a study of samples from a single subject, which prevents further generalization. It is well known that bone adapts itself to its mechanical environment, which implies a non-negligible inter-individual variability (Wolff, 1892). Fractures due to falls are often observed at the femoral neck and in the radius diaphysis. These are respectively weight bearing and non-weight bearing bones (Court-Brown and Caesar, 2006), which might influence their fracture properties. However, there is no data available on the effect of a fall for these anatomical sites.

Therefore the aims of the present study are to determine whether:

- quasi-static toughness differs between the femoral neck, femoral , tibial and radius diaphyses,
- there is an influence of the strain rate on toughness at each of these anatomical sites, and
- fall-like loading toughness differs between four anatomical sites.

2. Materials and Methods

i. Sample preparation

Thirty-one human cadaver subjects were used in this study (18 women, age 81 ± 12 y.o.; 14 men, age 79 ± 8 y.o.). No additional information regarding disease status or medication history was available. Whole femurs, tibias and radii were collected from these fresh cadaveric subjects. Extracted bones were wrapped in gauze soaked with saline to keep them hydrated, then stored at -20°C until sample preparation. Because some bones were broken or not available, the final database consisted of 29 femoral diaphyses, 29 femoral necks, 22 tibial diaphyses and 31 radial diaphyses. From each bone, 25 mm long rectangular notched samples, with a width W=2.08 ± 0.06 mm and a thickness B=1.01 ± 0.02 mm, were extracted using a low speed saw with a diamond coated blade (ISOMET 4000, Buehler, USA). The dimensions were chosen based on the available cortical thickness in the femoral neck and radius (Kilappa et al., 2011; Treece et al., 2012). While the available cortex is thicker in the femur and tibia, we decided to standardize the dimensions so that a direct comparison could be performed. The samples were prepared to have their long side parallel to the long axis of the bone, and consequently its osteons. A notch was then machined in the transverse direction of the bone, in order to initiate crack formation perpendicularly to the osteon structure within the tissue. To ensure consistent crack formation, the notch tip radius was reduced by the use of an ad hoc device sliding a cutter blade in the bottom of the initial notch, cutting the final notch to a controlled depth. The final notch was a_0=1.16 ± 0.06 mm long, half of the sample width, with a notch tip radius of approximately 10 µm. Since one objective of this study was to investigate the

effect of different strain rates, two contiguous samples were prepared from each bone; one to be tested under a quasi-static strain rate and the other at a rate representative of a fall. Thus, a total of 220 samples were prepared for this study. The samples were stored at -20°C after preparation, then de-frosted the night before the mechanical tests and kept at 21°C in a physiological solution from 6 h before testing for rehydration.

ii. Biomechanical experiments

Samples were tested in a three-point bending configuration with a 10 mm supporting span on a servo hydraulic testing machine (INSTRON 8802, High Wycombe, England) (The American Society of Mechanical Engineers (ASME), 2006). For the quasi-static loading, which is the standard for cortical bone toughness measurement, a strain rate of 10^{-4} s^{-1} was applied (Kasapi and Gosline, 1996; Yeni and Fyhrie, 2002; Zimmermann et al., 2014). Based on values found in the literature to represent a fall from a standing position, the samples were loaded at a strain rate of nearly 10^{-1} s^{-1} (Foldhazy, 2005) to emulate fall conditions. The corresponding displacement rates of the testing machine to the given strain rates were 10^{-3} $mm.s^{-1}$ for the quasi-static case and 10 $mm.s^{-1}$ for fall conditions. A load-displacement curve was recorded for each mechanical test and was used to obtain different parameters using the methods presented below.

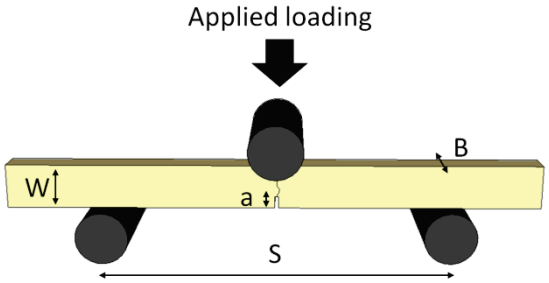

Figure 28 Illustration of human cortical bone sample with the different dimensional parameters

- ***Fracture toughness measurement***

Fracture toughness measurements were performed with a standardized apparatus and supporting span according to ASTM E-1820 for single-edge bending specimens (SENB) (The American Society of Mechanical Engineers (ASME), 2006). In order to take into account the elasto-plastic behavior of human cortical bone, we used the nonlinear path independent J-integral calculation introduced by Rice in 1968 (Rice, 1968). Contrary to linear elastic toughness K_{Ic}, the J-integral incudes the hypothesis of a non-negligible plastic zone, which is the case for bone ahead of the front

crack (Yang et al., 2006b). This mechanical parameter depends on both an elastic contribution, J_{el} ($N.mm^{-1}$) and a plastic one, J_{pl} ($N.mm^{-1}$):

$$J = J_{el} + J_{pl} = \frac{K_{Ic}^2}{E'} + J_{pl} \quad \text{(II.1)}$$

where *E'* is Young's modulus $E'=E/(1-\nu^2)$ (E=15.80 GPa (Zimmermann et al., 2014)) in plane strain conditions and ν=0.3 is Poisson's ratio. K_{Ic} is the linear-elastic fracture toughness, and correspond to the value of the stress intensity factor at which a crack will initiate from the notch:

$$K_{Ic} = \frac{PS}{BW^{\frac{3}{2}}} . f(\frac{a}{W}) \quad \text{(II.2)}$$

where *P* is the yield load determined at the intersection between the load-displacement curve and the secant line with a slope equal to 95% of the initial slope of the recorded curve as explained in ASTM E-1820 (The American Society of Mechanical Engineers (ASME), 2006), *S*=14 mm is the loading span and f(a/W) a geometrical polynomial function depending on the ratio between the initial crack length, *a*, and the width of the sample, *W* (The American Society of Mechanical Engineers (ASME), 2006). *B* is the thickness of the sample. The plastic contribution J_{pl} is given by:

$$J_{pl} = \frac{\eta A_{pl}}{B(W-a)} \quad \text{(II.3)}$$

where η is a geometrical factor equal to 1.9 for the SENB specimen (The American Society of Mechanical Engineers (ASME), 2006), A_{pl} the area under the plastic contribution of the load-displacement curve. With these different parameters, the fracture toughness K_{Jc}, corresponding to the mode I critical stress intensity factor, is computed as follows:

$$K_{Jc}=(JE')^2 \quad \text{(II.4)}$$

Figure 28 and Figure 29 show a summary of all the parameters needed to toughness parameter calculation.

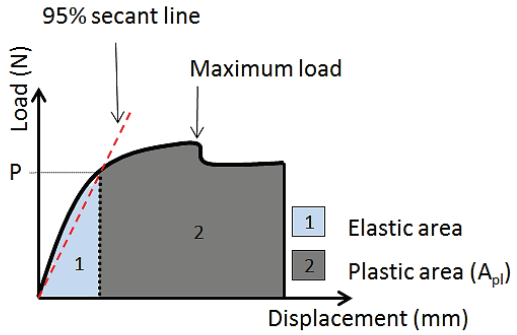

Figure 29 Typical load-displacement curve obtained for human cortical bone, 2 is the plastic area A_{pl}

- ***R-curve***

The R-curve gives the evolution of fracture toughness as a function of crack length (Swain, 1989). For short cracks in human cortical bone, this relation appears to be close to linear (Katsamenis et al., 2013; Koester et al., 2008). In order to track the evolution of the crack length during loading, the biomechanical tests were recorded with a camera (FASTCAM SA3, Photron, San Diego, USA) mounted with a macro lens (MACRO 180mm, F2.8 EX DG OS HSM, Sigma, Le Mans, France), yielding a pixel size of approximately 17 µm. The acquisition rate was 50 frames per second for the quasi-static rate and 6000 frames per second for the fall-like loading conditions. The image size was 512*256 pixels.

Crack follow-up was possible due to the light scattering induced by micro-defects, leading to an apparent whitening of the material (Katsamenis et al., 2013; Thurner et al., 2007) this whitening is called the process zone: the zone where non-linear mechanisms arise. A previous study (Katsamenis et al., 2013) found a strong linear relationship between the crack front and the whitening front: the distance between the two stays constant until catastrophic failure. The method consists of subtracting the current image from a reference image that is an image of the samples before the crack initiation. This operation enhances the difference between the current frame and the reference. The difference is mainly related to the said whitening due to initiation and propagation of a crack. Based on this method (Katsamenis et al., 2013), we then assume, that the variation of crack length is equal to the variation of the process zone that corresponds to the continuous whitening pattern that extends from the notch tip. In this study, we measured the projected length in the vertical direction (Figure 30), perpendicular to the direction of loading.

We decided to take four points of measurements between the yield load, P, and the maximum load (Figure 30) to determine the R-curves, based on the results showing a linear relationship between K_{Jc} and crack length for short length (smaller than 500 µm) in cortical bone (Katsamenis et al., 2013; Koester et al., 2008).

We can then use equations from ASTM E-1820 to calculate cortical bone fracture toughness for each i=1, 2, 3 and 4 corresponding to the four measured crack length $a_{(1)}$, $a_{(2)}$, $a_{(3)}$ and $a_{(4)}$. Each parameter correspond to the same as in 2.3 but for the actual crack length $a_{(i)}$, and for the load $P_{(i)}$ that correspond to the applied load at the considered load-displacement state (Figure 30).

We then have:

$$J_{(i)} = \frac{K_{Ic(i)}^2}{E'} + J_{pl(i)} \quad \text{(II.5)}$$

$$K_{Ic(i)} = \frac{P_{(i)}S}{BW^{\frac{3}{2}}} \cdot f\left(\frac{a_{(i)}}{W}\right) \quad \text{(II.6)}$$

$$J_{pl(i)} = \left[J_{pl(i-1)} + \frac{\eta}{(W-a_{(i-1)})}\left(\frac{A_{pl(i)}-A_{pl(i-1)}}{B}\right)\right] * \left[1-\frac{a_{(i)}-a_{(i-1)}}{(W-a_{(i-1)})}\right] \quad \text{(II.7)}$$

which gives

$$K_{Jc(i)} = \left(J_{(i)}E'\right)^2 \quad \text{(II.8)}$$

Once all the parameters are measured, we plot the evolution of K_{Jc} as a function of the crack length. Assuming a linear relationship between these two parameters, we can calculate the average slope $\Delta K_{Jc}/\ \Delta a$ (Katsamenis et al., 2013) as well as the coefficient of determination R^2 of the linear regression between toughness value and crack length. A sketch of the measurement protocol is shown in Figure 30.

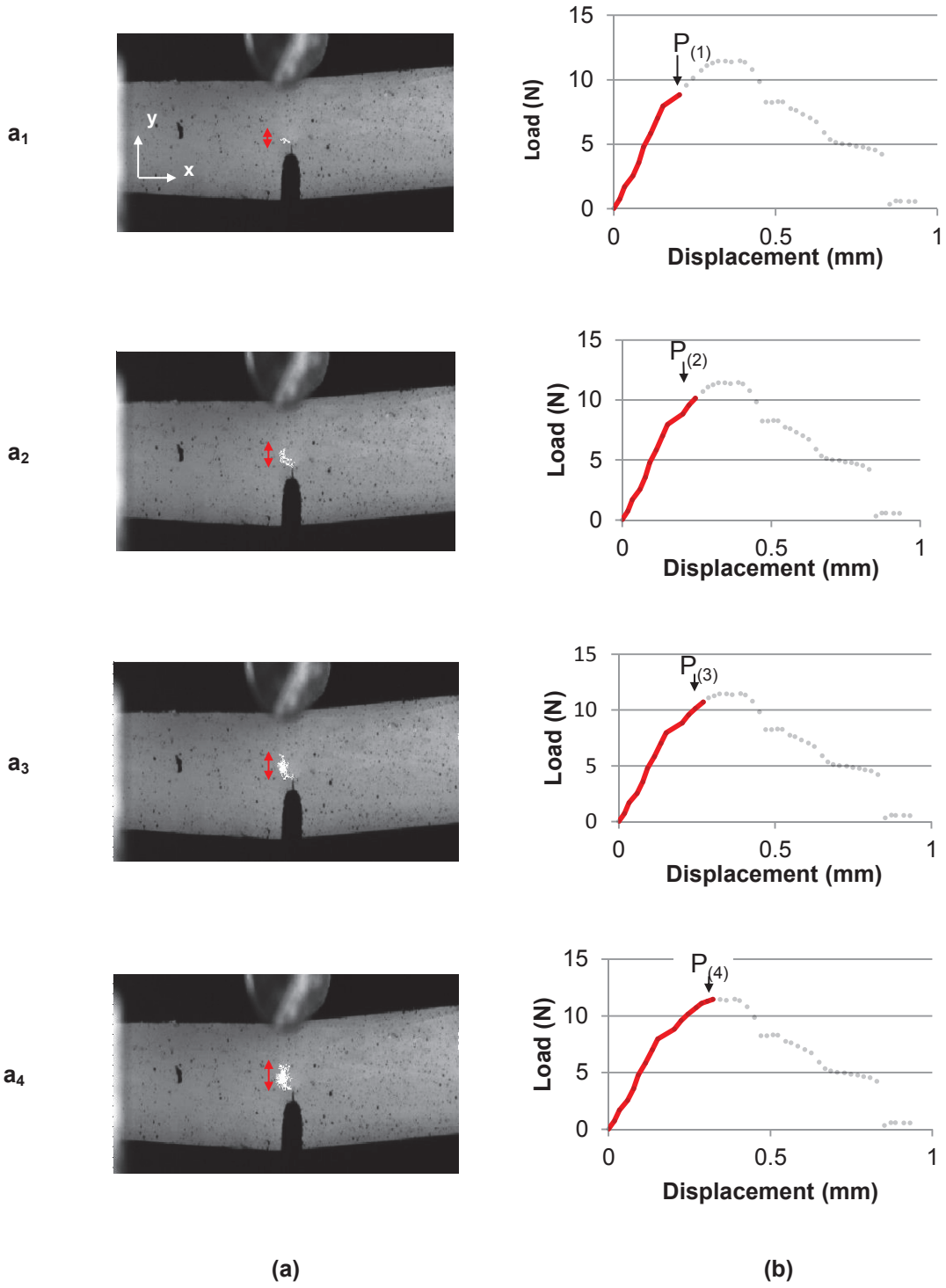

Figure 30 An example of the crack length measurement for the R-curve analysis. Each line represents measurements at different time points at. (a) shows the whitening front that correspond to the propagation of the crack, the red arrow shows the measured projected length; (b) shows the corresponding load-diasplcement curve (gray dots represent the whole curve, and red line corresponds to each particular crack length)

iii. Statistical tests

The normality of the distribution was assessed using Shapiro-Wilk's test. First a one-way analysis of variance (ANOVA) was performed in order to highlight potential differences between the series. Then t-tests for paired samples were used to evaluate these differences. If normality is not verified, then results were statistically tested using a non-parametric Wilcoxon test for paired samples, and a Kruskal-Wallis test for independent samples. These statistical tests were performed using R© software (The R foundation for Statistical Computing, Austria). P-values under 0.05 were considered as significant.

3. Results

Figure 31 shows an example of the obtained load-displacement curves. All the anatomical sites show a similar mechanical response under both quasi-static and fall-like loading conditions. First, human cortical bone exhibits elastic deformation until the yield load is attained. Then, a crack initiates from the notch followed by an inelastic deformation. This inelastic part of the curve is associated with a stable propagation of the crack that can be slowed down due to toughening mechanisms within the tissue (Zimmermann and Ritchie, 2015). The mechanical experiment ends with an unstable crack propagation that leads to complete fracture of the sample.

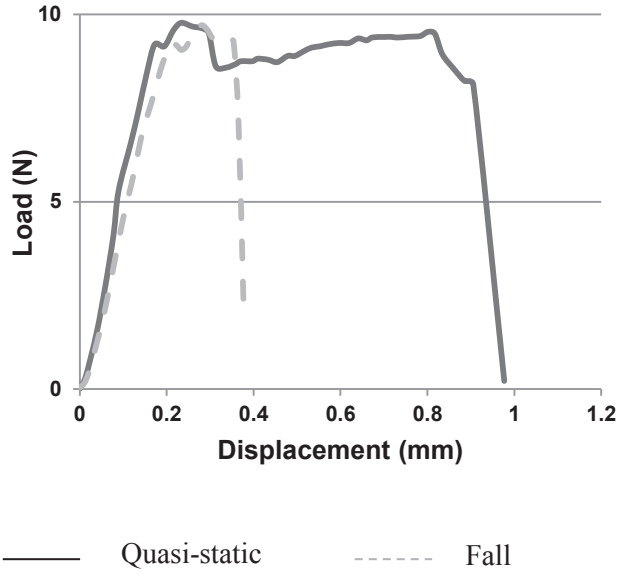

Figure 31 Load-displacement curves for tibia samples (male, 80 y.o.) under quasi-static and fall conditions.

Results for linear (K_{Ic}) and non-linear (K_{Jc}) fracture toughness for the four sites and two strain rates are shown in Figure 32. Table 3 summarizes the different values of toughness obtained.

i. Linear elastic fracture toughness

Results obtained from the femoral diaphysis under quasi-static loading conditions did not verify the hypothesis of the Shapiro-Wilk's normality test (p-value = 0.009). Non-parametric and parametric tests for paired samples were applied to this series. The p-value obtained for both of these tests were of the same order of magnitude. To standardize, the results obtained with the parametric tests are presented in the current study.

Under quasi-static loading rate, K_{Ic} values were found to be significantly higher in the radius and tibia compared to the femur. When comparing the radius and the femoral neck, a difference of ~21 % is found.

In the fall-like loading conditions, a significant increase of the linear elastic fracture toughness for both the diaphysis and the neck of the femur was found, as opposed to in the quasi-static case. No difference was found for the tibia and radius.

Further, in fall-like loading conditions, no significant difference in linear elastic fracture toughness was found between the different anatomical sites (Figure 32).

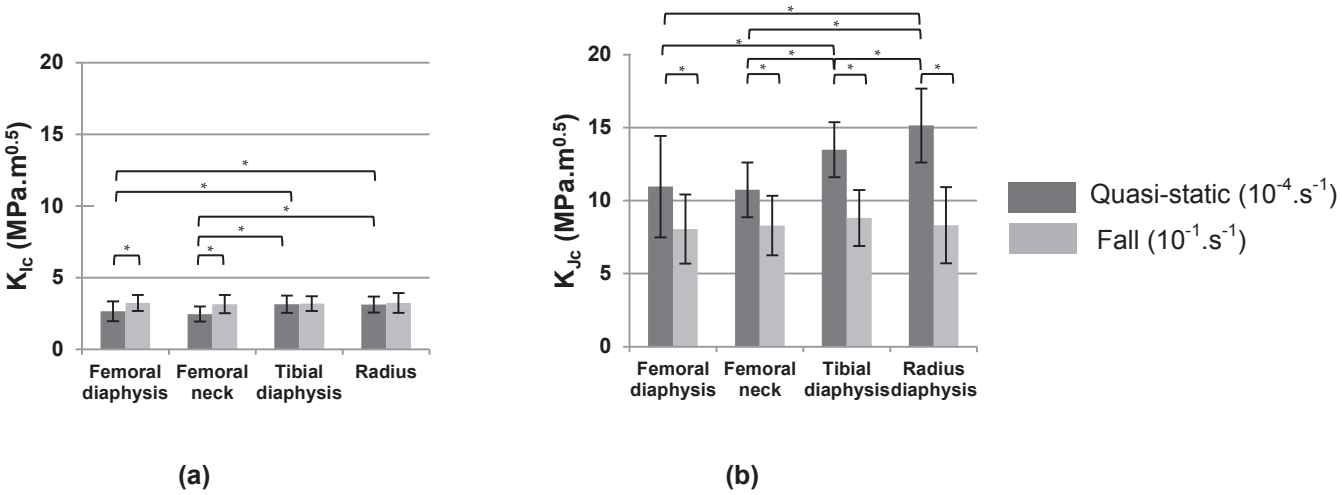

Figure 32 Histogram of toughness values for the four anatomical sites. (a) Linear elastic fracture toughness K_{Ic} values, and (b) Non-linear K_{Jc} values. * indicates that the difference is significant (p<0.05).

ii. Non-linear fracture toughness

Results obtained from the femoral diaphysis for both quasi-static and fall condition did not verify the hypothesis of the Shapiro-Wilk normality test (p-value = 0.05 and 0.0007 respectively for quasi-static and fall-like loading conditions). Non-parametric and parametric tests for paired samples were applied to this series. The p-value obtained for both of these tests were of the same order of magnitude. To standardize, the results obtained with the parametric tests are presented in the current study.

When considering both elastic and plastic contributions of cortical bone under quasi-static strain rate, a significant difference between the different studied anatomical sites was found. The femoral neck and femoral diaphysis present a non-linear toughness that is significantly lower than the tibia and radius. Further, the tibia showed significantly lower non-linear toughness than the radius. The non-linear toughness was 30 % higher in the radius than in the femoral neck and 11 % higher than in the tibia. Also, the strain rate significantly reduced the non-linear toughness in all sites (Figure 32**Erreur ! Source du renvoi introuvable.**). The majority of the toughness loss is due to a lower plastic contribution as, can be seen in Table 4. Finally, at the higher strain rate, there were no other differences in fracture properties between the four anatomical sites (Figure 32).

iii. R-curves

Measurements on the R-curves were performed only for the quasi-static case. Finally, measurements on 24 femoral diaphyses, 23 femoral necks, 22 tibial diaphyses and 24 radii diaphyses were realized. This is less than the available samples because of inadequate light for the video measurements during some of the tests. In the fall-like loading conditions, crack propagation was too fast despite the 6000 fps frame rate. Therefore, we could not report any intermediate crack length. Further, the whitening due to micro-crack initiation was too limited, precluding a proper measurement (Zimmermann and Ritchie, 2015).

All the results obtained from the r-curves analysis do not verify the normality condition (p-value<0.05). Moreover, there were not enough paired results to use a Wilcoxon test for paired samples. Hence, the non-parametric Kruskal-Wallis statistical test for independent samples was used to analyze the results.

Figure 33 shows the mean value of $\Delta K_{Jc}/\Delta a$ measured from the R-curves for the four anatomical sites. It also provides the values of the coefficient of determination of the regression between toughness value and crack length for each anatomical site.

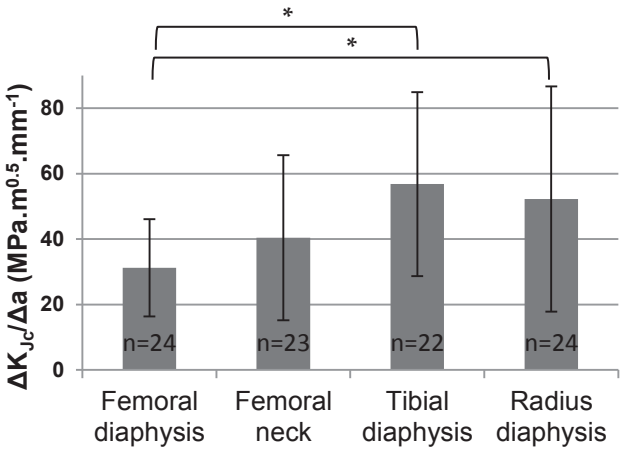

R²	0.91 ± 0.08	0.87 ± 0.13	0.85 ± 0.15	0.89 ± 0.07

Figure 33 Mean values of the slope of the toughness as a function of crack extension, derived from the R-curves in quasi-static loading conditions with the coefficient of determination associated to each site (mean value (SD)) (* independent Kruskal-Wallis test, $p<0.05$).

The R-curve analysis shows also that femoral diaphysis (31 $MPa.m^{0.5}.mm^{-1}$ ± 15) shows a significant lower value of $\Delta K_{Jc}/\Delta a$ than tibial diaphysis (57 $MPa.m^{0.5}.mm^{-1}$ ± 28) from 45% and from radius diaphysis (52 $MPa.m^{0.5}.mm^{-1}$ ± 34) from 40%. There is no significant difference between femoral neck and femoral, tibial and radius diaphyses (40 $MPa.m^{0.5}.mm^{-1}$ ± 25).

Table 3. Linear (K_{Ic}) and non-linear fracture toughness (K_{Jc}) toughness for the four different anatomical sites: mean (standard deviation); n is the number of subjects. P-values of t-tests for comparison between quasi-static and fall conditions are reported. In the case of p < 0.05, the relative difference between the two loadings is given. (2-column fitting table)

Toughness	Strain rate	Femoral diaphysis n=29	Femoral neck n=29	Tibial diaphysis n=22	Radius diaphysis n=31
K_{Ic} ($MPa.m^{0.5}$)	Quasi-static	2.75 ± 0.48	2.46 ± 0.52	3.15 ± 0.60	3.11 ± 0.56
	Fall	3.23 ± 0.56	3.15 ± 0.63	3.19 ± 0.51	3.23 ± 0.70
p-value		2.10^{-3}	$1.\ 10^{-4}$	NS*	NS*
Relative difference (%)		17	28	-	-
K_{Jc} ($MPa.m^{0.5}$)	Quasi-static	11.39 ± 2.78	10.75 ± 1.87	13.48 ± 1.88	15.15 ± 2.53
	Fall	8.06 ± 2.37	8.29 ± 2.05	8.82 ± 1.92	8.32 ± 2.61
p-value		$3.\ 10^{-8}$	$1.\ 10^{-4}$	2.10^{-9}	4.10^{-12}
Relative difference (%)		-29	-21	-33	-42

*NS: Non-Significant (p-value>0.05, t-test for paired samples)

Table 4. Elastic (J_{el}) and plastic (J_{pl}) energies values for the four different anatomical sites: mean (standard deviation); n is the number of subjects. P-values of t-tests for comparison between quasi-static and fall conditions. In the case of p < 0.05, the relative difference between the two solicitations is given. (2-column fitting table)

Toughness	Strain rate	Femoral diaphysis n=29	Femoral neck n=29	Tibial diaphysis n=22	Radius diaphysis n=31
J_{el} (kN.m^{-1})	Quasi-static	0.45 ± 0.14	0.34 ± 0.14	0.59 ± 0.21	0. 58 ± 0.20
	Fall	0.62 ± 0.20	0.60 ± 0.22	0.58 ± 0.21	0.60 ± 0.24
p-value		1.10^{-3}	1.10^{-4}	NS*	NS*
Relative difference (%)		28	43	-	-
J_{pl} (kN.m^{-1})	Quasi-static	7.44 ± 4.18	6.51 ± 2.36	10.10 ± 2.90	12.41 ± 5.13
	Fall	3.42 ± 2.52	3.69 ± 2.07	4.03 ± 1.99	3.78 ± 2.55
p-value		1.10^{-6}	2.10^{-4}	1.10^{-8}	2.10^{-10}
Relative difference (%)		-118	-77	-150	-228

*NS: Non-Significant (p-value>0.05, t-test for paired samples)

4. Discussion

Fracture injuries in the elderly mainly occur after a fall from a standing position, implying a mechanical loading at a specific strain rate in the order of $10^{-1}.s^{-1}$ (Bergland and Wyller, 2004; Gryfe et al., 1977; World Health Organization, 2007). The aim of this study was to assess the effect of this strain rate on human bone toughness on four paired anatomical sites. Therefore, two strain rates were applied: $10^{-4}.s^{-1}$ representing a quasi-static case, which represents the standard case in most studies in the literature; and $10^{-1}.s^{-1}$ which has been shown to be the physiological rate during a fall from a standing position at the radius (Foldhazy, 2005).

The strain rate effect was assessed on samples from 29 human femoral diaphyses, 29 femoral necks, 22 tibial diaphyses and 31 radius diaphyses. Data reported in the literature on radius and femoral neck are limited Only quasi-static toughness measurements have been reported on the human femoral neck (Brown et al., 2000). To our knowledge there is no published information on the human radius toughness.

Considering the linear elastic fracture toughness, K_{Ic}, the values obtained for the femoral diaphysis in quasi-static loading conditions (2.75±0.48 MPa.m$^{0.5}$)), are in the range of the values found in the literature (from 1.77±0.19 MPa.m$^{0.5}$) (Barth et al., 2010) up to 3.47±0.40 MPa.m$^{0.5}$) (Akkus et al., 2000); (Yeni et al., 1997)). Linear elastic fracture toughness dependence on strain rate was reported in a recent study, where an increase of 30 % (Sanborn et al., 2016) was shown compared to 15 % in the current study. In their study, Sanborn *et al.* performed fracture experiments with a four point bending method on cortical bone samples extracted from the femoral shaft of 3 male subjects aged 36, 43 and 50 y.o. The current study includes a larger number of samples (n=29 for the femoral diaphysis) from older subjects. If we restrict our results to only the "young" subjects (from 50 to 68 y.o., n=6), we find a mean relative difference of 30%, that compares well to those found in the past (Sanborn et al., 2016). Their linear elastic toughness values were higher than in the current study (4.5 MPa.m$^{0.5}$ (Sanborn et al., 2016), as compared to 2.52 MPa.m$^{0.5}$ corresponding to the mean linear elastic toughness value for the 6 youngest subjects in a quasi-static condition in the current study). Experimental conditions could be the origin of the different linear elastic toughness found here. Four-point bending tests might provide different results compared to three-point bending, since the maximum flexural moment is spread over a larger area. In four-point bending, the mode I fracture condition, that is crack propagation perpendicularly to the applied load, is better respected, but might also encourage crack deflection. As the maximum load is spread on a larger area, and as cortical bone has a preferential direction that is parallel to the long bone axis, crack might first follow a path parallel to this preferential direction, before propagating perpendicularly to the applied load. The consequence would be a higher measured toughness. An argument for the use of three-point bending in this study is that it is better suited to the small size of the samples. It also reduces the risk of misalignment of the upper span compared to four point bending.

The non-linear fracture behavior of human cortical bone has been sparingly reported in the literature (Barth et al., 2010; Zimmermann et al., 2014). Cortical bone is constituted in a way that allows it to undergo several energy dissipating mechanisms before breaking (Yan et al., 2007). Large plastic deformation was seen under quasi-static load (**Figure 31**). In order to investigate the relative contribution of elastic and plastic deformation in resisting crack propagation in human cortical bone, we investigated the non-linear J-integral related toughness, K_{Jc}. For human cortical bone, values at the femoral diaphysis (11.9±2.8 MPa.m$^{0.5}$) are comparable to previously reported values (12.5 MPa.m$^{0.5}$ (Zimmermann et al., 2014) and 13.3 MPa.m$^{0.5}$ (Barth et al., 2010)). At the femoral shaft, we found a reduction of 29 % of the non-linear toughness at fall conditions compared to quasi-static loading, whereas Zimmermann *et al.* reported a reduction of 40%. This is not directly comparable, however, as the differences are probably due to the use of different strain rates for fall conditions. In Zimmermann *et al.*, 2014, a strain rate of 1.s^{-1} was used, whereas we applied a strain

rate of $10^{-1}.s^{-1}$. It should also be noted that in Zimmermann *et al.* , tests were performed on samples from a single subject. In the present study, reduction in K_{Jc} with rate ranged between 9 % and 60 %. Thus, the values obtained from a single donor reported by Zimmermann *et al.* falls within this range.

In order to investigate toughness evolution under strain, R-curves were plotted. We used a similar method that can be found in the literature (Katsamenis et al., 2013), assuming a linear increase of critical toughness K_{Jc} with crack length. The slopes of the increase of toughness during crack propagation (**Figure 33**) are close to those presented in literature (11.05 $MPa.m^{0.5}.mm^{-1}$ in the femoral diaphysis (n=3) (Katsamenis et al., 2013); 35.6 $MPa.m^{0.5}.mm^{-1}$ in the tibia (n=5) in (Koester et al., 2011)). Some differences compared to the results obtained in the current study (31 $MPa.m^{0.5}.mm^{-1}$ ± 15) can be noted. They might be due to the low number of subjects used in previous studies. An interpretation of our results is that in tibial and radius diaphyses, the toughening mechanisms of bone are more pronounced than in the femur during crack propagation.

Based on the results presented here, we can state that femoral diaphysis, femoral neck, tibial diaphysis and radius diaphysis do not have the same fracture properties under quasi-static loading conditions. The radius appears more resistant to crack propagation than the other sites. This is a finding that has not been reported previously. For all the four sites, toughness decreases under fall-like loading conditions, compared to quasi-static loading, with a major decrease in plastic deformation. It should be noted that all the four anatomical sites have the same fracture toughness in the fall-like loading conditions. Since plastic contribution is the main component that is different in the case of a fall, and plastic deformation during crack propagation is associated to toughening mechanisms (Zimmermann et al., 2014), it seems that a high strain rate, compatible with conditions in a fall, negatively influences the energy dissipating mechanisms in bone.

As mentioned, human cortical bone incorporates several energy dissipating mechanisms, effectively decreasing the driving force of the crack propagation. Such mechanisms occur at every length scale of cortical bone, from interfibrillar sliding at the nanometer scale to crack deflection at the interface between osteonal and interstitial tissue at the hundreds of micrometer length scale. These toughening mechanisms have largely been studied under quasi-static loading conditions (Akkus et al., 2000; Bala et al., 2011; Brown et al., 2000; Follet et al., 2011; Koester et al., 2008; Viguet-Carrin et al., 2006; Yeni and Fyhrie, 2002; Zimmermann et al., 2014; Zimmermann and Ritchie, 2015). From the data obtained in the current study, one can assume that a potential difference in structural organization could explain the difference in fracture properties in the four different anatomical sites observed here. The multi-scale porous network (Volkmann-Haversian

system on the micron scale, and osteocyte-canaliculi lacunar network on the nano scale) should also be considered, as it potentially influences the human cortical bone fracture properties (Perilli et al., 2015). A future study can investigate the microstructure in the sites studied here and relate it to the corresponding toughness properties to elucidate which structural parameters significantly influence toughness at different strain rates.

There are some limitations to this study. First, the storage of extracted at -20°C could affect bone fracture properties. The effect of freezing has been studied in the past, but results found in the literature are not conclusive. Some studies showed that freezing cortical bones samples significantly affects some of their mechanical properties, whereas others reported that mechanical behavior remains unchanged (Borchers et al., 1995; Itoman and Nakamura, 1991; Moreno and Forriol, 2002; Nazarian et al., 2009; Panjabi et al., 1985; Pelker et al., 1984; Sedlin and Hirsch, 1966; Van Haaren et al., 2008). Considering that all the 220 samples tested in this study have followed the same storage and preparation protocol, we can assume there is no inter-group bias. Hence a comparative study is pertinent, even if the storage conditions may affect the material properties. Second, sample-specific Young's modulus was not taken into account in analysis of the results. There might be variability in the elastic properties between subjects, but also between the different anatomical sites. However, most studies of cortical bone toughness found in the literature used a single Young's modulus value for all the samples. Further, in the current study, strain rate influence was studied comparing two samples from the same donor that excludes potential inter-individual elastic properties variation. Moreover, linear fracture toughness, K_{Ic}, and the plastic contribution of the energy needed to propagate a crack, J_{pl}, that provide interesting information on the observed differences are not dependent on Young's modulus (see section 2.3). Finally, the small size of our samples might also be a consideration, mainly with respect to the 1 mm remaining ligament between the end of the notch and the edge of the sample. In most previous work on cortical bone toughness, larger sized samples were used, mainly due to samples being extracted from the femoral diaphysis, where the available cortical thickness is much higher than in other sites. We chose to perform biomechanical tests on small samples in order to have the same sample dimensions in the four anatomical sites. The cortical thickness in the radius and the femoral neck did not permit the extraction of larger samples, and thus effectively set the upper limit for a standardized sample size. It should be noted, however, that the toughness values found here for the femoral diaphysis are in good agreement with those found in the literature. Finally, the studied population can be considered as old (79 ± 11 y.o.). It is well known that bone mechanical properties, and more specifically its toughness, change with age (Zimmermann et al., 2012). Considering the significant evolution of the structural organization with age (Perilli et al., 2015), crack propagation mechanisms could be different in old and young subjects. This point is important to consider when interpreting our

results; studies on samples with a wider age distribution may lead to different results. Nonetheless, the samples used in this study are representative of those that suffer the most from fractures (Nanes and Kallen, 2014), and as such provides insight into the factors that contribute the most to cortical bone strength in this age group. More generally, the goal of our work is to understand human cortical bone fracture mechanisms. Others aspect of bone quality (e.g., structural and architectural parameters such as collagen quality and orientation, and tissue mineral density) could be further studied as it is well known that they influence bone mechanical properties (Bala et al., 2012, 2011). A comparison between fracture mechanisms at different locations could also be of great interest. The estimation of micro-cracks density and geometry (eg. using X-ray micro-computed tomography (Larrue et al., 2011)) would thus be made. These types of measurements would allow refining the study of differences in fracture behavior at different locations with respect to its microstructure even further.

5. Conclusions

In this study, we investigated the effect of a fall-like strain rate on the toughness of human cortical bone from several anatomical sites. The most important findings are that under a quasi-static strain rate, femoral diaphysis, femoral neck, tibial diaphysis and radius diaphysis do not have the same fracture properties. Cortical bone from the radius exhibits a higher crack propagation resistance than other tested sites. Resistance to fracture in all four sites is decreased at a fall-like loading rate, mainly due to a major loss of the plastic component of the fracture resistance. Under the chosen fall-like strain rate, there is no significant difference in fracture properties between all the four anatomical sites. These results suggest that models for fracture risk prediction at strain rates that are representative of falls can use femoral diaphysis fracture properties, even when modelling fracture risk in the radius or the femoral neck. To our knowledge, this is the first study providing data on human radius toughness for both quasi-static and fall strain rates. Moreover, this study provides data on the variation between four anatomical sites, with both weight bearing (femur, tibia) and non-weight bearing (radius) bones, on a relatively large population of 31 subjects. Future work includes measurement and analysis of the microarchitecture of the studied anatomical sites in order to investigate its correlations to the different behaviors reported here under quasi-static and fall-like strain rates.

Chapter III Synchrotron radiation micro-CT imaging of paired human femoral diaphysis, femoral neck and radial diaphysis

Abstract: It is known that human cortical bone toughness depends on the anatomical locations when studied under quasi-static loading condition. Recent results also show that under fall-like loading condition, cortical bone toughness is similar for different paired anatomical locations. If cortical bone toughening mechanisms are known to be dependent on the tissue architecture under quasi-static condition, there is a lack of knowledge concerning fracture mechanisms during a fall. In the current study, we analyzed structural parameters of 8 paired femoral diaphyses, femoral necks and radial diaphyses mechanically tested under quasi-static and fall-like loading conditions. Using synchrotron radiation micro-CT imaging, we were able to quantify the multiscale pore network of the cortical tissue, including Haversian, lacunar network and micro-damages. Results showed that the three locations have significant different morphometric parameters. The amount of micro-cracks formed during loading is significantly higher within the specimens loaded under quasi-static condition. These results confirm that microstructure have an influence on human cortical bone toughness. We also showed that the fracture mechanisms depend on the loading condition.

1. Introduction

Bone fragility is a complex problem involving its architectural and material properties of bone at different scales (Seeman and Delmas, 2006).

Bone porosity has been shown to be a major determinant on biomechanical properties (Bala et al., 2016, 2015; Dong et al., 2014; Hesse et al., 2015; Jones et al., 2004; Langer and Peyrin, 2015; Parnell and Grimal, 2009) and related to its mechanical behavior.

The main porosity in cortical bone is related to the so-called Haversian and Volkmann canals forming a network containing blood vessels and nerve. These canals, approximately 50 μm in diameter and a few millimeters in length, are known to act as mechanical units for cortical bone elastic properties (Bala et al., 2016, 2015; Jowsey, 1966). Their specific orientation in bone, parallel to the long axis of the diaphysis for the Haversian canals, and perpendicular to this axis for the Volkmann's canals, are one on the main contributor to the anisotropic mechanical properties of bone. The blood vessels passing within these canals, thus in proximity to the bone tissue and the LCN, implies that they play a major role in the remodeling process. The resorption and formation of bone tissue is initiated on these porosities (Zebaze et al., 2010). This involves an osteonal arrangement surrounding these canals. The newly formed osteons are less mineralized that the interstitial bone tissue (Kazanci et al., 2007; Phelps et al., 2000).

Throughout the lifetime of tissue, different types of damages also occur. The main types are linear micro-cracks (D Vashishth, 2007). They form porosity that can be observed within the tissue at a higher length scale (Larrue et al., 2011; O'Brien et al., 2000). The planar cracks defects that can span hundreds of μm length and a gap on the order of 1 μm, are a result of fatigue of the bone material due to external loading: they form due to stored mechanical energy and serve to dissipate (Larrue et al., 2011; Nalla et al., 2004b).

At the micrometer scale, the cellular arrangement of osteocytes cortical bone may be of great importance as it is assumed that these cells play a major role for bone capacity to adapt to a particular mechanical environment (Bonewald, 2011). Osteocytes differentiate from osteoblast cells that become trapped in the mineralized matrix during bone formation. The space they occupy is called osteocyte lacunae. They remain as porosity after cells apoptosis. These small ellipsoidal porosities (Marotti, 1979) are connected together by canals formed by the processes of the osteocytes, called canaliculi, thus forming a complex and densely interconnected network called lacuno-canalicular network (LCN). The LCN has recently been

investigated by synchrotron radiation CT at micrometric and sub-micrometric scales (Dong et al., 2014; Hesse et al., 2015; Langer et al., 2012; Langer and Peyrin, 2015; Pacureanu et al., 2012; Schneider et al., 2011).

If the investigation of the influence of Haversian or micro-cracks density and morphology and cortical bone fracture behavior has already been performed in the past (Diab and Vashishth, 2005; Granke et al., 2011; Nalla et al., 2004b; Yeni and Norman, 2000b; Zioupos et al., 2008), there are only a few studies dealing with the role of osteocytes lacunae on tissue mechanical behavior (Milovanovic et al., 2015), and particularly its toughness (Granke et al., 2016). In the later study, Granke et al. found a significant positive correlation between the density of lacunae and cortical bone fracture toughness properties measured on femoral diaphysis in 2D, but no information are provided concerning lacunae morphology.

The observation of micro-cracks and osteocytes is usually performed using imaging, such as Scanning Electron Microscopy (SEM) (Granke et al., 2016; Milovanovic et al., 2015), visible light microscopy (Wang et al., 2005), confocal microscopy (Lai et al., 2015; Verbruggen et al., 2012). However, most of these different techniques only provide 2D images micro-cracks and LCN. Schneider and al. used a SEM coupled with focused ion beam milling to investigate a three dimensional region containing lacunae (Schneider et al., 2011). Although this technique can provide high-resolution 3D analysis of osteocyte lacunae, the size of the region of interest (ROI) remains limited to one or two lacunae due to the extensive scanning time. Micro Computed tomography (μCT) was also used to investigate morphometric properties of osteocytes lacunae on a larger region (van Hove et al., 2009; Vatsa et al., 2008). Synchrotron radiation (SR) CT was previously used to image and analyze osteocyte lacunae in human femoral cortical bone (Dong et al., 2014; Hannah et al., 2010). The advantage of this technique compared to standard CT is that it can offer a higher signal to noise ratio even at higher spatial resolution (Salomé et al., 1999), thus facilitating the segmentation of lacunae and its quantitative analysis. Synchrotron radiation also provides a high flux allowing a significant decrease of scanning time.

To our knowledge, there is no data on lacunae morphology investigated with SR-μCT on other anatomical sites than human femoral diaphysis. When dealing with human cortical bone fracture properties, other sites where *in vivo* fracture may occur, such as the radius or the femoral neck should be considered (Court-Brown and Caesar, 2006). We showed that these bones have different fracture behavior (Gauthier et al., 2017). These differences may arise from several factors, one of them being their internal architecture. This microstructural

arrangement depends on the bone's function within the organism and more specifically its mechanical environment (Wolff, 1892). In that way, the radius, that does not support the body's weight in a standing position, may present a different morphology than the femur.

The aim of this study is thus to investigate the multi-scale three-dimensional porosity network on paired human femoral diaphysis femoral neck and radial diaphysis subjected to a mechanical loading.

2. Materials and methods

i. Sample preparation

Paired femoral diaphyses, femoral neck and radial diaphyses were collected from 8 women cadaver subjects (70 ± 14 y.o., min: 50 y.o., max: 91 y.o.). These 8 women donors represent a sub-population of the complete population considered in Chapter II. As μCT imaging is time consuming, we had to reduce the number of samples. We decided to consider only women because it is known they are more exposed to bone diseases. No additional information regarding disease status or medication history was available. Extracted bones were wrapped in gauze soaked with saline to keep them hydrated, then stored at -20 °C until sample preparation. Two rectangular samples, with a width of W = 2.1 ± 0.1 mm and a thickness B = 1.0 ± 0.1 mm, were extracted from each bone using a low speed saw with a diamond coated blade (ISOMET 4000, Buehler, USA). The samples were prepared so that their long axes were parallel to the osteons. A notch was cut in the middle of each sample, perpendicularly to the long surface, on the wide side. The samples were subjected to three-point bending mechanical test until fracture. One of the samples from each donor and site was loaded in quasi-static (10^{-4} s^{-1}), while a contiguous sample was laoded with a strain rate representative of a (10^{-1} s^{-1}, (Foldhazy, 2005)). The aim was to evaluate the effect of strain rate on fracture behavior (Gauthier et al., 2017). One of the resulting sample pieces (the samples were broken in two parts) from the mechanical test was imaged for analysis, resulting in an imaged population of 24 samples. Before image acquisition, they were stored at -20 °C, then a delipidation protocol was applied one week before imaging. Before image acquisition, the samples were immerged in acetone for 30 minutes, then rinsed with water, and finally dehydrated by successive immersion in 70 % and nearly 100 % ethanol baths for maximum 2 days. On each sample, two volume of interest (VOI) were chosen. The first one (VOI1, Figure 34) was chosen to lie outside of the support rollers used for the mechanical test. There was thus no particular mechanical stress applied there. This VOI was used as control group.

The second VOI (VOI2, Figure 34) was chosen to include the fracture surface and the surrounding damaged region, where the main crack has propagated during the mechanical test, therefore having been subjected to a high stress concentration state. The imaging experiment thus comprised 96 acquisitions.

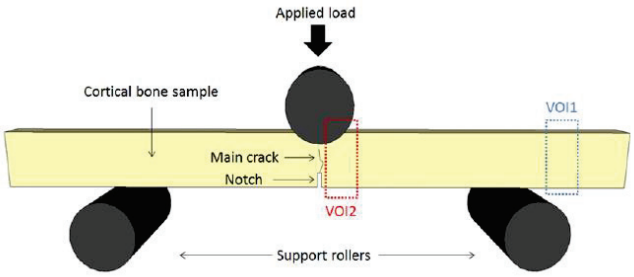

Figure 34 Schematic of the mechanical apparatus, and illustration of the two VOI

Table 5 Summary of imaged VOIs

	Femoral diaphysis	Femoral neck	Radial diaphysis
Quasi-static			
Control VOI	8	8	8
Cracked VOI	8	8	8
Fall			
Control VOI	8	8	8
Cracked VOI	8	8	8

ii. Synchrotron radiation micro-computed tomography (SR-µCT)

SR-µCT was performed on beamline ID19 at the ESRF (European Synchrotron Radiation Facility), Grenoble, France. For each sample, 2000 projections images were recorded over a total rotation of 360 ° in a" pink beam" undulator radiation with an effective energy of 31 keV. The detector was composed of a scintillator screen and a CCD camera and visible light microscope to yield a pixel size of 0.7µm. Phase contrast was obtained by placing the detector at 40 mm from the sample. Tomographic reconstruction was performed using a filtered back-projection algorithm yielding 3D images with 2048^3 voxels. Both phase and absorption CT images were obtained. Phase retrieval was performed using Paganin's method (Paganin et al., 2002), with delta/beta set to 572. As there were 96 volumes scanned, that bot

absorption and phase contrast images were reconstructed, and that and individual sample represents a volume of 32 Go, the final dataset represents a total of 6144 Go.

To reduce processing time, the initial VOIs were cropped so that the final volume size was B x 500 µm x 500 µm (B is the thickness of the sample, and is variable between the samples, min: 800 µm, max: 1200 µm). For the VOIs containing the fracture surface, the cropped volumes start at the initial notch tip and follow the main crack over 500 µm where the main crack propagation mechanisms occurs (Koester et al., 2008)

We could observe a variation of the average gray level with the slice number in VOIs 2 as is illustrated on the 3D display of a cracked volume on Figure 35 (a). This was related to the irregular shape of the sample, larger at the bottom, and thus did not always fit in the field of view of the detector. Thus part of the projection data was truncated which is commonly known as "local tomography", causing a loss of the absolute reconstructed value of the attenuation coefficient. Since, at least approximatively, this mainly results in a shift of the gray levels; the image was corrected by applying an offset slice by slice on each volume. The offset for each slice was estimated by fitting the gray level histogram of the slice with two Gaussian functions. The first Gaussian corresponds to the air and the second one to the bone. The mean of the first Gaussian was used to correct the offset. All volumes were then corrected considering the offset values for each slice (Figure 35). On this figure we can see the entire VOI before and after offset correction (a and b), and the cropped VOI used for the analysis (c).

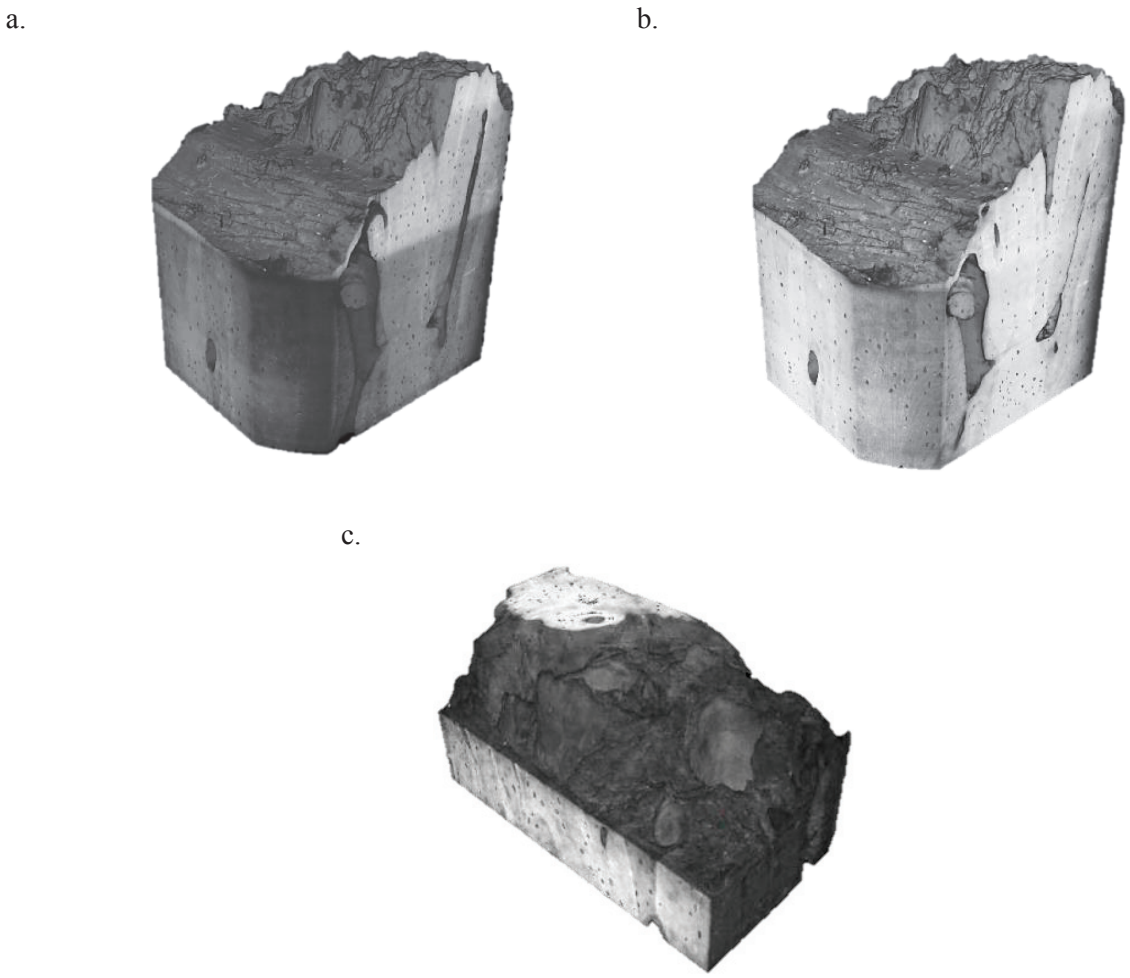

Figure 35 3D Volume rendering of human femoral diaphysis sample tested under fall-like loading conditions: a. and b. are the reconstructed volumes before and after offset correction, respectively; c. is the rendering of the cropped VOI

- ***Absorption coefficient***

The absorption coefficient (μ) of bone tissue was measured on the complete control VOIs. A quantitative bone mineral density value could not be calculated because of the local aspect of the acquisition (meaning some part of the samples were not in the field of view of the detector). As the complete control VOIs were subjected to the same acquisition conditions, we assumed that we can use the μ coefficient as a qualitative result for further comparison between the different groups.

- ***Bone and canals masks***

The first step consisted in the creation of a bone and canals masks by applying a median filter. A binarisation was then performed using the Otsu's method.

- ***Haversian canal analysis***

The analysis of the Haversian canals was done on the whole control VOIs in order to make the analysis on a bigger volume, as they are bigger porosities. Cracked VOI bone masks were difficult to have because of the complex shape of the bone cortex. The segmentation of this network was realized by binarisation and by fitting a convex hull on the sample cortex (Figure 36). Analysis of the Haversian canals was done with an automated method using commercial software (CTAnalyser Software V 1.14.4, Skyscan NV, Kontich, Belgium).

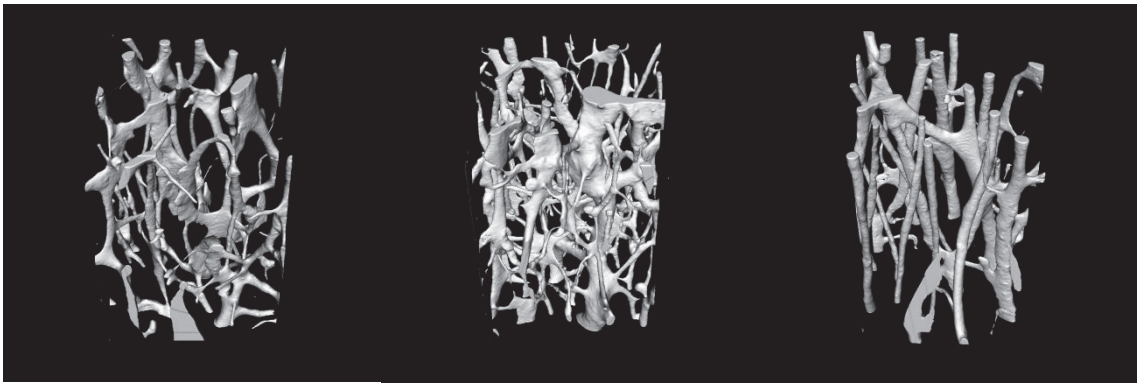

a. b. c.

Figure 36 Volume rendering of Haversian network segmented on the control complete VOIs on a. femoral diaphysis, b. femoral neck and c. radial diaphysis of a same subject

On these segmented VOIs, the canal volume fraction Ca.V/BV (%) was evaluated. The mean diameter of the canals, Ca.Dm (μm), and the standard deviation were also measured.

- ***Segmentation of lacunae***

Lacunae were segmented using a hysteresis threshold. First, the mask of the canals was applied to the VOI to only get the bone cortex and the small objects, such as the lacunae or the micro-cracks, within. Then the hysteresis threshold, with a low and a high value as input

parameters, was applied on the different VOIs. The low value of the threshold was used to select voxels that belong to the osteocytes lacunae or micro-cracks. The higher threshold was used to refine the segmentation by selecting the voxels with higher intensity values but only if they were connected to the previously detected voxels. Finally, a binarized volume was obtained containing osteocytes and micro-cracks (Figure 37). Bone volume (BV) was calculated multiplying the inverse of the final binarized VOI with the canals mask.

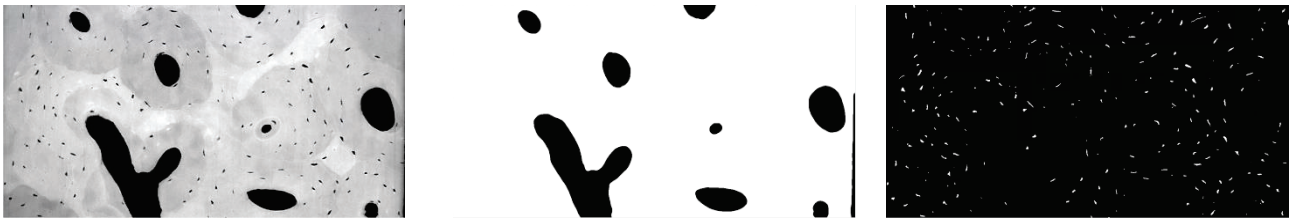

a. b. c.

Figure 37 VOI slice from a femoral diaphysis bone sample; a. is the phase contrast initial image, b. is the canals mask and c. is the final binarized image containing osteocytes and micro-cracks

- ***Morphometric parameters on lacunae and micro-cracks***

The aim was to calculate morphometric descriptors of each object in the binarized VOI. The methods used in the current study are those developed in (Dong et al., 2014). The first step was to perform a connected component analysis to label each object (as either lacuna or micro-crack). Then, a number of parameters are caObjulated on each labeled object:

- Volume of object (Obj.V): this parameter was defined as the sum of all the voxels within the cell multiplying by the volume of one voxel (0.7*0.7*0.7 μm^3)
- The Length (Obj.L1), width (Obj.L2) and depth (Obj.L3) of the object: an osteocyte can be described as an ellipsoid (Marotti, 1979); L1, L2 and L3 are the three axis of the best fitting ellipsoid, with L1 being the main axis.
- The thickness of object (Obj.Th): the actual thickness of the cell was assessed using an automated algorithm assigning the value of the diameter of the maximal fitting sphere within the cell (Martín-Badosa et al., 2003).
- The surface area of object (Obj.S), structure model index (OBJ.SMI), and Euler number (Obj.χ): These different parameters are calculated using the geometric invariant intrinsic volumes Obj.V_0, Obj.V_1 and Obj.V_2 by applying the following equations (Schladitz et al., 2006):

$$Lc.S = 2Lc.V_2, \quad Lc.\chi = Lc.V_0, \qquad \text{III.1}$$

$$Lc.SMI = \frac{12\pi Lc.VLc.V_1}{Lc.S^2}$$

The Euler number is a descriptor of the topological property of the object. It is to the number of connected component minus the number of tunnels plus the number of cavities (A.Rosenfeld and A.Kak, 1982; Di Zenzo et al., 1996). The SMI's value ranges between 0 and 4 and defines the global shape of the object: SMI = 0 for a pure plate, SMI = 3 for a rod and SMI = 4 for a sphere (Hildebrand and Rüegsegger, 1997).

- ***Osteocytes and micro-cracks separation***

So far, the segmented structures analyzed as described above can be either lacunae or micro-cracks. Since we want to evaluate if micro-cracks that occur during fracture is dependent of the morphology of the surrounding tissue, it is necessary to distinguish whether a segmented object is an osteocytes lacunae (Lc) or a micro-cracks (μCr). Since these structures have quite different shapes, it was possible to define criteria based on the different descriptors enounced above to identify them. First, objects with a volume smaller than 82 μm^3 were considered as noise incorrectly classified as porosity and therefore subsequently removed. Cells with a volume larger than 10000 μm^3 were also excluded from the lacuna class, considered as either an incorrectly segmented object or crack. Criteria were also applied on some geometrical ratios: cells with a Obj.L1/Obj.Th ratio higher than 15 and a Obj.L2/Obj.Th ratio higher than 8 were excluded, considered as micro-cracks. Obj.SMI and Obj.χ were also exploited as exclusion criteria: lacunae were considered as having a SMI higher than 1.6 and an Euler number ranged between 0 and 2. Here is a summary for the rules applied to select only the lacunae in each VOI:

- Obj.V > 82 μm^3
- Obj.V < 10000 μm^3
- Obj.L1/Obj.L3< 15 and Obj.L2/Obj.L3 < 8
- Obj.SMI > 1.6
- 0 < Obj.χ < 2

To extract micro-cracks, we selected cells with a volume higher than 500 μm^3, to exclude small objects due to noise. To exclude lacunae, we used the opposite criteria as previously on Obj.L1/Obj.Th and Obj.L2/Obj.Th ratios, since micro-cracks have relatively small

thicknesses compared to other objects. Objects with Obj.L1/Obj.L3 ratios lower than 5 and features with ObjL2/Obj.L3 lower than 3 were considered as ring artefact, since these incorrectly segmented objects had a relatively short smallest ellipsoid axis L3 compared to cracks. Finally we defined that objects with a SMI lower than 2.5 to exclude other type of artefacts. The different rules applied to conserve micro-cracks are thus:

- Obj.V > 500 μm^3
- Obj.L1/Obj.Th > 15 and Obj.L2/Obj.Th> 8
- Obj.L1/Obj.L3 > 5 and Obj.L2/Obj.L3 > 2
- Obj.SMI < 2.5.

By qualitatively assessing VOI 1, another type of cracks, different from the micro-cracks enounced above, but also due to external loading was observed. These cracks, which we will call secondary cracks (2ndCr) appear to be much bigger than previously segmented micro-cracks. They present a high value of L1, L2 and also L3, meaning a complex shape in the three dimensions of the VOI (Figure 38). In order to select only secondary cracks, we used the same criteria as previously concerning Obj.SMI, in order to exclude a certain type of artefacts. The other criteria concern the ratios between the ellipsoid's three dimensions and the thickness of the segmented object. The criteria are Obj.L1/Obj.Th > 35; Obj.L2/Obj.Th > 35 and Obj.L3/Obj.Th > 20. This last criterion is important because it relates the difference between the best fitting ellipsoid and the actual objects thickness which is small for cracks since they are roughly locally planar. These objects were not selected with the micro-cracks criteria because of their low Obj.L1/Obj.L3 and Obj.L2/Obj.L3 ratios.

- Obj.V > 500 µm^3
- Obj.L1/Obj.Th > 35, Obj.L2/Obj.Th> 35 and Obj.L3/Obj.Th > 20
- Obj.SMI < 2.5.

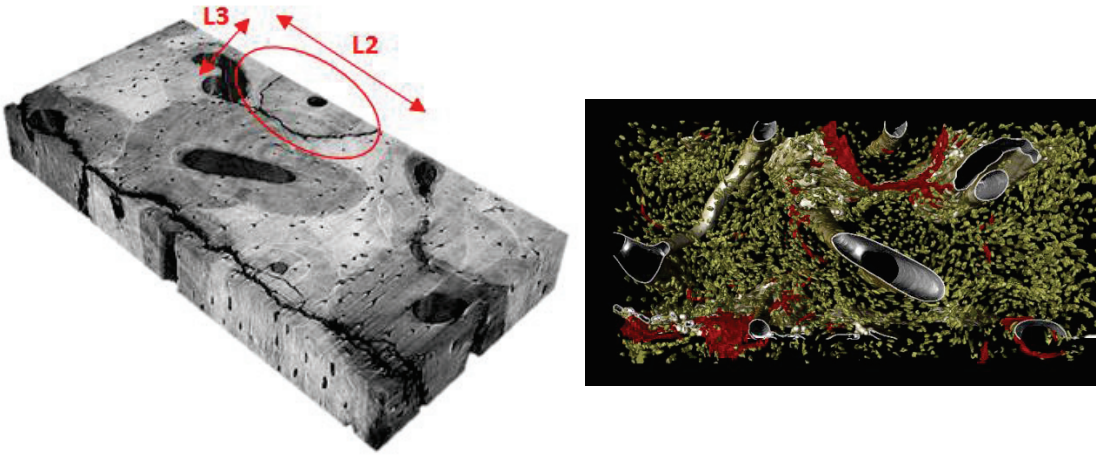

a. b.

Figure 38 Volume rendering of radial diaphysis cortical bone samples loaded under quasi-static conditions. a. note the secondary crack surrounding the osteon. The best fitting ellipsoid for this crack has high dimensions in the three directions; b. osteocytes lacunae are in yellow and cracks in red.

- ***Lacunae and cracks analysis***

The different geometric parameters listed above were analyzed for the three different features (i.e. lacunae, micro-cracks and secondary cracks). The dimensions of the lacunae were taken as the thress axes of an ellipsoid, Lc.L1 (µm), Lc.L2 (µm) and Lc.L3 (µm) in the three dimensions. The mean individual volume and surface, Lc.V (µm^3) and Lc.S (µm^2) were evaluated. In order to characterize the curvature at the top of the elliptic lacunae, we introduced Lc.ρ_1 (µm) and Lc.ρ_2 (µm) as following:

$$Lc.\rho_1 = \frac{Lc.L2^2}{Lc.L1} \; and \; Lc.\rho_2 = \frac{Lc.L3^2}{Lc.L1} \qquad 2.$$

A high Lc.ρ_i is indicative of a less elliptical lacuna (either sphere or disc-shaped depending on Lc.ρ_2).

The corresponding geometrical parameters were also calculated for the micro-cracks, µCr.L1 (µm), µCr.L2 (µm), µCr.Th (µm), µCr.V (μm^3) and µCr.S (μm^2) as well as their standard deviation (SD). For the secondary cracks, the three axes of the best fitting ellipsoid, 2dCr.L1 (µm), 2ndCr.L2 (µm) and 2ndCr.L3 (µm), were also analyzed to qualitatively report their extension in the three dimensions.

The lacunar, micro-crack, secondary crack and total crack volume fraction, Lc.V/BV (%), µCr.V/BV (%), 2dCr.V/BV (%) and TotCr.V/BV (%), which is the sum of the two previous, were calculated. The tissue volume (TV) for the cracked VOIs was difficult to measure because of the complex shape of the bone cortex. Finally, the lacunar density, Lc.N/BV (mm^{-3}), was measured.

iii. Statistical analysis

Since we analyzed different anatomical locations on a same subject, and also different loading conditions on a same region, Wilcoxon tests for paired samples were performed using StatView (Abaqus, USA) to analyze differences between the different groups. The Spearman correlation coefficient was also assessed to reach correlations between the different structural parameters. Results with p-value < 0.05 were considered as significant.

3. Results

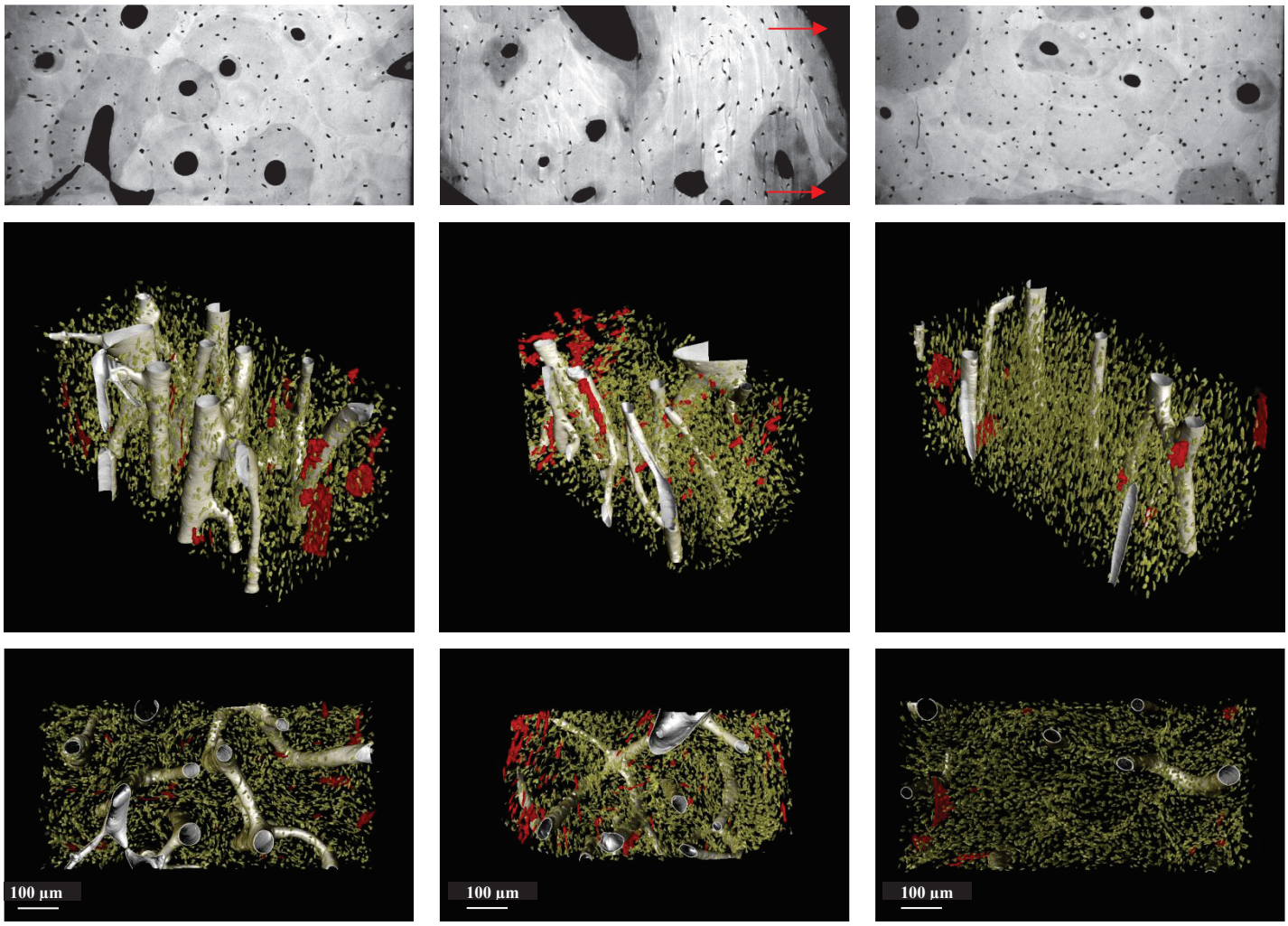

Femoral diaphysis **Femoral neck** **Radial diaphysis**

Figure 39 Phase contrast slice and volume rendering of control VOIs of human femoral diaphysis, femoral neck and radial diaphysis (Woman, 50 y.o.). Lacunae are represented in yellow, and micro-cracks in red. Note that on femoral neck slice, the detector edges are seen (red arrows). Note that the initial amount of micro-cracks is particularly high for this subject.

i. Osteocyte lacunae

Figure 39 present 3D rendering of control VOIs for the 3 anatomical locations. Table 6 presents the mean values over the eight subjects of the lacunae morphometric parameters. Significant differences between paired anatomical locations are also indicated. It can be noticed that individual geometrical parameters of osteocyte lacunae are significantly different in the radius than in the femur, diaphysis and neck. Lc.L1 at the radius is 15 % larger than in the femoral diaphysis and femoral neck, and Lc.L2 is from 8 % and 7 % smaller than in the femoral diaphysis and femoral neck, respectively. These differences lead to a sharper ellipsoid for the radius, with a 25 % lower Lc.ρ_1 and a 14 % and 12 % smaller Lc.ρ_2 than in the femoral diaphysis and femoral neck, respectively. The average individual lacuna volume and surface, on the other hand, remain the same in all the studied anatomical locations. Lc.N/BV is 13 % and 21 % higher in the femoral neck than in the radial and femoral diaphysis, respectively. This difference in lacunar density leads to a 14 % and 15 % higher Lc.V/BV in the femoral neck than in the femoral and radial diaphysis, respectively.

Table 6 Mean values for lacunae morphometric parameters

Morphometric parameters	Femoral diaphysis	Femoral neck	Radial diaphysis
Lc.L1 (µm)	22.08 (1.02)^{r*}	22.27 (1.46)^{r*}	25.49 (2.04)$^{d*\ n*}$
Lc.L2 (µm)	11.83 (0.44)^{r*}	11.89 (0.58)^{r*}	10.98 (0.67)$^{d*\ n*}$
Lc.L3 (µm)	5.44 (0.43)	5.52 (0.41)	5.46 (0.30)
Lc.ρ_1 (µm^{-1})	6.35 (0.59)^{r*}	6.39 (0.72)^{r*}	4.78 (0.74)$^{d*\ n*}$
Lc.ρ_2 (µm^{-1})	1.35 (0.20)^{r*}	1.38 (0.21)^{r**}	1.19 (0.17)$^{d*\ n*}$
Lc.S (µm^2)	517.00 (33.40)	526.57 (45.41)	558.27 (48.58)
Lc.V (µm^3)	570.95 (66.01)	561.12 (66.51)	599.52 (53.68)
Lc.N/BV (mm^{-3})	23034.92 (1771.43) $^{n*\ r*}$	26562.29 (4790.19) $^{d*\ r*}$	20765.05 (1476.92) $^{d*\ n*}$
Lc.V/BV (% x 10^3)	1323.58 (130.94)	1502.38 (279.57) ^{r*}	1257.46 (131.46) ^{n*}
Lc.N	5075	5487	4565

[d] different from femoral diaphysis, [n] different from femoral neck, [r] different from radial diaphysis

[*] $p < 0.05$

ii. Micro-cracks

Table 7 shows the mean values over the 8 subjects for the morphometric parameters of micro-cracks measured in control VOIs. In contrast to the osteocytes lacunae, micro-cracks appear to have nearly the same morphometric parameters in all three anatomical locations. A 48 % lower volume fraction of micro-cracks could be measured in the femoral diaphysis than the femoral neck, however.

i. Haversian canals

Table 8 presents Haversian canal morphometric parameters means and standard deviation values over the 8 subjects in control VOis. The radius shows a lower canal volume fraction than the femur. Ca.V/BV is 43 % and 29 % lower in the radius than in the femoral diaphysis and femoral neck, respectively. Haversian canals in the radius are also thinner by 31 % and 33 % than those observed in the femoral diaphysis and femoral neck, respectively. The standard variation of canal thickness within the tissue was also 47 % higher in the femoral neck and 51 % higher than the femoral diaphysis than in the radius. The femoral neck has a more heterogeneous Haversian system.

Table 7 Mean values for cracks morphometric parameters measured in the control VOIs.

Morphometric parameters	Femoral diaphysis	Femoral neck	Radial diaphysis
µCr.L1 (µm)	72.94 (38.39)	67.12 (17.77)	69.69 (32.09)
µCr.L2 (µm)	28.61 (6.92)	30.04 (7.59)	30.91 (10.76)
µCr.Th (µm)	1.92 (0.15)	1.99 (0.21)	2.06 (0.10)
µCr.S (μm^2)	3181.16 (1692.27)	4445.50 (4413.37)	5183.01 (4989.62)
µCr.V (μm^3)	2257.43 (1183.09)	3735.25 (4324.08)	4291.97 (4288.53)
µCr.V/BV (% x 10^3)	16.47 (9.49)	23.61 (19.39)	24.32 (17.66)

Table 8 Mean values for Haversian morphometric parameters measured in the control VOIs.

Morphometric parameters	Femoral diaphysis	Femoral neck	Radial diaphysis
Ca.V/BV (%)	8.45 (2.80)^{r*}	9.94 (4.40)	4.34 (2.46)^{d*}
Ca.Dm (µm)	73.01 (16.81)^{r*}	86.27 (35.76)^{r*}	49.24 (46.65)$^{d* n*}$
SD Ca.Dm (µm)	28.44 (8.13)^{n*}	57.52 (19.64)$^{d* r*}$	26.36 (12.29)^{n*}

^{d} different from femoral diaphysis, ^{n} different from femoral neck, ^{r} different from radial diaphysis

* $p < 0.05$ (Mann – Withney test)

ii. Influence of mechanical loading

Figure 40 and Figure 41 show 3D rendering of samples loaded under quasi-static and fall-like loading condition for femoral diaphysis and radial diaphysis, respectively. Table 9 presents the differences between loaded samples and controls, expressed as the relative difference (%) with respect to the control group, in geometrical (µCr.S and µCr.V) and volume fraction (µCr.V/BV and TotCr.V/BV) parameters; both for quasi-static and fall-like loading conditions. Mechanical loading changes the morphology of micro-cracks in the sites studied.

Under fall-like loading, these geometrical parameters were affected only in the femoral diaphysis, but significantly so ($p < 0.05$). For the two different loading rates, the micro-crack volume fraction (μCr.V/BV) and the total crack volume fraction (TotCr.V/BV) increased (p-value < 0.05).

Table 9 Relative difference (in %) between parameters before and after loading. Mechanical loading has a significant effect on bone micro-structure.

Morphometric parameters	Femoral diaphysis	Femoral neck	Radial diaphysis
		Quasi-static	
µCr.S	ns	ns	ns
µCr.V	ns	ns	ns
µCr.V/BV	403*	137*	922*
TotCr.V/BV	980*	647*	972*
		Fall	
µCr.S		ns	ns
µCr.V		ns	ns
µCr.V/BV	136*	198*	209*
TotCr.V/BV	262*	259*	679*

* **p < 0.05, ns non-significant**

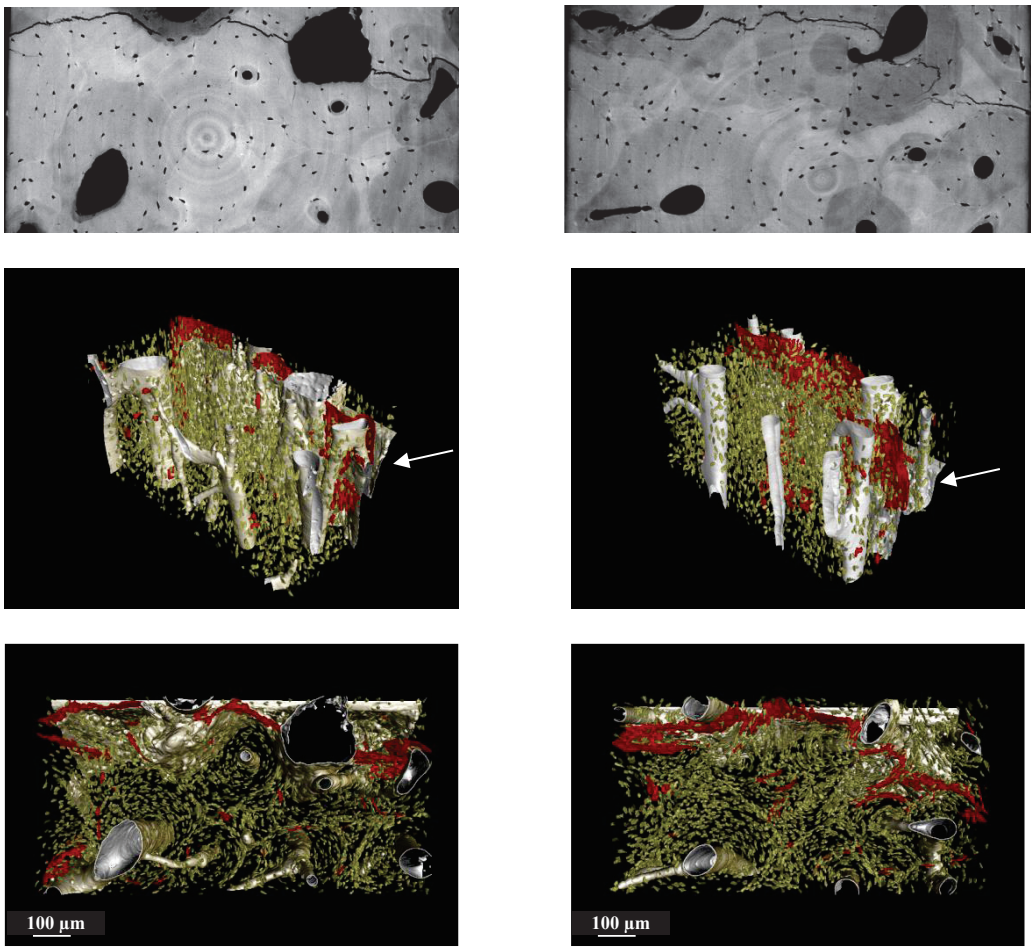

Figure 40 Phase contrast slice and volume rendering of femoral diaphysis samples under quasi-static and fall-like loading conditions (woman, 50 y.o.). Lacunae are represented in yellow, and cracks in red. White arrow points the fracture surface that could not be separated from the Haversian network.

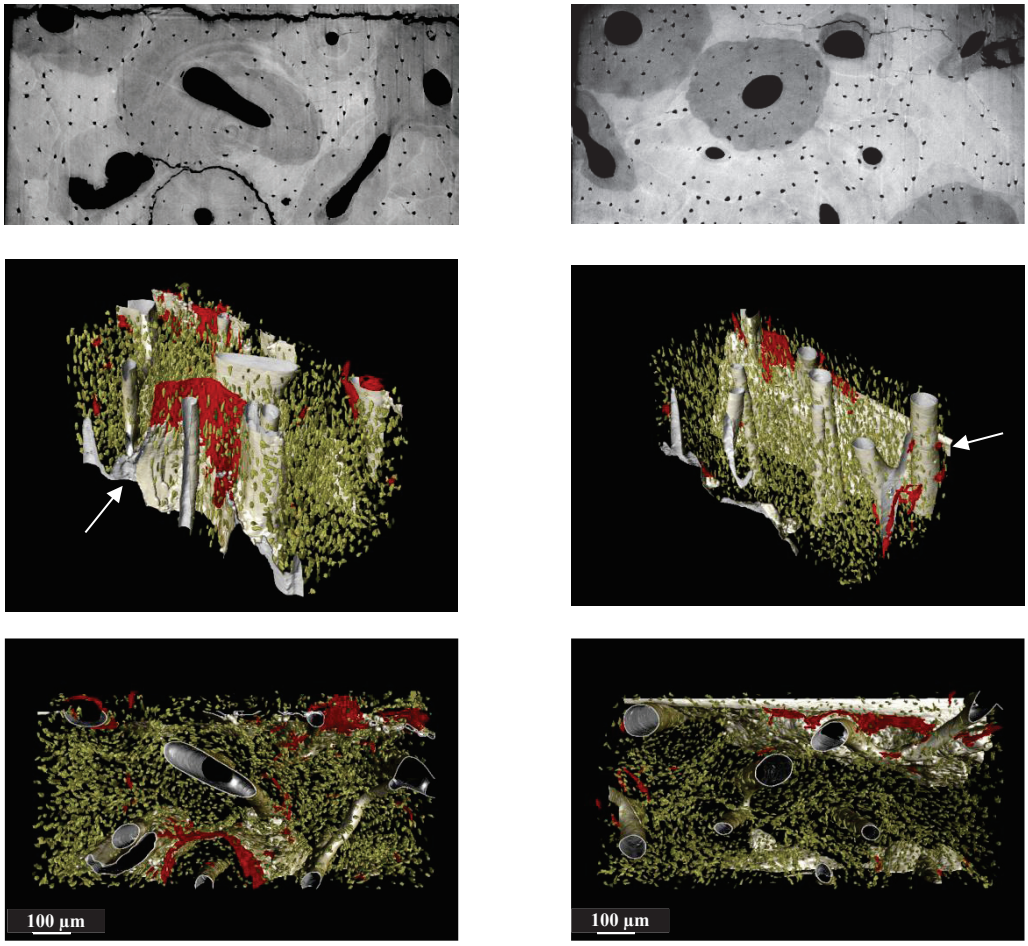

Figure 41 Phase contrast slice and volume rendering of radial diaphysis samples under quasi-static and fall-like loading conditions (woman, 50 y.o.). Lacunae are represented in yellow, and cracks in red.

A global result is that when there are differences in the morphometric parameters of the cracks between locations under quasi-static loading, the there are no differences under fall-like loading.

Considering the quasi-static loading conditions, micro-cracks observed in the radius have a higher individual surface (µCr.S) than in the femoral diaphysis and femoral neck, by 42 % and 48 % respectively. The individual crack volume (µCr.V) is only higher (by 53 %) in the femoral neck, however.

Concerning secondary cracks, in the radius, these cracks have a larger third axis than in the femoral diaphysis (27 % higher) and the femoral neck (28 % higher).

Regarding micro-crack volume fraction (μCr.V/BV), a significant difference was only measured in the radius, where the volume fraction was higher by 48 % under quasi-static loading. Considering the total amount of cracks formed within the tissue, a significant difference was observed between the femoral diaphysis and radius, with a TotCr.V/BV higher by 41 % and 78 % respectively, under quasi-static condition.

In Table 10, we present the values for geometrical parameters and volumes fractions of the two types of cracks found within the tissue and the significant differences between paired anatomical locations. For the volume fraction, the relative difference is expressed when significant.

A global result is that when there are differences in the morphometric parameters of the cracks between locations under quasi-static loading, there are no differences under fall-like loading.

Considering the quasi-static loading conditions, micro-cracks observed in the radius have a higher individual surface (μCr.S) than in the femoral diaphysis and femoral neck, by 42 % and 48 % respectively. The individual crack volume (μCr.V) is only higher (by 53 %) in the femoral neck, however.

Concerning secondary cracks, in the radius, these cracks have a larger third axis than in the femoral diaphysis (27 % higher) and the femoral neck (28 % higher).

Regarding micro-crack volume fraction (μCr.V/BV), a significant difference was only measured in the radius, where the volume fraction was higher by 48 % under quasi-static loading. Considering the total amount of cracks formed within the tissue, a significant difference was observed between the femoral diaphysis and radius, with a TotCr.V/BV higher by 41 % and 78 % respectively, under quasi-static condition.

Table 10 Geometrical parameters (mean standard deviation) on cracked VOIs loaded under quasi-static and fall-like conditions

Morphometric parameters	Loading rate	Femoral diaphysis	Femoral neck	Radial diaphysis
µCr.S (10^3 µm^2)	Quasi-static	4.79 (2.03)^{r*}	4.56 (1.70)^{r*}	10.56 (4.09)$^{d*\ n*}$
	Fall	3.96 (3.30)	5.98 (2.39)	4.15 (3.62)
µCr.V (10^3 µm^3)	Quasi-static	3.93 (1.82)	3.49 (1.52)^{r*}	9.34 (4.32)^{n*}
	Fall	3.11 (4.17)	4.73 (2.47)	3.52 (3.45)
µCr.V/BV (% x 10^3)	Quasi-static	82.82 (39.85)^{r*}	56.00 (39.02)^{r*}	248.53 (156.61)$^{d*\ n*}$
	Fall	38.86 (17.47)^{n*r*}	70.45 (20.23)^{d*}	75.16 (29.13)^{d*}
	Relative difference (%)	ns	ns	- 70*
2dCr.L3 (µm)	Quasi-static	82.48 (32.85)^{r*}	76.02 (18.07)^{r*}	96.45 (15.83)$^{d*\ n*}$
	Fall	77.94 (32.94)	70.73 (20.28)	71.96 (12.34)
2ndCr.S (10^3 µm^2)	Quasi-static	155.81 (69.72)	152.84 (91.59)	211.59 (170.71)
	Fall	121.63 (85.77)	119.51 (164.27)	184.61 (57.44)
2ndCr.V (10^3 µm^3)	Quasi-static	151.49 (84.58)	151.73 (64.03)	200.20 (163.17)
	Fall	119.14 (86.68)	104.44 (164.96)	151.88 (49.33)
TotCr.V/BV (% x 10^3)	Quasi-static	345.87 (177.81)^{r*}	203.76 (176.40)^{r*}	625.63 (260.15)$^{d*\ n*}$
	Fall	132.84 (128.29)	118.14 (84.68)	125.69 (84.68)
	Relative difference (%)	- 62*	ns	- 80*

^{d} different from femoral diaphysis, ^{n} different from femoral neck, ^{r} different from radial diaphysis

* p < 0.05, ns : Non-Significant

iii. Correlations

Annex 1 shows the Spearman's correlation coefficient matrix obtained between different tissue structural parameters for the different anatomical locations.

For the three anatomical locations, the Haversian parameters (Ca.V/BV, Ca.Th and SD Ca.Th) are positively correlated.

In the femoral diaphysis, the micro-crack density (μCr.V/BV) within the tissue after quasi-static loading is positively correlated to the lacunar volume fraction, whereas the total crack volume fraction (TotCr.V/BV) was positively correlated to the volume fraction of micro-cracks after quasi-static loading ($p < 0.05$). Under fall-like loading, the total volume fraction of cracks is positively correlated to the volume fraction of micro-cracks formed after a loading.

In the femoral neck, μ is negatively correlated to Ca.V/BV and SD Ca.Th. The lacunar volume fraction is also negatively correlated with the variation of the canal thickness. The volume fraction of micro-cracks formed after quasi-static loading is positively correlated to the initial volume fraction. Finally the total volume fraction of cracks is positively correlated to the volume fraction of micro-cracks formed under quasi-static loading.

In the radius, μ is negatively correlated to the Haversian volume fraction (Ca.V/BV), mean and SD thickness (Ca.Th and SD.Ca.Th).. The volume fraction of micro-cracks formed under quasi-static load is also positively correlated to the Haversian parameters. The total volume fraction of cracks formed under fall-like conditions is positively correlated to the variation of Haversian canal thickness (SD Ca.Th, p-value < 0.05).

Table 11 presents the matrix of Spearman correlation coefficient calculated between geometrical parameters measured on the three paired anatomical sites. In this table, we can note that $Lc.\rho_2$, which characterizes lacunae sharpness, is positively correlated to the individual surface of micro-cracks formed under fall-like loading in the femoral diaphysis (p-value < 0.05). There is no correlation with the geometrical parameters measured on the radius.

Table 11 Spearman's correlation coefficient between different geometrical parameters on the three anatomical locations

Femoral diaphysis				
	Lc.ρ_1	**Lc.ρ_2**	**µCr.MeanSurf$_{QS}$**	**µCr.MeanSurf$_F$**
Lc.ρ_1	1	ns	ns	ns
Lc.ρ_2		1	ns	**0.91***
µCr.S			1	ns
µCr.V				1
Femoral neck				
	Lc.ρ_1	**Lc.ρ_2**	**µCr.MeanSurf$_{QS}$**	**µCr.MeanSurf$_F$**
Lc.ρ_1	1	**0.88****	ns	ns
Lc.ρ_2		1	ns	ns
µCr.S			1	ns
µCr.V				1
Radial diaphysis				
	Lc.ρ_1	**Lc.ρ_2**	**µCr.MeanSurf$_{QS}$**	**µCr.MeanSurf$_F$**
Lc.ρ_1	1	ns	ns	ns
Lc.ρ_2		1	ns	ns
µCr.S			1	ns
µCr.V				1

$_{QS}$ Quasi-static, $_F$ Fall, non-indication means control

* p < 0.05, ns non-significant

4. Discussion

Bone fragility is a complex problem that has to be considered to prevent the elderly from traumatic fractures. Human cortical bone fracture mechanisms depend on its global organization, involving geometrical, compositional or architectural arrangement (Augat and Schorlemmer, 2006; Berteau et al., 2015; Poole et al., 2012; Seeman and Delmas, 2006). We focused on the bone porosity at different length scale as it may play a role in bone capacity to resist fracture (Bala et al., 2016; Granke et al., 2016, 2011; Perilli et al., 2015). The aim of this study was to measure morphometric parameters of different type of porosity on eight paired human femoral diaphysis, femoral neck and radial diaphysis.

Considering lacunar morphometric parameters measured on the femoral diaphysis, values of Lc.L1, Lc.L2 and Lc.L3 are in the same order of magnitude than values found in the literature

(Lc.L1 /Lc.L2 /Lc.L3 = 22.08 ± 1.02 /11.83 ± 0.44 /5.44 ± 0.43 µm in the current study, 18.9 ± 4.9 /9.2 ± 2.1 /4.8 ± 1.1 µm in (Dong et al., 2014)). Lc.S and Lc.V values are higher in the current study (Lc.S / Lc.V = 517.0 ± 33.4 μm^2 / 570.9 ± 66.0 μm^3 in the current study, 336.2 ± 94.5 μm^2 / 409.5 ± 149.7 μm^3 in (Dong et al., 2014)). These differences may come from the different size of the VOI. The size of the volumes scanned in the current study is about 0.225 mm^3 (this quantity is variable and depends on the thickness of the samples), involving an average number of osteocytes lacunae of 4250 whereas Dong et al. studied VOI of 0.686 mm^3 involving a number of lacunae of 12791. . The lacunar volume fraction are also comparable (Lc.N / BV / Lc.V / BV = 23035 ± 1771 / 1.3 ± 0.1 in the current study, 20573 ± 2850 / 0.9 + 0.1 in (Dong et al., 2014)). We can see that the lacunar volume fraction is nevertheless not comparable to values found in the literature (Lc.V / BV = 1.3 ± 0.1 in the current study, 0.9 + 0.1 in (Dong et al., 2014)). This difference can be explained by the same reason as for the surface Lc.S and the volume Lc.V of the lacunae. By overestimated each volume of lacunae, then we may overestimated the total volume of lacunae over the bone volume.

The lacunar geometrical differences between femur and radius might be the consequences of a different nature of the remodeling process. As femur is a weight bearing bone and radius not. The femur is more often subjected to high levels of loading involving a more rapid mechanical constraint. This mechanical damage is assumed to send a signal to the osteocytes network to initiate the turnover of bone (Burr et al., 1985; Lee et al., 2002). It has recently been shown that the shape of lacunae osteocytes is related to its mechanosensitivity. A flatter osteocyte, as observed in the radius, had been measured to be less mechanosensitive than a rounder one, as observed in the femur (van Oers et al., 2015). This point supports our hypothesis: since the radius experiences much less damage, it is replaced with less frequency, hence its osteocytes are not adapted to certain mechanical constraints and may therefore be less mechanosensitive.

The femoral neck appears to have a higher density and volume fraction of lacunae than the femoral and radial diaphysis. This may be due to the fact that the femoral neck is an anatomical region that is highly loaded, even during physiologically normal movement such as walking (Lotz et al., 1995; Verhulp et al., 2008). Mechanical stimuli being a driver for bone remodeling, a higher loading may involve a higher turnover rate, meaning a higher activity of osteoblasts and osteoclasts. As it has been assumed that it is osteoblasts that differentiate into osteocytes (Bonewald and Johnson, 2008), a higher turnover rate may involve a higher production of osteocytes. This is corroborated by the difference being higher between the femoral neck and the radius.

The geometrical parameters of micro-cracks are difficult to compare with values found in literature. For the baseline case, data on three dimensional morphometric parameters of micro-cracks measured on human cortical bone are very limited. In 2011, Larrue et al. investigated geometries of micro-cracks observed on human trabecular bone (Larrue et al., 2011). Considering that the main axis of the microcracks is parallel to the orientation of the osteon, length values obtained in Sobelman et al., 2004 or in Haupert et al., 2014, correspond to our µCr.L2. The values presented in the current study are lower than those reported in the two previous studies (µCr.L2 = 26.6 ± 6.9 µm in the current study, 75 ± 26 µm in (Sobelman et al., 2004), 72.6 ± 13 µm in (Haupert et al., 2014)). These differences may come from the sample preparation protocol, as cutting may introduce new cracks within the tissue. To our knowledge there is no study comparing different preparation protocol on the morphology of damages within cortical tissue. The size of the analyzed volume may also influence the measurement. In the two other studies, the measured area is much higher (0.45 mm^2 in the current study, 400 mm^2 in (Sobelman et al., 2004), 5.6 mm^2 in (Haupert et al., 2014)). We can also notice that, in the current study, µCr.L2 ranged between 13 µm and 91 µm over the eight subjects on the femoral diaphysis. Considering the parameters measured in the cracked VOIs, a comparison with data found in the literature is also difficult, because in previous studies, samples are not tested until complete fracture but subjected to fatigue tests (Mohsin et al., 2006; O'Brien et al., 2000). The consequence of a complete fracture is that a large number of previously formed micro-cracks (due to loading) are incorporated into the propagation of the main crack. The initiation and propagation of this main crack might thus be due to the coalescence of previously formed micro-cracks (Akkus et al., 2000; Danova et al., 2003). Therefore the morphometric parameters of micro-cracks after loading are highly dependent on the experimental conditions.

It is interesting to note that there are no differences in geometrical parameters of the pre-existing micro-cracks before loading between the different anatomical locations. This might indicate that the accumulation of micro-cracks proceeds similarly in all three studied sites (albeit at different time scales). However, it might also be due to the bone tissue reacting in a similar way between the sites during cutting for sample preparation, in terms of geometry of defects. We can therefore observe a difference of micro-crack volume fraction between femoral diaphysis and neck. This might be due to a higher density of micro-cracks *in vivo* in the femoral neck, due to its highly loaded state. But it might also be due to a different behavior between the sites in response to the sample preparation protocol. This might be an interesting point for future studies. Here, the main interest was to analyze the effect of loading on micro-crack morphometric parameters, however.

Dealing now with the parameters of the Haversian network, the volume fraction of vascular porosity measured on the femoral diaphysis in the current study are in the same order of magnitude as values also measured in 3D found in the literature (Ca.V/BV = 9.34 ± 3.40 % here, 12.26 ± 3.15 % in (Perilli et al., 2015),11.48 ± 7.0 in (N J Wachter et al., 2001)). The canal diameter measured in the femoral diaphysis is also in accordance with the data found in literature (Ca.Dm = 73.04 ± 16.81 in the current study, 55.09 ± 14.33 in (Jowsey, 1966), up to 72 μm in (Zimmermann et al., 2011)).

For the three anatomical sites, a negative correlation was found between the X-ray attenuation coefficient and the canal volume fraction. Higher is the volume fraction of vascular porosity, lesser the bone tissue is mineralized. This may be due to the osteonal bone surrounding the Haversian canals. This tissue is less mineralized than the surrounding tissue (Kazanci et al., 2007; Phelps et al., 2000). If there are more canals, there are more osteons and thus less mineralized bone, because of the remodeling process.

The significant differences of morphometric parameters at all length scale found between the femur and the radius may also come from the non-weight bearing nature of the radius. As pointed out above, the radius might experience less remodeling due to a mechanical environment involving less mechanical damage formation. The Haversian canals are structural features where the remodeling process may initiate due to the passage of blood vessels (Zebaze et al., 2010). A higher thickness variation is also observed in the femoral neck. In this region, the cortical thickness is close to 2 mm (Treece et al., 2010). The sample thickness for mechanical testing was also roughly 2 mm. It may thus be possible that samples were extracted at the transition zone between cortical and trabecular bone, involving a variate map of vascular porosity.

In this study we found that both quasi-static and fall-like loading conditions have a significant influence on micro-crack morphology. During the propagation of the main crack through the bone micro-structure, energy is stored within the tissue. The final propagation of the main crack involves the dissipation of a large part of this stored energy. Formation of micro-cracks is also an energy dissipating mechanism that manifest both under quasi-static and fall-like loading conditions (Diab and Vashishth, 2005; Sobelman et al., 2004; Turnbull et al., 2014).

More and larger micro-damage, in terms of volume fraction, appears to form in the radius than the femoral diaphysis and femoral neck under quasi-static loading. Considering the energy-dissipating nature of the formation of micro-cracks in the bone tissue, this would mean that more energy is dissipated through crack formation in the radius than the other sites

under quasi-static loading. This is consistent with our previous work stating that the radius is more resistant to crack propagation than femoral diaphysis or neck under quasi-static loading because more energy is dissipated with the formation of micro-cracks whether that for the main crack propagation (Gauthier et al., 2017). The same result and hypothesis are obtained considering all the cracks, micro-cracks and secondary cracks.

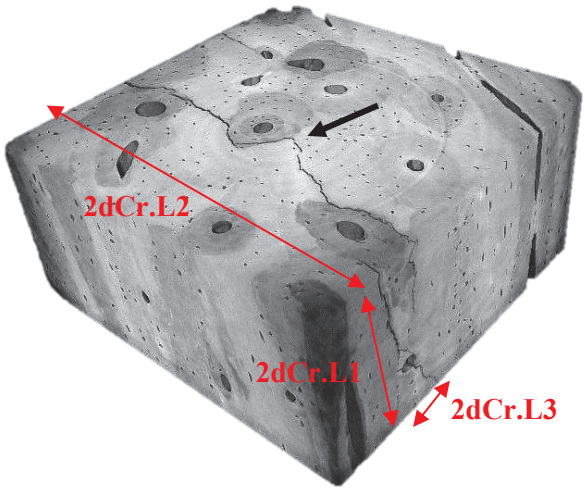

Figure 42 3D rendering of radius cortical bone sample loaded under quasi-static conditions. Secondary cracks third axis characterizes their deviation among osteons. Note the deviation shown by the black arrow

The secondary cracks formed under quasi-static loading within the radius present a higher μCr.L3, characterizing their deviation among the osteons (Figure 42). More crack deviations may thus occur in radius than in the femoral diaphysis or femoral neck. This may be due to a lower Haversian canals volume fraction within the radius, which might be related to the osteonal volume fraction. A high volume fraction of osteonal bone may be negative for the activation of some dissipation mechanisms, such as micro-crack formation, and therefore limited energy dispersal (Mischinski and Ural, 2011; Zimmermann et al., 2011). Osteons are complex mechanical features that can both act as crack propagation barriers and micro-crack initiation sites, as well as stress concentration sites (Burr et al., 1988; O'Brien et al., 2005a). In the radius the canals are organized in a way that they are seldom close to each other. They may thus play the role of individual sites of stress concentration; there is no interference between the stresses experienced by the osteons. In that way each of them can act as an initiation site in the favor of micro-crack formation. In the femoral diaphysis and neck, the canal volume fraction may be too high to promote micro-cracks initiation.

In the femoral diaphysis, the lacunar volume fraction acts in favor of micro-cracks formations. The positive correlation found between Lc.V/BV and μCr.V/BV_{QS} means that a higher amount of lacunae within bone tissue may enhance the formation of micro-cracks under quasi-static mechanical loading. Moreover, the shape of individuals' lacunae may also be involved in the shape of the observed micro-cracks Lacunae may act as small stress concentrators within the bone matrix, thus playing the role of guides for the micro-cracks. The stress concentration at the tip of a small objects is dependent of its radius of curvature: the more the object is pointed, the more the stress measured at its tip is high (Griffith, 1921). The hypothesis is that, the rounder lacunae found in the femoral diaphysis may allow micro-cracks to develop and coalesce, and as their stress concentration state is low because of their high roundness, they may act as weak defects which micro-cracks can pass through. This hypothesis is therefore not supported by our measurements in the femoral neck, which had similar lacunar roundness as the femoral diaphysis. As for the Haversian canals, a too high volume fraction of canals may be disadvantageous for this hypothetic micro-crack propagation mechanism, by encountering too much lacunae, micro-cracks development may be arrested because of a possible too much tortuous path. These different hypotheses are difficult to verify experimentally. Numerical models are in development to analyze mechanical fields at the lacuna scale (Rath Bonivtch et al., 2007; Varga et al., 2014).

Under fall-like loading, the resulting micro-crack volume fraction is significantly lower than under quasi-static loading within the radius. Considering the total amount of cracks formed, this significant difference can also be seen in the femoral diaphysis. These results mean that there is less energy dissipation due to micro-crack formation when cortical bone is loaded under fall-like conditions. Moreover, there is no difference in crack volume fraction between the different anatomical locations. This is consistent with our previous results stating that there is significantly less dissipated energy in the femoral diaphysis, femoral neck, and radial diaphysis when they are loaded under fall-like conditions (Gauthier et al., 2017). Further, it was shown that while there were different fracture behavior between the sites under quasi-static loading, there was no difference under fall-like conditions (Gauthier et al., 2017). This result is therefore also observed for the femoral neck considering the fracture behavior. In the current study, the loading rate had no significant effect on crack volume fraction. Microcrack formations might therefore not be the only energy dissipating mechanism during crack propagation. Other might be the collagen stretching, interfibrillar sliding or crack deflection (Zimmermann and Ritchie, 2015).

The current study presents some limitations. First, the micro-cracks were quantified by considering an ellipsoid fit, which might not accurately relay their actual geometrical parameters. Micro-cracks can undergo some deviation, which may increase their geodesic length but not the length of the best fitting ellipsoid. As the aim of this study was to evaluate inter-site differences, and since all the samples were treated using the same protocol, we propose that the comparative investigation is consistent. Further, the sample preparation method might have introduced micro-defects post-hoc. The initial amount of micro-cracks observed in our samples might not be representative of bone tissue *in vivo*. Since we investigated the effect of loading on the morphometric parameters of micro-cracks, the result is expressed as an evolution beyond the initial state. In the current study, both quasi-static and fall-like loading conditions bring out significant changes in micro-crack properties with respect to the initial state; measured using the same technique in a non-loaded zone and tested using a test for paired samples (Wilcoxon test).

The size of the VOIs used in the current study might also be limiting, since it is small compared to other studies found in literature (Dong et al., 2014; Hannah et al., 2010; Haupert et al., 2014; Sobelman et al., 2004). Due to the large number of volumes (96), we had to widely reduce the size of the analyzed region to avoid a too long time for processing. Finally our population involved only eight female subjects, all of which could be qualified as aged (50 to 91 y.o.). It is known that, e.g., the porosity network is dependent of the age *and* sex of the subject (Bala et al., 2012; Vashishth et al., 2005). In the current study no correlation was found between age and any measured morphometric parameters, probably due to the limited age range. We note, however, that the samples used are representative of a population of elderly women.

To our knowledge this is the first study investigated the multi-scale pore network of paired human femoral diaphysis and neck and radial diaphysis using SR-µCT with a voxel size of 0.7 µm. In summary, our results confirm that micro-cracks play a major role in cortical bone fracture behavior. Further, micro-crack formation may be dependent on the pre-existing porosity network, but this mechanism seems to differ in each anatomical site: micro-damage development is related to the Haversian system within the radius whereas in the femoral diaphysis, micro-cracks rather seem related to the osteocyte lacunae network. Finally, while micro-crack formation seems to play a major role in the crack propagation mechanisms in bone, other parameters should also be considered. Analysis on these µCT images can be deepened in order to identify other structural related fracture mechanisms such as crack deflection at the cement line, or roughness of the fracture surface. Future work could be

performed outside the range of length scales studied here, involving for example the chemical characteristic of the collagen or the morphology of the mineralized collagen assemblies.

5. Conclusion

In the current study, we assessed morphometric parameters of human cortical on eight paired femoral diaphyses, femoral necks and radial diaphyses. Results found show that thesis anatomical locations have different microstructures, from the Haversian system down to the lacunar network. Differences are particularly observed between the femur and the radius. This result confirms that the internal organization of the tissue depends on the weight bearing or non-weight bearing nature of the bone as discussed by Wolf (Wolff, 1892). These observed differences can also explain the previous results found on human cortical bone toughness. It is well known that bone fracture mechanisms are related to the Haversian network under standard condition. The different properties of this network assessed on the three paired locations can explain the different observed mechanical behavior. The difference of lacunar morphometric parameters investigated in the current study on paired femur and radius suggest that this network might also play a role in human cortical bone fracture process.

Chapter IV On the relationships between human cortical bone toughness and collagen cross-links maturation

Abstract: Human cortical bone fracture process depends on the internal porosity network down to the lacunar length scale. Recent results showed that at the collagen scale, the maturation of collagen cross-links may have a negative influence on bone mechanical behavior. If the effect of pentosidine on human cortical bone toughness has been studied in the past, influence of mature and immature enzymatic cross-links has only been studied in relation to other mechanical parameters. The aim of the current study was thus to assess the relationships between both enzymatic and non-enzymatic collagen cross-links and human cortical bone toughness considering 32 paired femoral diaphyses, femoral necks and radial diaphyses. Maturation of collagen was defined as the ratio between immature and mature cross-links. Results show that this ratio is not correlated to bone capacity to undergo plastic mechanisms. This study suggests that collagen cross-links maturation is not involved in crack propagation mechanisms in human cortical bone.

1. Introduction

Collagen fibres are of a great importance in human cortical bone's mechanical integrity (Gupta et al., 2013; Oxlund et al., 1995; Saito and Marumo, 2010; Viguet-Carrin et al., 2006; Wang and Elbanna, 2014; Zioupos et al., 1999). Its maturation is assumed to be involved in bone mechanical properties decline with age (Berteau et al., 2015; Granke et al., 2015; Vashishth et al., 2001).

One of the most important mechanism of collagen evolution with time is the formation of cross-links between molecules (Bailey, 2001). Two different process of cross-linking can be outlined. The first one is a stabilisation of the collagen fibres regulating by lysyl oxidase that converts the amino groups of lysine and hydroxylysine to form the allysine and hydroxyallysine. These molecules can then condensate with some residues of lysine or hydroxylysine to form didhydroxylysinonorleucine (DHNL) and hydroxylysinonorleucine (HLNL) divalent immature cross-links. By undergoing another reaction with lysine or hydroxylysine molecules, formation of pyridinoline (PYD) and deoxypyridinoline (DPD) trivalent mature cross-links can occur (Bailey, 2001; Bailey et al., 1998; Saito and Marumo, 2010; Viguet-Carrin et al., 2006). If the conversion from immature to mature cross-links have been shown to be independent of the turnover rate, their relative amount is age-dependent (Berteau et al., 2015; Viguet-Carrin et al., 2006). This relative amounts expressed as the ratio between immature and mature cross-links, and called CX in the current study (CX = [HLNL + DHLNL] / [PYD + DPD], has also been shown to be related to the decrease of bone mechanical properties decline with age (Berteau et al., 2015). Divalent immature and trivalent mature cross-links can be measured by high performance liquid chromatography (HPLC) (Gineyts et al., 2010).

The second maturation mechanism involves non-enzymatic reaction with glucose. The so-called glycation reaction is at the origin of the presence of advance glycation end-products (AGEs) within bone tissue (Bailey, 2001; Saito and Marumo, 2010). These non-enzymatic cross-links are thought to be involved in the decline of cortical mechanical properties with age (Vashishth et al., 2001; Zimmermann et al., 2012). Pentosidine (PEN), that is one over many AGEs, can accurately be quantified in bone tissue using HPLC by natural fluorescence (Saito et al., 2006; Saito and Marumo, 2010; Viguet-Carrin et al., 2006). It has been shown that content of pentosidine within cortical tissue is strongly related to the content of all AGEs (Deepak Vashishth, 2007; Vashishth et al., 2001).

If relation between collagen crosslinking and cortical bone mechanical properties can be found in the literature (Berteau et al., 2015; Poundarik et al., 2015; Saito and Marumo, 2010; Vashishth et al., 2001; Viguet-Carrin et al., 2006; Zimmermann et al., 2012), there is only few information on a relative difference between different anatomical locations (Saito and Marumo, 2010). The aim of

this study is thus to quantify contents of both enzymatic and non-enzymatic collagen cross-links on paired femoral diaphysis (medial and lateral regions), femoral neck and radial diaphysis on which toughness testing were performed at two different strain rates (Gauthier et al., 2017).

2. Materials and methods

i. Bone samples

Thirty-two human cadaver subjects were used in this study (18 women, age 81 ± 12 y.o.; 14 men, age 79 ± 8 y.o.). No additional information concerning eventual disease or medication history was available. Whole femurs and radii were collected from these fresh cadaveric subjects. Extracted bones were kept hydrated in saline soaked gauze; then stored at -20 °C until sample preparation. Because of the non-availability of some of these bones, the final database is constituted of 29 femoral diaphyses, 29 femoral necks and 31 radial diaphyses. On the femoral diaphysis, both the medial and the lateral region were studied.

ii. Biomechanical measurements

The biomechanical experiments protocol used here is the same as in a previous study (Gauthier et al., 2017)(see Chapter II). A summary of the methodology is recalled below.

- ***Sample preparations***

From each bone, 25 mm long rectangular notched samples, with a width W=2.08 ± 0.06 mm and a thickness B=1.01 ± 0.02 mm, were extracted using a low speed saw with a diamond coated blade (ISOMET 4000, Buehler, USA). The dimensions were chosen based on the available cortical thickness in the femoral neck and radius (Kilappa et al., 2011; Treece et al., 2012). While the available cortex is thicker in the femur, we decided to standardize the dimensions so that a direct comparison could be performed. The samples were prepared to have their long side parallel to the long axis of the bone, and consequently its osteons. A notch was then machined in the transverse direction of the bone, in order to initiate crack formation perpendicularly to the osteon structure within the tissue. To ensure consistent crack formation, the notch tip radius was reduced by the use of an ad hoc device sliding a cutter blade in the bottom of the initial notch, cutting the final notch to a controlled depth. The final notch was a_0=1.16 ± 0.06 mm long, half of the sample width, with a notch tip radius of approximately 10 µm. Since one objective of this study was to investigate the effect of different strain rates, two contiguous samples were prepared from each bone; one to be tested under a quasi-static strain rate and the other at a rate representative of a fall. Thus, a total of 236 samples were prepared for this study. The samples were stored at -20°C after preparation, then

de-frosted the night before the mechanical tests and kept at 21°C in a physiological solution from 6 h before testing for rehydration.

- ***Biomechanical experiment***

Samples were tested in a three-point bending configuration with a 10 mm supporting span on a servo hydraulic testing machine (INSTRON 8802, High Wycombe, England) (The American Society of Mechanical Engineers (ASME), 2006). For the quasi-static loading, which is the standard for cortical bone toughness measurement, a strain rate of 10^{-4} s^{-1} was applied (Kasapi and Gosline, 1996; Yeni and Fyhrie, 2002; Zimmermann et al., 2014). Based on values found in the literature to represent a fall from a standing position, the samples were loaded at a strain rate of nearly 10^{-1} s^{-1} (Foldhazy, 2005) to emulate fall conditions. The corresponding displacement rates of the testing machine to the given strain rates were 10^{-3} $mm.s^{-1}$ for the quasi-static case and 10 $mm.s^{-1}$ for fall conditions. A load-displacement curve was recorded for each mechanical test and was used to obtain different parameters using the methods presented below.

- ***Fracture toughness measurement***

The non-linear J-integral introduced by Rice in order to consider both elastic and plastic properties of human cortical bone was measured (Rice, 1968). Thus, J_{el} ($N.mm^{-1}$) and J_{pl} ($N.mm^{-1}$) were calculated from toughness experiments. They are the strain energy release rate associated to the elastic contribution and plastic contribution, respectively. Formula needed to calculate these mechanical parameters can be found in Gauthier et al., 2017

As cross-links may have an influence on cortical bone capacity to undergo plastic deformation before breaking, we decided to divide the non-linear part of the load-displacement curve into two different areas associated to two different non-linear deformation mechanisms (Berteau et al., 2015). Based on the shape of curves obtained during toughness experiment on human cortical bone, we choose to associate a parameter, $J_{process}$ ($N.mm^{-1}$), to the area between the yield load and the maximum load that would correspond to the development of a process zone due to rearrangement of the internal organization of cortical bone (Vashishth et al., 1997; Yang et al., 2006a). The second parameter, J_{prop} ($N.mm^{-1}$), is associated to the final part of the curve, from the maximum load until the final breakage, and would correspond to the actual formation of a main crack that would propagate through cortical bone microstructure until fracture. These two parameters can be assessed as follows (Figure 43):

$$J_{process} = \frac{\eta A_{process}}{B(W-a)} \quad (4.a)$$

$$J_{prop} = \frac{\eta A_{prop}}{B(W-a)} \quad (4.b)$$

We thus find the relationship between the different parameters:

$$J_{pl} = J_{process} + J_{prop} \quad (5)$$

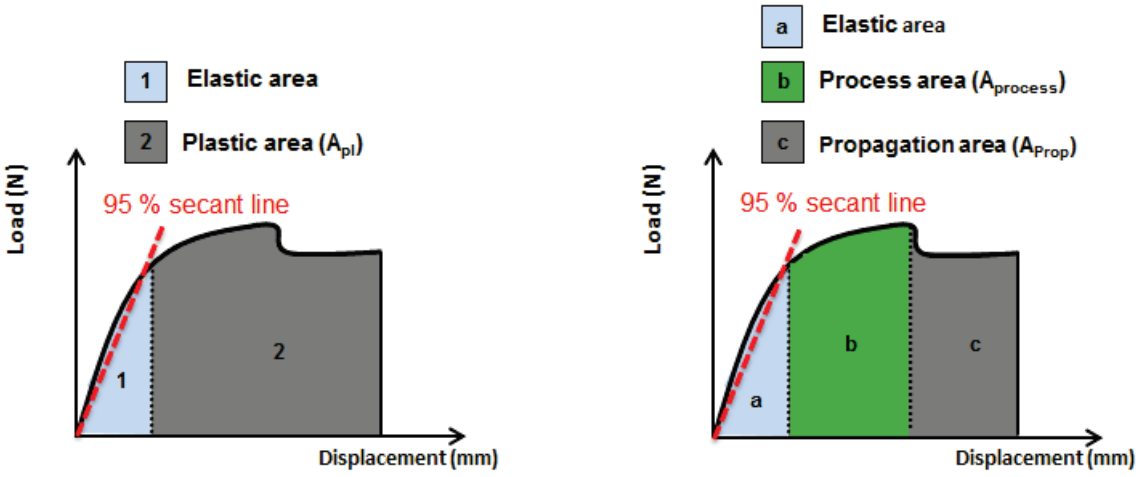

Figure 43 Typical load-displacement curve obtained for human cortical bone toughness experiments. On the left is the ASTM E-1820 suggestion of division (The American Society of Mechanical Engineers (ASME), 2006)**; on the right is the current study choice of division.**

iii. Biochemical measurements

- ***Sample preparation***

The cortical bone falls stemmed from the previously enounced sample preparation were kept frozen at -20 °C. They were cut into small pieces, powered in liquid nitrogen-cooled freezer mil (Spex Centriprep, Metuchen, USA), demineralized with daily changing of 0.5 M EDTA in 0.05 M in Tris buffer, pH 7.4 for 96 h at 4 °C. The demineralized powder was then extensively washed with deionized water. The samples were then suspended in phosphate buffered saline (0.15 M sodium chloride, 0.1 M sodium phosphate buffer, pH 7.4) and reduced in $NaBH_4$ at room temperature for 2 h using a reagent/sample ratio of 1:30 (w/w). The reduced bone residues were washed, freeze-dried and hydrolyzed in 6 M hydrochloric acid at 110 °C for 20 h. These hydrolysates were used for the measurement of cortical bone cross-links and for the assessment of collagen studying

hydroxyproline. Because of availability of matter, the final database for biochemical measurements is composed of 29 femoral diaphyses, 25 femoral necks and 30 radial diaphyses.

- ***Cross-links measurements***

Pyridinoline (PYD) and deoxypyridinoline (DPD) mature cross-links and didhydroxylysinonorleucine (DHNL) and hydroxylysinonorleucine (HLNL) immature cross-links stabilized by NaBH4 reduction were extracted from the hydrolysates using a solid phase extraction column (Bond Elut Cellulose, Agilent Technologies, Santa Clara, CA, USA) to remove interfering molecules. The wanted DHLNL, HLNL, PYD and DPD cross-links were then investigated using an Alliance 2695 separation HPLC system equipped of with Waters Micromass® ZQ™ Single Quadrupole Mass Spectrometer, a 2647 Multi λ fluorescence detector and Empower2 chromatography data software (Waters Corp. Milford, MA, USA). They were separated on a C18 Atlantis® T3, 3µm, 4.6×100mm reversed-phase column protected by an Atlantis® T3, 3µm, 4.6×20mm guard cartridge (Waters Corp. Milford, MA, USA), maintained at 25 °C, and using a gradient between an aqueous phase composed of 0.12 % of heptafluorobutyric acid in 18 ohms pure water and an acetonitrile organic phase at a flow rate of 1ml/min. The detection of the different molecules was performed by electrospray ionization mass spectrometry in a positive ion mode (Gineyts et al., 2010).

The ratio CX = [DHLNL + HLNL] / [PYD + DPD] was used to express the state of cross-links maturation allowing thus the assessment of the collagen matrix maturation (Berteau et al., 2015).

Pentosidine (PEN) quantification was performed investigating its natural fluorescence at an emission of 385 nm for PEN and at an excitation of 334 nm (Viguet-Carrin et al., 2009).

The weight proportion of bone collagen in the sample was analyzed by measuring hydroxyproline using a HPLC assay (Bio-Rad, Munich, Germany) (Follet et al., 2011; Gineyts et al., 2010; Saito et al., 1997).

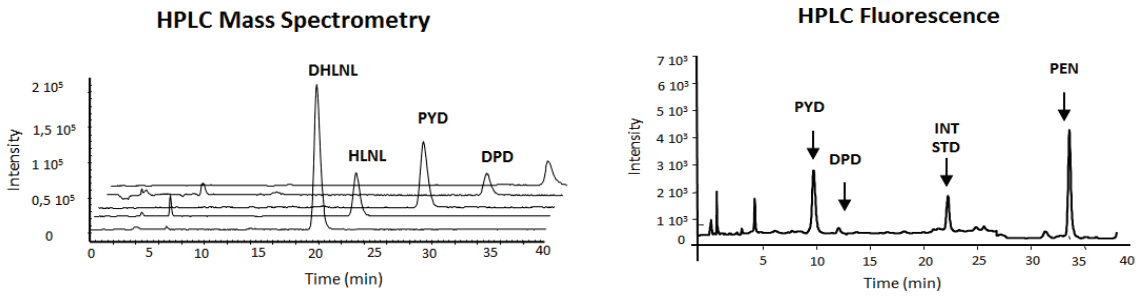

Figure 44 On the left is typical chromatogram of DHLNL, HLNLD, PYD and DPD of human cortical bone assessing with a mass spectrometry system. On the right is typical chromatogram of PYD, DPD and PEN of human cortical bone assessed with fluorescence system.

iv. Statistical tests

The normality of the distribution was assessed using Shapiro-Wilk's test. First a one-way analysis of variance (ANOVA) was performed in order to highlight potential differences between the series. Then t-tests for paired samples were used to evaluate these differences. If normality was not verified, then results were analyzed using a non-parametric Wilcoxon test for paired samples, and a Kruskal-Wallis test for independent samples. Correlation tests were performed between the different measurements modalities. These statistical tests were performed using R© (The R foundation for Statistical Computing, Austria) and Statview® (SAS Institue Inc, Campus Drive, Cary, NC 27513). P-values under 0.01 were considered as significant. For data sets that don't satisfy the Shapiro-Wilk condition, both non-parametric and parametric tests for paired samples were thus performed on the data set.

3. Results

The final results obtained from the two kind of statistical tests were from the same order of magnitude. To standardize, and for comprehension reason, only the results obtained with the parametric tests are presented here.

i. Biomechanical experiments

Mean values for the four toughness parameters are presented in Figure 45 and Table 12.

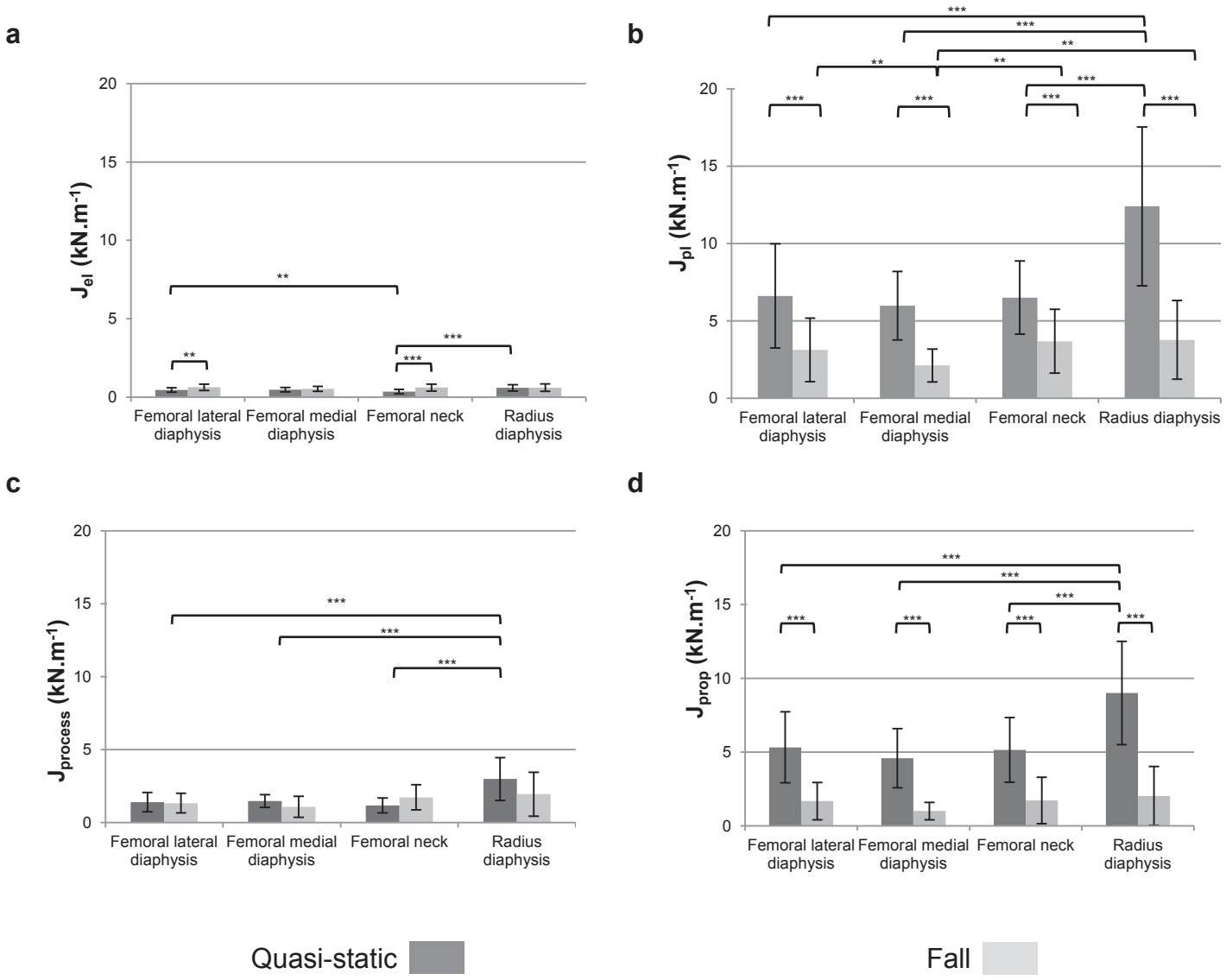

Figure 45 Histograms of the mean values of J_{el} (a), J_{pl} (b), $J_{process}$ (c) and J_{prop} (d) under quasi-static and fall-like loading condition. (* p-value < 0.0001; **p-value < 0.01; * p-value < 0.05)**

- ***Linear elastic strain energy release rate***

All the results obtained verify the condition of the Shapiro-Wilk's normality test (p-value > 0.05). T-tests for paired samples were thus realized to analyze this parameter.

Under quasi-static loading rate, the femoral lateral diaphysis and the radius present a significant higher elastic strain energy release rate than the femoral neck, with a maximum difference between the femoral neck and the radius (- 45%).

Dealing with the influence of strain rate, a significant difference is observed only on the femoral lateral diaphysis and femoral neck: the elastic strain energy release rate increases when the rate is higher. The toughness increases of about 27 % for the lateral region of the diaphysis, and of 43 % for the femoral neck.

- ***Non-linear elastic strain energy release rate***

Some J_{pl} values obtained both from the quasi-static and fall-like loading conditions on the femoral lateral diaphysis and femoral neck, and $J_{process}$ and J_{prop} obtained under fall-like loading conditions on the femoral neck and the radial diaphysis, did not verify the condition of the Shapiro-Wilk's normality test (p-value < 0.05).

A clear influence of strain rate can be observed on the non-linear contribution of the deformation: under fall-like conditions, strain energy release rates decrease. When distinguishing a process and a propagation area on the load-displacement curve, we can observe a significant decrease of J_{prop} for the four locations, from -199 % for the femoral neck to -345 % for the radius; whereas the behavior in the process development area there is no significant influence of loading condition.

Both under quasi-static and fall-like loading conditions, the overall non-linear deformation, represented by J_{pl}, appears to be higher than the elastic contribution J_{el}. When defining different regimes within the plastic contribution, under quasi-static condition, propagation energy release rate, J_{prop}, is higher than the elastic, J_{el}, and the process, $J_{process}$, contribution; whereas under fall like loading conditions, the process zone development and the propagation contributions are comparable.

Table 12 The ASTM J_{el} and J_{pl}, and the indtroduced $J_{process}$ and J_{prop} values obtained for the different anatomical locations: mean (SD); n is the number of subjects. P-values of t-tests for comparison between quasi-static and fall conditions are reported. In the case of a significant difference (p-value < 0.01), the relative difference is given.

Toughness	Strain rate	Femoral lateral diaphysis n=29	Femoral medial diaphysis n=29	Femoral neck n=29	Radius diaphysis n=31
J_{el} (kN.m^{-1})	Quasi-static	0.45 ± 0.2	0.46 ± 0.21	0.34 ± 0.14	0.58 ± 0.20
	Fall	0.60 ± 0.24	0.52 ± 0.21	0.60 ± 0.22	0.60 ± 0.24
p-value		1.10^{-3}	ns*	1.10^{-4}	ns*
Relative difference (%)		27	-	43	-
J_{pl} (kN.m^{-1})	Quasi-static	6.61 ± 4.18	5.99 ± 2.21	6.51 ± 2.36	12.41 ± 5.13
	Fall	3.13 ± 2.04	2.12 ± 1.06	3.69 ± 2.07	3.78 ± 2.55
p-value		7.10^{-8}	8.10^{-11}	1.10^{-4}	2.10^{-10}
Relative difference (%)		-111	-183	-77	-228
$J_{process}$ (kN.m^{-1})	Quasi-static	1.40 ± 0.67	1.47 ± 0.44	1.18 ± 0.51	2.98 ± 1.47
	Fall	1.33 ± 0.67	1.07 ± 0.72	1.73 ± 0.86	1.94 ± 1.50
p-value		ns*	ns*	ns*	ns*
Relative difference (%)		-	-37	32	-54
J_{prop} (kN.m^{-1})	Quasi-static	5.32 ± 2.40	4.58 ± 2.01	5.15 ± 2.19	9.01 ± 3.51
	Fall	1.68 ± 1.27	1.00 ± 0.60	1.72 ± 1.58	2.03 ± 2.00
p-value		2.10^{-7}	4.10^{-9}	2.10^{-6}	4.10^{-10}
Relative difference (%)		-218	-359	-199	-345

*ns: Non-Significant (p-value>0.05, t-test for paired samples)

ii. Biochemical measurements

CX values obtained on the femoral lateral diaphysis, and PEN measurements on the radius did not satisfy the Shapiro-Wilk's conditions of normality ($p < 0.05$).

The mean values (SD) of enzymatic immature cross-links, enzymatic mature cross-links, CX, Pen and collagen are reported in the Table 13.

Figure 46 shows the mean values obtained for CX and PEN measurements on the four anatomical locations. Significant differences are observed depending on the anatomic location. In particular, CX and PEN are higher in femoral neck than in femoral and radial diaphyses. The maximum

difference is noted with the femoral medial diaphysis of about 80 % for CX and 110 % for PEN (p-value < 0.0001). Radius also presents a significant higher CX than femoral diaphysis with a higher difference of about 38 % with the medial region (p-value < 0.0001). There is no difference between femoral lateral and distal diaphysis for CX and PEN.

Annex 2 presents correlations measurement for biochemical parameters between the different anatomical locations. Lateral and medial diaphysis PEN content and CX are significantly positively correlated (p-value < 0.0001). CX was also significantly correlated between femoral neck, and femoral diaphysis, both for medial and lateral region (p-value < 0.01). No correlation was found between the radius and any part of the femur.

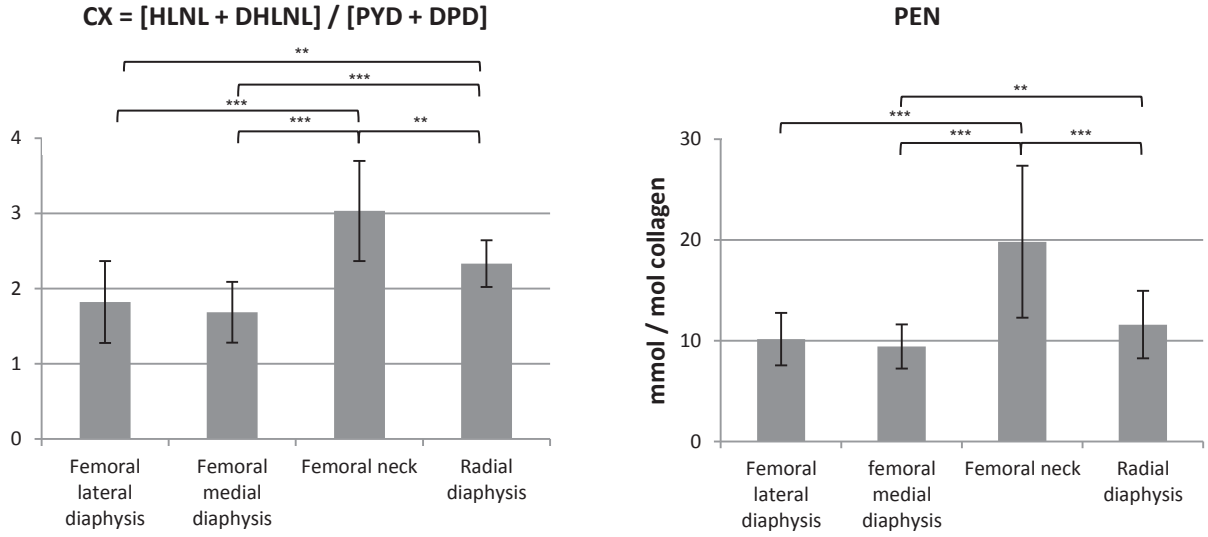

Figure 46 Histograms the mean values for CX and PEN measurements for the four anatomical locations. (* p-value < 0.0001; ** p-value < 0.01; * p-value < 0.05)**

Table 13 Mean values obtain for the different biochemical parameters

Anatomical location	n	[HLNL + DHLNL] (mmol / mol collagen)	[PYD + DPD] (mmol / mol collagen)	CX	PEN (mmol / mol collagen)	Collagen (%)
Femoral lateral diaphysis	29	818.81 (248.76)	439.11 (48.16)	1.82 (0.54)	10.17 (2.60)	13.72 (0.63)
Femoral medial diaphysis	29	779.97 (212.98)	462.60 (44.03)	1.68 (0.40)	9.43 (2.18)	13.35 (0.50)
Femoral neck	25	1008.69 (254.38)	334.09 (40.84)	3.03 (0.67)	19.83 (7.53)	12.25 (0.61)
Radial diaphysis	30	815.46 (143.40)	355.02 (45.37)	2.33 (0.31)	11.59 (3.35)	12.94 (0.91)

iii. Relationships between age, mechanical and biochemical properties

Annex 4 shows the Pearson's coefficient matrix between the age, the mechanical and the biochemical measurements for the four anatomical locations. Figure 47, as an example, represents PEN in relation with age for the femoral diaphysis, and Figure 48 shows the CX in relation with age for the radial diaphysis.

For the femoral diaphysis and radial diaphysis, pentosidine measurements are significantly positively correlated to the age of the subject (Figure 47); whereas CX is negatively correlated to the age only for the radial diaphysis (Figure 48).

No significant correlations were found between CX and biomechanical parameters under quasi-static condition. A wick relation between CX and $J_{process}$ on the femoral diaphysis and radial diaphysis in nevertheless observed (p-value < 0.05).

On the femoral lateral diaphysis, J_{el} and J_{prop} under fall-like condition are correlated to CX.

On the femoral lateral diaphysis, PEN was found to be negatively correlated to J_{el} and J_{prop} under fall-like loading condition.

No significant correlation was found between mechanical and biochemical parameters on the three other locations.

A significant correlation between this CX ratio and $J_{process}$ is found when we investigate the gathered population of femoral and radial diaphysis. In a same was, this correlation was significant but weaker, for J_{pl} and J_{prop}. These correlations were no more significant if we include the femoral neck in the investigated population (Figure 49).

Finally, a significant negative correlation was found between PEN and CX on femoral diaphysis and neck (p-value < 0.01).

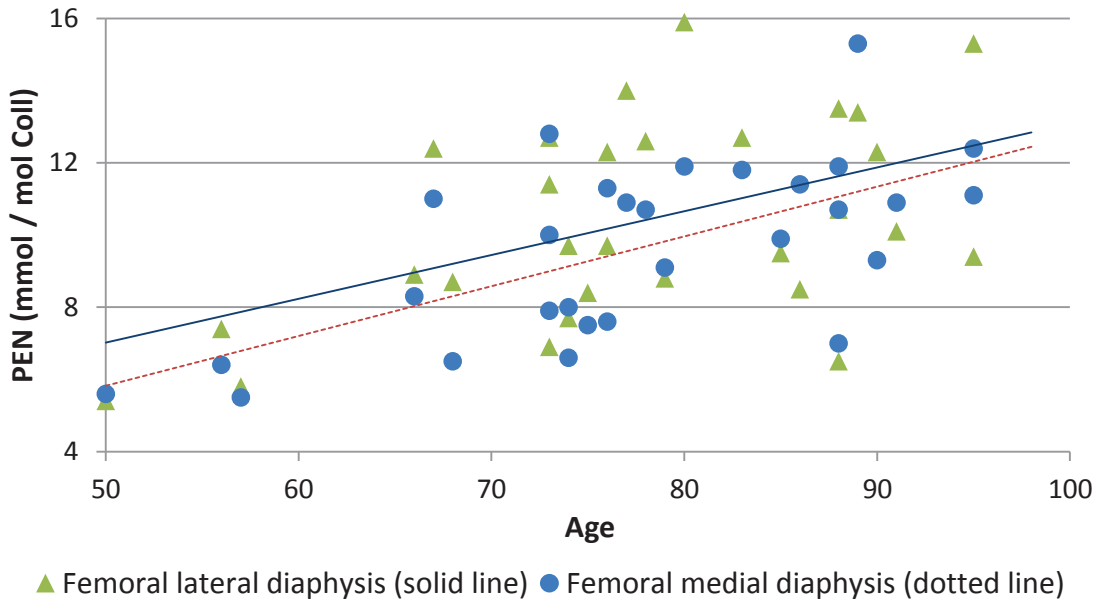

Figure 47 PEN in function of the age for the femoral diaphysis, lateral and medial region (p-value < 0.01)

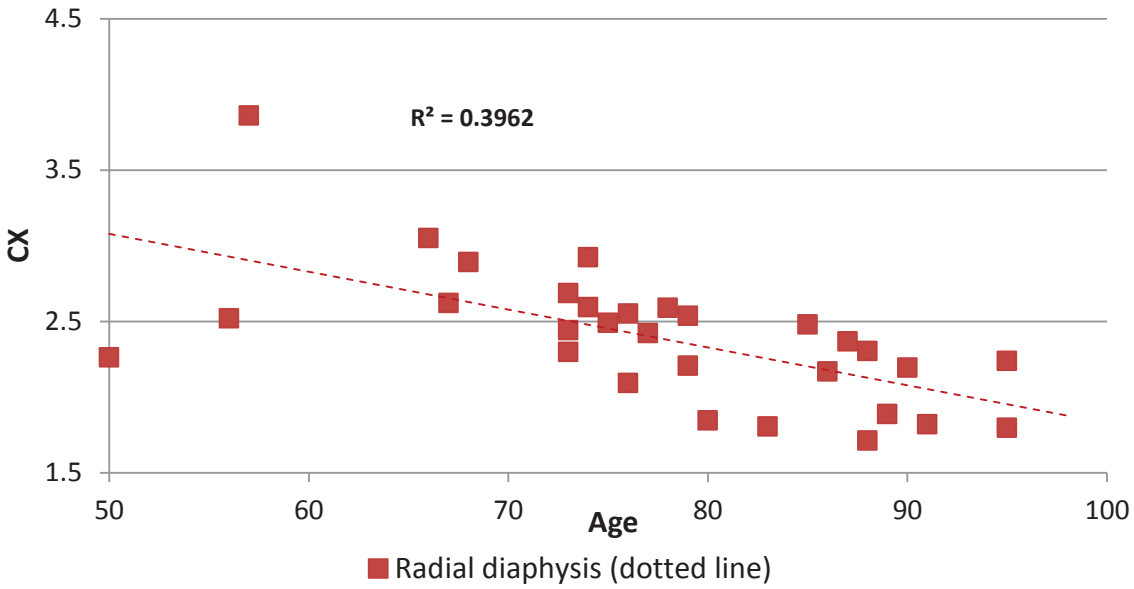

Figure 48 CX in function of the age for the radial diaphysis

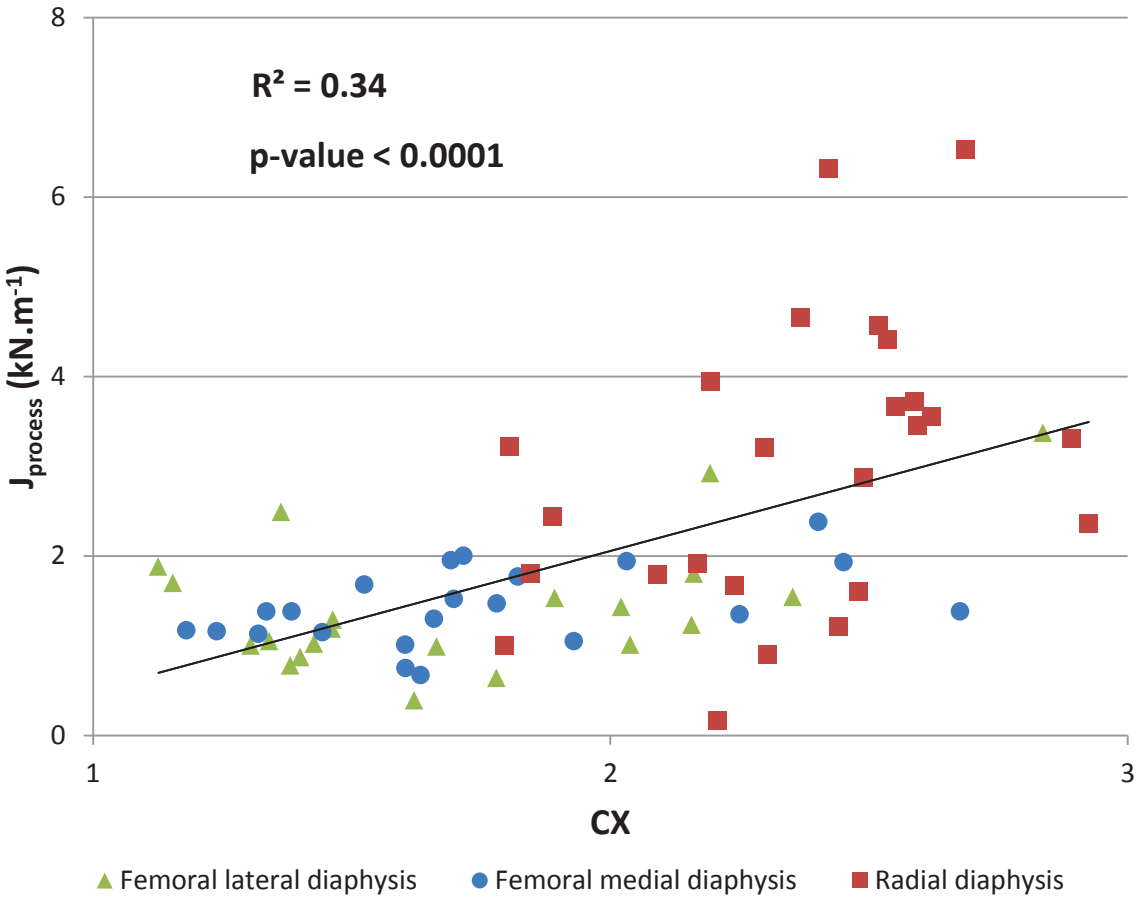

Figure 49 $J_{process}$ under quasi-static loading condition in function of CX. Femoral and radial diaphysis are gathered in a same population for the correlation.

4. Discussion

The main aim of this study was to investigate the potential relation that can be found between fracture behavior, both under quasi-static and fall-like loading condition, and collagen maturation of human cortical bone considering four paired anatomical locations extracted from a population of 32 cadaveric subjects (18 women, age 81 ± 12 y.o.; 14 men, age 79 ± 8 y.o.).

It is known that cortical bone mechanical properties are altered with the maturation of bone collagen (Berteau et al., 2015; Granke et al., 2015; McNerny et al., 2015; Oxlund et al., 1995; Saito and Marumo, 2010; Tang and Vashishth, 2010; Vashishth et al., 2001; Viguet-Carrin et al., 2006; Willett et al., 2013; Zioupos et al., 1999). The majority of these studies considered only one anatomical location, and only few results can be found comparing different bones mechanical and biochemical parameters (Saito and Marumo, 2010). In bone collagen, the maturation of enzymatic

cross-links evaluated by the CX and the increase of non-enzymatic glycation crosslinking measured by PEN content is a reflect of tissue aging and induces changes in its mechanical properties, in particular its ability to undergo nonlinear deformation (Berteau et al., 2015).

A mechanism governing non-linear deformation in human cortical bone is known to manifest as a sliding between collagen fibrils within the tissue (Gupta et al., 2013; Zimmermann et al., 2012). By increasing their content, trivalent mature cross-links and advanced glycation end products, such as PEN, may stiffen the interface between collagen fibrils, thus limiting them to move between each other (Bailey, 2001; Depalle et al., 2015; Granke et al., 2015; Poundarik et al., 2015; Vashishth et al., 2001; Zimmermann et al., 2012).

In a previous study, the effect of strain rate on human cortical bone toughness has been discussed, resulting in a significant decrease of the non-linear strain energy release rate (J_{pl}) with an increased strain rate (Gauthier et al., 2017). In the current study, we introduced the notions of $J_{process}$ and J_{prop} that cut this plastic contribution into two different mechanisms. $J_{process}$ would represent the development of a process zone in front of the notch tip, due to the formation of micro-cracks. J_{prop} may quantify the energy needed to propagate the crack once cortical bone cannot accumulate energy anymore. The results show that, under quasi-static loading condition, non-linear mechanisms are mainly due to propagation mechanism. But under fall-like loading rate, $J_{process}$ and J_{prop} are at the same order of magnitude, reflecting an equivalent contribution to the non-linear crack propagation mechanisms. The effect of strain rate on the propagation mechanism, J_{prop}, is the same as observed previously: there is a lower value at higher rate. For the process zone development mechanism, there is no influence of the loading condition. The difference of J_{prop} between the anatomical locations is the same as the overall plastic contribution J_{pl} under quasi-static loading conditions (Figure 45). Dealing with the difference of biomechanical parameters between the four anatomical locations, the results are the same for $J_{process}$ and J_{prop} as J_{pl}. Under quasi-static condition, radius presents a greater capacity to undergo non-linear mechanisms, both for the process zone development than for the propagation mechanisms. Under fall-like loading condition there is no difference considering the $J_{process.}$ This implies that this is the propagation contribution that is mostly affected by the increase of rate.

In summary, even considering two regimes during the plastic part of the deformation mechanisms, radius appears to resist better to crack propagation in these two regimes than the other locations. Strain rate has a significant negative influence on the toughness for all the anatomical locations for propagation regimes. Finally, under fall-like loading condition, there is no more difference between the different locations.

Biochemical parameters values obtained are in the range of results found in the literature (Berteau et al., 2015; Follet et al., 2011; Karim et al., 2013; Saito et al., 2006, 1997; Saito and Marumo, 2010). Saito et al. also reported a positive correlation between the content of PEN and the age of subjects measured on femoral neck and radial diaphysis, with in their study a larger age range (0 – 80 y.o.) with younger donors than in the current study (50 – 98 y.o.) (Saito and Marumo, 2010). A higher content of PEN in old bone tissue was also measured on human humeri (Zimmermann et al., 2012). A negative correlation between the ratio CX and the age of the subject was also found in (Berteau et al., 2015) on the fibula, as found in the current study the radius. These results are in accordance with the fact that PEN and enzymatic cross-links changes reflect the maturation of cortical bone tissue (Eyre et al., 2010; Sroga et al., 2015; Viguet-Carrin et al., 2006), even if the age of the tissue

is not exactly the age of the subject. Eventual differences can be explained by the age range for the studied population, or the anatomical locations used to measure biochemical parameters (Saito and Marumo, 2010). The values obtained on the femoral neck appear to be slightly different to the literature (Karim et al., 2013; Saito et al., 2006). For example, PEN content measured in the current study (19.83 ± 7.5 mmol / mol collagen) is higher than in (Saito et al., 2006) (7.82 ± 3.45 mmol / mol collagen) or in (Karim et al., 2013) (~ 10 mmol / mo collagen). These differences may come from the bone samples used to measure biochemical parameters in the current study. As a major part of cortical bone on the femoral neck was used to prepare samples for biomechanical experiments, the remaining part of cortical was thin. As femoral neck is mainly composed of trabecular bone, it is possible that this remaining part of bone contained some region of trabeculae. It has been shown in the past that the PEN content of trabecular bone is higher than in cortical bone (Karim et al., 2013; Saito and Marumo, 2010).

In the present study, we showed that, in term of enzymatic cross-links composition (meaning CX), femur is a strictly different material than the radius, whereas femoral medial and lateral diaphyses are highly correlated ($r = 0.92$), and are both correlated to the femoral neck ($r = 0.77$ and $r = 0.81$, for lateral and medial, respectively).

The difference seen between the anatomical locations might be explained by different remodeling mechanisms. The amount of immature and mature cross-links are directly linked to the bone tissue turnover rate (Bailey et al., 1998; Viguet-Carrin et al., 2006). It has been shown that a low CX is typical of osteoporotic patients (Viguet-Carrin et al., 2006). A high content of PEN might alter tissue remodeling process (Tang et al., 2009; Viguet-Carrin et al., 2006) which is confirmed in the current study on the femur, as PEN is negatively correlated to CX (meaning a decrease of the immature form within the tissue). These differences of remodeling might be due to the specific function of each bone in the skeleton (Wolff, 1892).

Results concerning the relationships between biomechanical and biochemical properties found in the literature show that maturation of collagen has an influence on the cortical bone capacity to undergo non-linear deformation [8]. Values found in the current study are different from those found in the literature. Maturation of bone, represented by a decrease of CX ratio (meaning an increase of mature cross-links beside immature ones) is not correlated to the decrease of J_{pl}, $J_{process}$ or J_{prop} under quasi-static condition, considering individual locations. This may be due to the difference of population. In Berteau et al., the age of subject is ranged from 5 to 99 years old separated into two groups (7 children of 10 y.o. in average, 3 elderly adults of 79 y.o. in average).

This different of age between the two groups involves a high difference of mechanical and compositional properties of the tissue between the two groups.

By gathering femoral and radial diaphysis, we found that there were a significant correlation between CX ratio and $J_{process}$ thus suggesting that by investigating a larger population of donors, we may have found significant correlations between collagen maturation and human cortical fracture behavior under quasi-static loading condition. But still the correlation coefficient remains small ($r^2 = 0.34$). This result also confirms the difference of femoral neck maturation of collagen among the other anatomical locations.

To our knowledge, no information is available concerning the relationship between biomechanical properties under fall-like loading condition and biochemical parameters. In the current study we found that there was a correlation between PEN and J_{el} and J_{prop} under fall-like loading conditions only on the femoral lateral diaphysis ($r = - 0.59$ and $r = - 0.54$ for J_{el} and J_{prop}, respectively).

These results confirm that human cortical bone is a complex material that depends on its location and function in the organisms. We have shown here that crack mechanisms are different from a location to another and depend on the loading rate. If the main contribution under quasi-static loading condition is assigned to the propagation mechanisms, under fall-like condition, an equivalent contribution of the development of a process zone and of the actual crack propagation is observed on the four locations. Strain rate has a major influence on cortical bone capacity to control crack growth when it is initiated.

Regarding biochemical parameters correlations, we can affirm that collagen maturation mechanism is dependent on the anatomical location of the bone. The weight bearing bones, femoral diaphysis and neck, appear to have significantly correlated maturation mechanisms that are different from the radius, a non-weight bearing bone (Annex 2), even if femoral neck presents a significantly higher CX ratio. This result may be explained by considering that bone turnover rate is dependent on its mechanical environment during life. In this study we also confirm that the PEN content is related to the age of the subject and may alter the turnover rate.

Comparing to some results found in the literature, the results found in the current study don’t allow confirming that collagen maturation is associated to a decrease in human cortical bone fracture behavior.

This study presents some limitations. Concerning the biomechanical experiments, limitations are discussed in (Gauthier et al., 2017). Regarding the biochemical measurements, the main limitation

is that sample were taken from cadaveric subjects, and were then stored at –20 °C until measurements. Some studies show that the action of freezing may not affect the measured concentration with an HPLC system (Bergmann and Sypniewska, 2016). As all our samples followed the same preparation protocol, we may assume that we can perform comparative analysis within our samples population. Considering that all the 236 samples tested in this study have followed the same storage and preparation protocol, we can assume there is no inter- group bias. Hence a comparative study is pertinent, even if the storage conditions may affect the material properties. Second, the studied population can be considered as old (79 ± 11 y.o.). It is well known that bone chemical composition changes with age. This point is important to consider when interpreting our results; studies on samples with a wider age distribution may lead to different results. Nonetheless, the samples used in this study are representative of those that suffer the most from fractures (Nanes and Kallen, 2014), and as such provides insight into the factors that contribute the most to cortical bone strength in this age group. That is also the reason why relation with age are not that obvious than in other studies where age range is larger (Berteau et al., 2015; Saito and Marumo, 2010).

In the current study we have found that there was no influence of collagen cross-links maturation on human cortical bone fracture behavior considering individually the four paired anatomical locations. A significant correlation was found by gathering femoral and radial diaphysis. Fibrillar sliding mechanism is although known to play a major role in human cortical bone crack propagation mechanisms. It is also assumed that the inter-fibrilar sliding efficiency may depend on loading condition [19]. Further work should be done investigating the influence of other compositional parameters, as the osteopontin, on this particular sliding mechanism [42–44]. Future investigations can also be performed evaluating the influence of some structural parameters on human cortical bone fracture behavior as it is known that some structural features, such as the osteons, play a major role in crack propagation mechanisms in human bone [45].

5. Conclusion

The maturation of collagen cross-links is thought to be associated to a decline in human cortical bone fracture properties under quasi-static loading. However, in the current study we have shown that the relationship between collagen cross-links maturation and cortical bone toughness is not significant enough to state that there is an influence of collagen composition in human bone fracture behavior. Although a wick correlation has been measured between the CX ratio and cortical bone capacity to develop a process zone implying the need of a better understanding of the different mechanisms involved this particular mechanical regime. This process zone development is assume to be associated with the emergence of micro-damages within the tissue.

Chapter V What is the influence of strain rate on human cortical bone crack propagation mechanisms?

Abstract: Cortical bone fracture mechanisms are well known under quasi-static loading condition. However the influence of strain rate on this mechanical process need to be better understood as bone fractures mainly occur after a fall from a standing position. Previous results show that the whole porosity network, from the Haversian system to the lacunar network, as well as the collagen cross-links maturation might be involved in the decrease in bone capacity to resist crack propagation. Thus, the aim of the current study is to gather morphometric and biochemical parameters to make an overall characterization of human cortical bone organization considering 8 paired femoral diaphyses, femoral necks and radial diaphyses. Results showed that if collagen cross-links are involved in the elastic contribution of the fracture process, the plastic one is governed by the porosity network under quasi-static loading. Under fall-like loading condition, the cortical porosity is less involved in crack propagation mechanisms.

1. Introduction

From a clinical point of view, the prediction of bone fracture risk remains limited to reach an accurate diagnostic (Siris et al., 2014, 2004). Clinical gold standard methods are based on the assessment of bone density using Dual X-rays Absorptiometry (DXA) (Genant et al., 1996).

Bone density measurement is however not sufficient to accurately predict the fracture risk: almost 50 % of the patients diagnosed as "not at risk" will still suffer from a bone fracture (Siris et al., 2014, 2004). This single parameter does not describe the overall mechanical response of bone in a fall loading configuration. Other parameters, such as geometrical, compositional or architectural have to be considered to understand bone fracture process (Seeman and Delmas, 2006).

From a mechanical point of view, the fracture risk can be defined as the ratio between load that is applied on the organ and its failure load (Hayes et al., 1991). Bone fracture generally occurs after a fall from a standing position involving thus high loading rate (Dubousset, 2014; Gryfe et al., 1977; World Health Organization, 2007). Thus it was assumed that to improve fracture risk prediction the effective fracture load in a fall loading configuration has to be considered.

Cortical bone toughness appears as a good candidate to improve biomechanical knowledge on this fracture process as it provides information on the energy needed to propagate a crack through the complex cortical bone structure (Ritchie, 1988). During crack propagation, number of toughening mechanisms occur in order to arrest the crack and thus increase the energy needed to break the material (Gupta et al., 2013; Nalla et al., 2004b; Tang and Vashishth, 2010; Zimmermann et al., 2011; Zioupos et al., 2008). These mechanisms depend on the organization of the cortical tissue. For example, micro-cracks formation is dependent on the Haversian network (O'Brien et al., 2005a), crack deflection on the osteons (Burr et al., 1988; Koester et al., 2008), interfibrillar sliding may depend on the collagen maturation (Berteau et al., 2015; Depalle et al., 2015). If the role of the Haversian systems is established, little is known about the lacunae because of the complexity to assess accurately this network (Granke et al., 2016).

Human cortical bone toughness has been largely studied under quasi-static loading condition. As bone fractures occur at higher rate, it seems important to analyze the influence of this loading rate. Recent studies show that at higher strain rate, bone toughness significantly decreases (Gauthier et al., 2017; Zimmermann et al., 2014). The understanding of these

significant differences with regards to the microstructure might be of interest. Moreover, as discussed previously, bone microstructure is different from an anatomical location to another, similarly to the toughness under a quasi-static loading condition (Gauthier et al., 2017).

The aim of this study is thus to pool biomechanical results with composition and morphometric analyses on 8 paired femoral diaphyses, femoral necks and radial diaphyses to first understand the difference seen between these anatomical locations under quasi-static loading. The second objective is to understand the significant decrease of toughness due to the increase in strain rate.

2. Materials and methods

Samples studied in this current section are the same as those studied with the synchrotron radiation (Chapter III).

Paired femoral diaphyses, femoral neck and radial diaphyses were collected from 8 women cadaveric subjects (70 ± 14 y.o., min: 50 y.o., max: 91 y.o.). No additional information regarding disease status or medication history was available. Extracted bones were wrapped in gauze soaked with saline to keep them hydrated, then stored at -20 °C until sample preparation. Two rectangular samples, with a width of W = 2.1 ± 0.1 mm and a thickness B = 1.0 ± 0.1 mm, were extracted from each bone using a low speed saw with a diamond coated blade (ISOMET 4000, Buehler, USA). The samples were prepared so that their long axes were parallel to the osteons. A notch was performed in the middle of each bone, perpendicularly to the osteon. A quasi-static (10^{-4} s^{-1}) toughness experiment was performed on one of them. The other was tested at a strain rate representative of a fall (10^{-1} s^{-1}, (Foldhazy, 2005)) to evaluate the effect of strain rate (Gauthier et al., 2017). Due to mechanical testing, samples were split in two parts. Only one part was used for image acquisition, resulting in a population of 48 samples (24 under quasi-static condition, 24 under fall-like condition). They were stored at -20 °C, a defatted protocol was performed one week before the images acquisition. Cortical bone specimen were immerged in acetone for 30 minutes, then rinsed with water, and finally dehydrated by successive immersion in 70 % and 100 % alcohol baths for maximum 2 days. On each sample, two volume of interest (VOI) were chosen. The first one (VOI1 on Figure 34) corresponds to a control area located outside of the support rollers where no particular mechanical stress were applied. The second one (VOI2 on Figure 34) corresponds to a damaged region, where a main crack propagates during mechanical test, involving a high stress concentration state. The final imaging protocol consists thus of 48 acquisitions. The cortical bone falls stemmed from the previously

enounced sample preparation were cut into small pieces, powered in liquid nitrogen-cooled freezer mil (Spex Centriprep, Metuchen, USA), demineralized with daily changing of 0.5 M EDTA in 0.05 M in Tris buffer, pH 7.4 for 96 h at 4 °C. The demineralized powder was then extensively washed with deionized water. The samples were then suspended in phosphate buffered saline (0.15 M sodium chloride, 0.1 M sodium phosphate buffer, pH 7.4) and reduced in $NaBH_4$ at room temperature for 2h using a reagent/sample ratio of 1:30 (w/w). The reduced bone residues were washed, freeze-dried and hydrolyzed in 6 M hydrochloric acid at 110 °C for 20 h. These hydrolysates were used for the measurement of cortical bone collagen cross-links.

i. Biomechanical measurements

Biomechanical parameters discussed in this current section are the different strain energy release rates: J_{el} ($N.mm^{-1}$), $J_{process}$ ($N.mm^{-1}$), $J_{propagation}$ ($N.mm^{-1}$) and J ($N.mm^{-1}$) both under quasi-static and fall-like loading conditions (Figure 50). The parameter $J_{el} + J_{process}$ ($N.mm^{-1}$) will also be discussed as the total stored energy within cortical tissue before the actual main crack propagation.

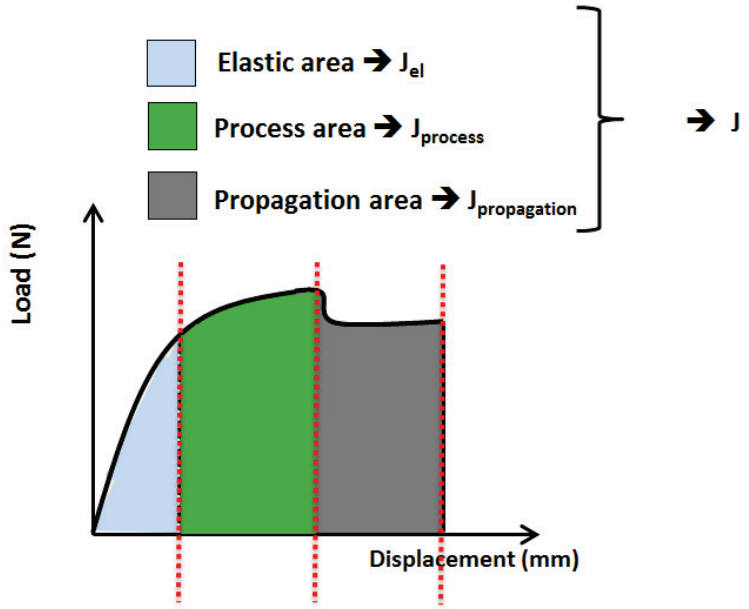

Figure 50 Typical load-displacement curve obtained for human cortical bone toughness experiments with definition for the different biomechanical parameters.

ii. Morphometric measurement

Morphometric parameters of the haversian and osteocytes systems were investigated with SR-μCT (see Chapter III): We report the most important parameters in the context of this study: Haversian volume fraction Ca.V/BV (%), Haversian canals diameter Ca.Dm (μm), lacunar density Lc.N/BV (mm^{-1}) and the radius of curvature of the ellipsoidal lacunae Lc.ρ_1 (μm) were used for discussion in the current section. In addition the distribution of the absorption coefficient μ (cm^{-1}) was also available.

iii. Biochemical measurements

Pyridinoline (PYD) and deoxypyridinoline (DPD) mature cross-links and didhydroxylysinonorleucine (DHNL) and hydroxylysinonorleucine (HLNL) immature cross-links were measured (Chapter IV). The sum of mature [PYD + DPD] and immature [HLNL + DHLNL] as well as their ratio CX [HLNL + DHLNL] / [PYD + DPD] was discussed here.

iv. Statistical tests

In order to make statistical tests on more than 8 samples, all the three anatomical locations were clustered to finally have a population of 24 samples for each biomechanical parameter (8 femoral diaphyses, 8 femoral necks and 8 radial diaphyses). Analyses were also performed for each individual site to have information on their respective contributions.

Shapiro-Wilk's normality tests were not satisfied for some of the different parameters discussed in the current study, thus Spearman's coefficient was measured to investigate correlations between the measured parameters.

Multiple linear regressions using backward stepwise elimination to remove the non-significant parameters were performed until obtaining significant relation to explain the variance of the biomechanical parameters. Statistical significance were considered for p-value < 0.05.

Statistical analyses were performed using StatView (StatView, Abaqus, USA).

3. Results

Table 14 presents the contribution of each strain energy release rate to the global parameter J. Under the quasi-static loading condition, the energy dissipating mechanisms are mainly due to the crack propagation, whereas the elastic contribution is small. Under the fall-like

condition, the contributions are more equilibrated, with a higher dissipation of energy during the process zone development.

Table 14 Relative contribution of each parameter to the overall strain energy release rate J

	J_{el}	$J_{process}$	$J_{propagation}$
Quasi-static	5 %	20 %	75 %
Fall	24 %	43 %	33 %

Table 15 presents the Spearman's coefficients between the biomechanical and biochemical or morphometric parameters. The correlation for each anatomical location is shown on Annex 5. Haversian canals diameter appears to have a negative influence in the three regimes of deformation of cortical (see Figure 50) under quasi-static loading (p-value < 0.01). Lacunar radius of curvature, $Lc.\rho_1$ is positively correlated to strain energy release rate, particularly considering the plastic contribution of the deformation (p-value < 0.01). Under fall-like loading conditions, results are less clear. Haversian system has a negative influence on J_{el} and collagen divalent immature cross-links are positively correlated to J_{el} and J (p-value < 0.05). Considering the respective contribution of each location (Annex 5), Haversian canals diameter appears to be highly negatively correlated to $J_{el} + J_{process}$ for the femoral and radial diaphysis under fall-like loading condition (p-value < 0.05). But this correlation is not significant when considering the three locations in a same population (Table 15).

Table 15 Spearman's coefficient between biomechanical and biochemical or morphometric parameters.

Biomechanical parameter	Rate	Immature	Mature	μ	Ca.Dm	Lc.N/BV	Lc.ρ_1
J_{el}	QS	0.03	0.23	**0.55****	**-0.55****	-0.27	**-0.51***
	F	**0.52***	0.34	0.23	**-0.41***	-0.19	-0.17
$J_{process}$	QS	0.08	0.05	0.30	**-0.59****	-0.07	**-0.57****
	F	0.03	0.00	0.32	-0.23	-0.15	0.02
$J_{el} + J_{process}$	QS	0.04	0.12	0.034	**-0.62****	-0.10	**-0.59****
	F	0.28	0.01	0.23	-0.17	-0.20	-0.16
J	QS	0.15	0.04	0.32	**-0.58****	-0.14*	**-0.67****
	F	**0.46***	0.13	-0.03	-0.02	-0.15	-0.13

** p-value ≤ 0.05; ** p-value ≤ 0.01; QS: quasi-static; F: fall

Table 16 presents the best multivariate linear regression explaining biomechanical variances with biochemical and morphometric parameters. Figure 51 and Figure 53 show the linear regressions between J under quasi-static loading condition and the co-variates that best explain its variance.

Dealing with the elastic contribution, both for the quasi-static and the fall-like loading condition, biomechanical variance can be explained up to 43 %. The absorption coefficient μ and the mature cross-links content are co-variates for both of the parameters. Lc.ρ_1 is the co-variate that shows the better individual correlation for the quasi-static. For fall-like condition, the immature cross-links content appears to be the main predictor co-variate.

Best prediction considering the process strain energy release rate was found with Ca.Dm and Lc.ρ_1 as co-variates, with a variance explanation up to 50 % for $J_{el} + J_{process}$ under quasi-static loading conditions. No statistically significant prediction was found for the fall-like condition. No more correlation with collagen cross-links were found.

Considering the whole deformation, J variance under quasi-static condition can be explained up to 56 % using immature cross-links content, Ca.Th and Lc.N/BV as co-variates. Cross-links content appear to play a minor role in the prediction. The better fit for J under fall-like loading were find with Immature cross-links content and Lc.N/BV as co-variates, with a variance explanation up to 19 %. The contribution of cross-links on the elastic part is not

significant on this global parameter considering both elastic and plastic deformation. As the plastic deformation represents 95 % of the all curve, the elastic deformation contribution is not significant when considering J.

Table 16 Multivariate linear regression explaining the variance of biomechanical parameters.

		Best combination	p-value	Adj-R^2
J_{el}	QS	$-4.249 + 0.001 * Mature + 2.941 * \mu - 0.0741 * Lc.\rho_1$	**0.005**	**0.43**
	F	$-16.578 + 0.001 * Immature + 0.001 * Mature + 8.294 * \mu$	**0.004**	**0.44**
$J_{process}$	QS	$8.926 - 0.023 * Ca.Dm - 0.854 * Lc.\rho_1$	**0.0009**	**0.47**
	F	-	-	-
$J_{el}+J_{process}$	QS	$10.015 - 0.024 * Ca.Dm - 0.939 * Lc.\rho_1$	**0.0008**	**0.53**
	F	-	-	-
J	QS	$27.874 + 0.007 * Immature - 0.093 * Ca.Dm - 2.640 * Lc.\rho_1$	**0.0004**	**0.57**
	F	-	-	-

QS: quasi-static; F: fall

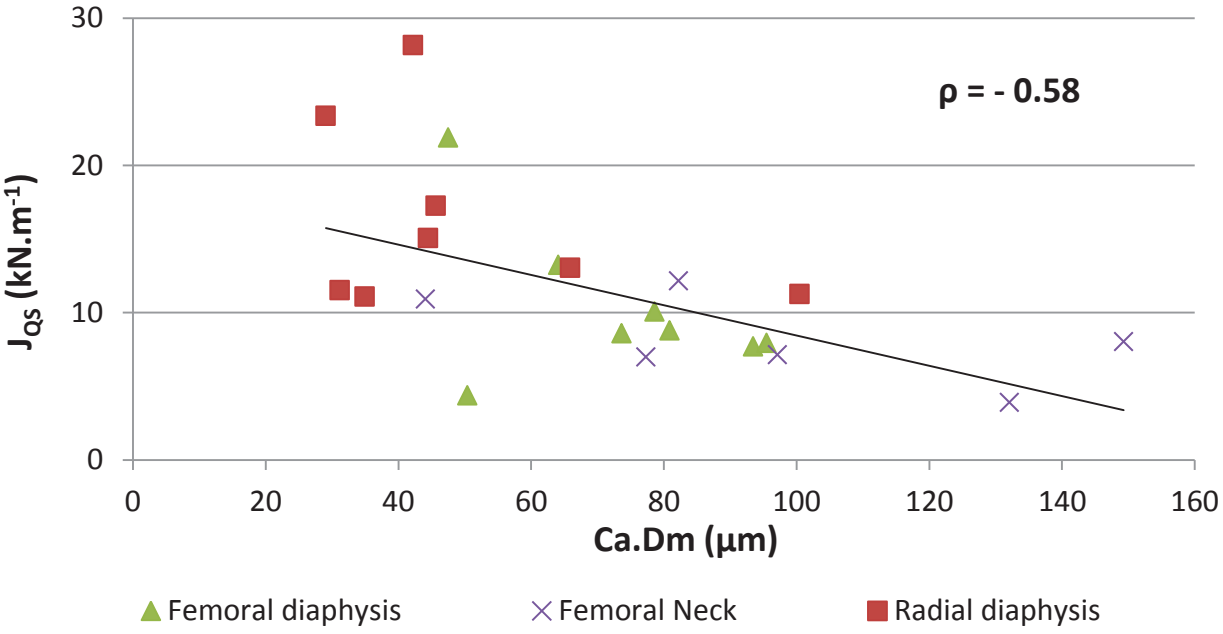

Figure 51 Ca.Dm in function of J under quasi-static loading condition; ρ is Spearman's coefficient (p-value < 0.01)

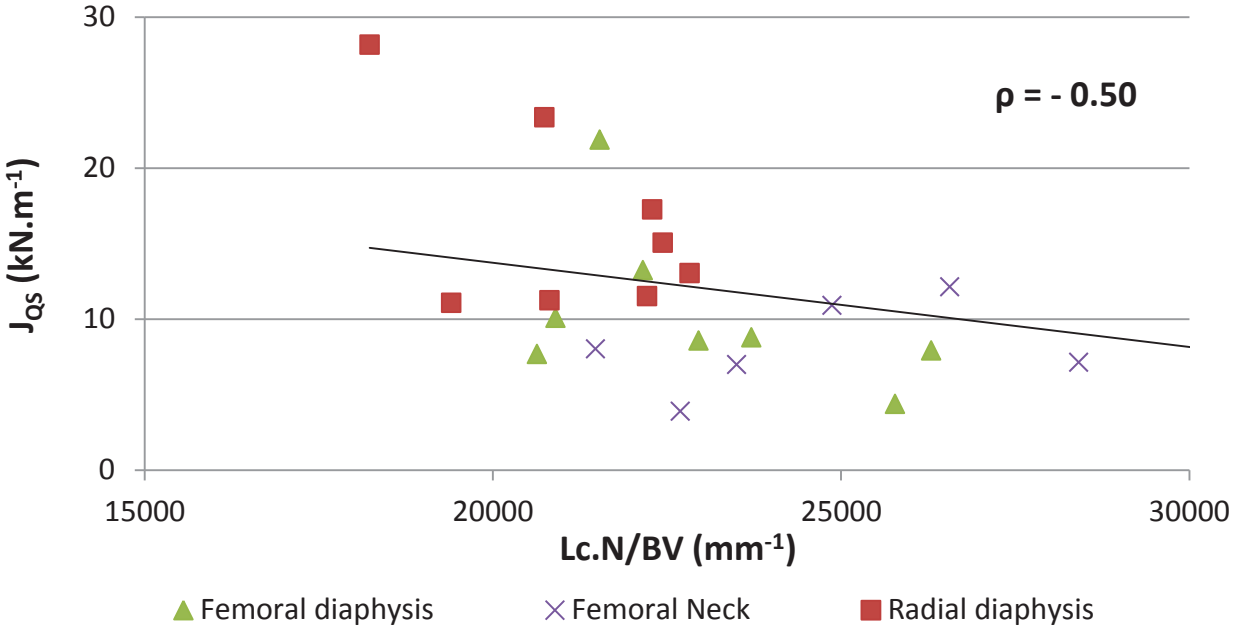

Figure 52 Lc.N/BV in function of J under quasi-static loading condition; ρ is Spearman's coefficient (p-value < 0.01)

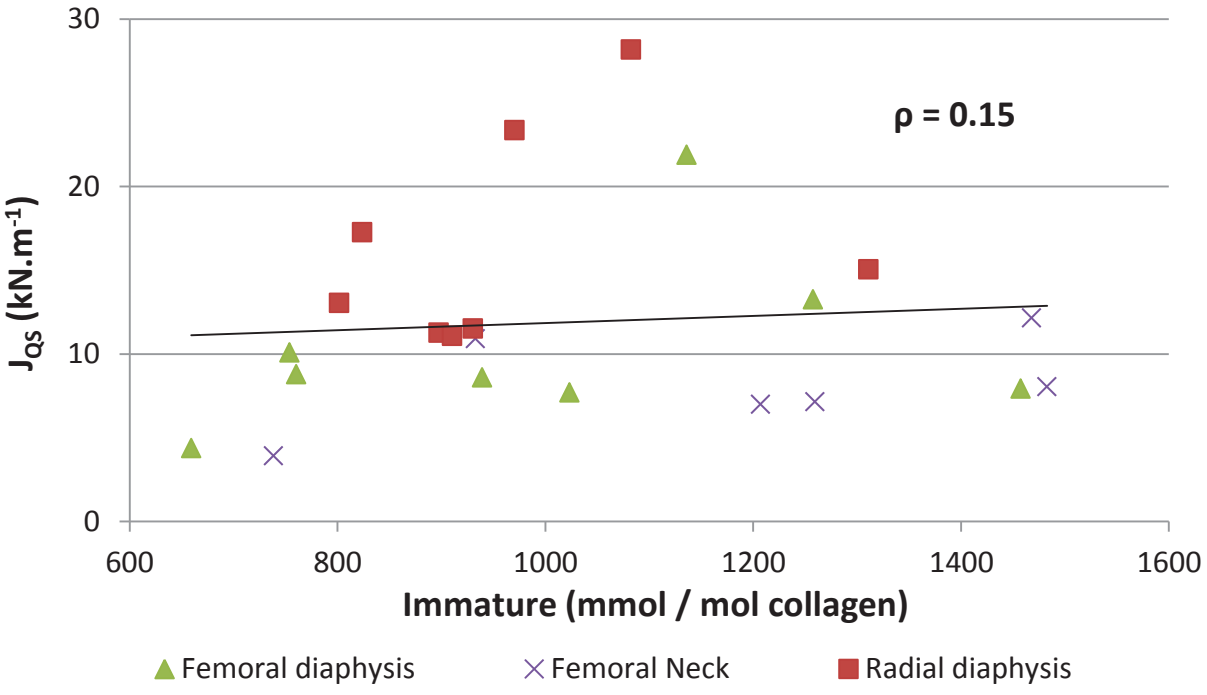

Figure 53 Immature in function of J under quasi-static loading condition; ρ is Spearman's coefficient

4. Discussion

A better knowledge of human cortical bone fracture properties is of great interest for a better understanding of bone fracture risk. Cortical bone is a complex material showing a multi-scale arrangement of organic and mineral (Rho et al., 1998). During crack propagation, the overall organization of cortical tissue is harvested in order to slow down the fracture process (Seeman and Delmas, 2006). From the osteons to the collagen fibers, all the possible sources of crack arrest were discussed in the past (Abraham et al., 2015; Berteau et al., 2015; Granke et al., 2016, 2015; Gupta et al., 2013; Poundarik et al., 2015; Viguet-Carrin et al., 2006; Yeni and Norman, 2000b; Zimmermann et al., 2012). The majority of these studies assessed the role of cortical structure in crack propagation mechanisms under quasi-static loading condition. Only one group studied the effect of loading rate on human cortical bone toughness and discussed the results with regard to the tissue architecture (Zimmermann et al., 2014). As strain rate has a significant influence on bone toughness (Gauthier et al., 2017; Zimmermann et al., 2014) and that fractures occur at higher rate than those investigating in the literature, the aim of this study was to analyze the influence of the cortical bone microstructure on both human cortical bone toughness under quasi-static and fall-like loading conditions.

Considering the elastic contribution under quasi-static loading, a positive correlation was found with absorption coefficient μ, confirming previous results. The later can therefore give information on the density of the tissue, the higher is μ the denser is the material. The presence of mineral within collagen matrix has been shown to improve its stiffness and thus increase the energy needed to stretch collagen fibrils (Buehler, 2007). Elastic toughening mechanism may be mainly governed by a molecular uncoiling and stretching (Depalle et al., 2015; Gupta et al., 2013; Launey et al., 2010).

Few results are available concerning the relationships between lacunar morphometric parameters and elastic mechanical behavior. Granke et al. found a positive correlation between linear elastic toughness and the volume fraction of lacunae (Granke et al., 2016). In the current study, we found a negative correlation with the morphometric parameter $Lc.\rho_1$: the pointer are the lacunae, higher is their capacity to concentrate stress and thus relax the main crack tip. This process involves that more energy is needed to propagate the crack through cortical bone microstructure. This difference may come from that Granke et al. made a 2D analysis, whereas we have a three dimensional information in the current study (Granke et al., 2016). Recent results show that lacunae act as strain amplifiers (Langer and Peyrin,

2015; Rath Bonivtch et al., 2007). In that way, they may play the role of small stress concentrators, dissipating thus the energy at the notch tip of the sample. With a sharper ellipsoidal shape, the stress concentrators might be more efficient to localize stress (Nishida et al., 1994).

Mature cross-links content also appear to improve the prediction of J_{el} under quasi-static loading. These trivalent enzymatic cross-links may stiffen the tissue when increasing their content (Depalle et al., 2015; McNerny et al., 2015; Viguet-Carrin et al., 2006). A higher stiffness implies more energy needed to stretch the collagen molecules.

Under fall-like loading condition, there is no more contribution of the lacunar network, and a higher contribution of the biochemical parameters considering the elastic contribution. It has recently been assumed that at higher strain rate, the elastic behavior of cortical bone, due to molecular stretching, becomes more important due to the viscoelastic nature of the deformation of collagen chains (Zimmermann et al., 2014). However, no accurate results are available concerning these elastic energy dissipating mechanisms under fall-like loading condition. The high level of prediction (explaining the variance up to 43 %) is not negligible for this parameter as it represents 24 % of the overall toughness (Table 14).

We can observe that, under quasi-static condition, considering the process zone development alone, or with the elastic contribution, the result is nearly the same, as the elastic contribution represents only 4 % of the J parameter, whereas J_{proces} accounts for 20 %. The Haversian diameters appears to be a better co-variate as the absorption coefficient, these two parameters being correlated (ρ = -0.82, p-value w 0.01). The Haversian system is assumed to be a major determinant for bone crack propagation mechanisms as it is related to the amount of osteon within the tissue, cement lines are known to influence on crack path during propagation (Burr et al., 1988; Mischinski and Ural, 2011; Yeni and Norman, 2000a). Here we found that samples with smaller canals (that also mean lower volume fraction of canals, see chapter III) may consume more energy to develop the process zone. This may be analyzed as the capacity to create longer micro-cracks (O'Brien et al., 2005a).

No significant relation were found to explain the variance of the process parameters ($J_{process}$ and (J_{el} + $J_{process}$) under fall-like loading condition. With the increase of strain rate, microstructure may have less influence on the capacity bone has to undergo micro-cracks formation during the process zone development.

Considering now the overall strain energy release rate, we can see that the haversian system also play a role in slowing down the fracture process. And as the propagation regime account for a major part in this process, we can assume that canal diameter does have an influence on the crack path under quasi-static loading condition. Smaller are these canals, higher is the energy consumed within the tissue to propagate the crack. This Haversian canals related mechanism during propagation is probably related to the osteons. Smaller canals may imply smaller osteon. It is assumed that cement lines act as barrier to arrest crack propagation. Smaller osteons imply less barriers to crack propagation within the tissue. Another point to highlight the determinant role of Haversian system in the cortical bone fracture process is the formation of the so-called secondary cracks (see chapter III). These cracks may be issued from a crack branching toughening mechanism during the propagation regime ($\rho = 0.50$, p-value < 0.05, Spearman's coefficient with $J_{propagation}$ under quasi-static loading) (Sumi et al., 1983). Our analysis showed that these secondary cracks are related to the Haversian system, and specifically to the canals volume fraction ($\rho = - 0.45$, p-value < 0.05).

The lacunar network also appears to have an influence on the overall fracture process under quasi-static loading condition. If the lacuna radius of curvature seems to individually have a greater contribution, the inclusion of the lacunar density and canals diameter improve prediction of the energy dissipated mechanisms. We can notice that $Lc.\rho_1$ and Lc.N/BV are significantly correlated ($\rho = 0.68$, p-value < 0.01). Regarding this point, we may assume that lacunae play the role of weak defects among which the crack path can be made. With a more important density of lacunae, the tissue might be easier to cut through. From a biological point of view, this latter result appears to be counter intuitive as lacunae play a major role in bone remodeling process so as it can replace its damaged regions in order reach a better mechanical resistance. A too high lacunar density may reflect a more frequent turnover because of a higher fatigue of the tissue. Femoral neck, that has a significantly higher lacunar density, may be subject to a more complex mechanical loading during daily life due to his anatomical location compare to femoral and radial diaphysis. For this reason it might undergo more turnover to insure its function.

We can also notice that the divalent immature cross-links content is a co-variate that enhances J prediction under quasi-static loading. The biochemical contribution is therefore much lower than morphometric parameters (Table 15, Figure 51 -Figure 53).

Dealing with the global parameters, J, under fall-like loading condition, the best fit multivariate prediction, even if significant, is quite low (Adj. $R^2 = 19$ %, p-value = 0.05).

This best fit also involves a negative influence of the lacunar density and a positive one of immature cross-links content. We can notice that Haversian network is not a co-variate in that case.

In summary, regarding these different results, we can confirm that microstructural parameters have more influence on the fracture process under quasi-static loading condition than the biochemical parameters. These structural properties have much lesser influence in a fall-like condition of loading.

This study presents some limitations. The first one concerns the particular population studied (8 women, 50 – 91 y.o.), and has already been discussed in the previous studies. Here we decided to cluster the three anatomical locations to enhance the statistical power and analyze a population of 24 specimens rather than 8. This is a questionable point as we have shown in the previous studies that femoral diaphysis, femoral neck and radial diaphysis are different material regarding toughness, microstructrual and biochemical parameters. When analyzing the individual correlations, we can notice that Ca.Dm is highly correlated to the $J_{process}$ under fall-like loading condition for femoral and radial diaphysis. It is therefore harder to list strong evidences on a small population of 8 samples. If the inter-site differences may first be seen as a limitation in the current study, we can also assume that if the correlation is confirmed despite these differences, then the conclusion on the results is reinforced. If results found in this study are not representative of the reality considering individual anatomical locations, it shows a real trend of what occurs during fracture process in human cortical bone.

5. Conclusion

The aim of this study was to enhance biomechanical knowledge on the fracture process of human cortical both under quasi-static and fall-like loading conditions. This study combines biochemistry and imaging data to assess both collagen links, and micro-structure in relation to biomechanical tests. Regarding the results we can affirm that bone crack propagation mechanisms depend on the complex architectural arrangement of the tissue. Under quasi-static loading, the Haversian system and the lacunar network are the main contributors for cortical bone toughness. Considering fall-like conditions, the contribution of the microstructure is less significant. The elastic contribution can be associated to collagen cross-links and tissue density for the fall-like condition. But no relation has been found for the plastic crack propagation mechanisms. Thus this study suggests different that human cortical bone undergoes different crack propagation mechanisms whether it is loaded under standard quasi-static or fall-like conditions.

Conclusion

This study brought new biomechanical knowledge related to bone fracture mechanisms. Bone fractures in the elderly still remains a major worldwide problem, involving both healthcare problems and high economic burden. A better understanding of the mechanisms of fracture within human cortical bone tissue seems to be a first step regarding the global clinical process of bone fracture prediction.

The first chapter of this document introduces the background on cortical bone fracture mechanisms and investigation techniques. Cortical bone toughness and fracture mechanisms have largely been studied in the past on both animal and human subjects under quasi-static condition. But a large proportion of these studies considered the femoral diaphysis whereas it is not the location of fragility in the elderly. The influence of loading conditions on this mechanical parameter also needs to be better understood as bone fracture mainly occurs after a fall. That is why we decided to analyze relationships between microstructural parameters of human cortical bone with its toughness.

The current work allowed us to assess human cortical bone fracture mechanisms on 32 paired femoral diaphyses, femoral necks, tibial diaphyses and radial diaphyses subjected to different loading conditions resulting in a total set of nearly 300 samples analyzed. Quasi-static analysis was first performed in order to well understand this complex fracture process under a standard condition. This also allowed us to compare our work with a large set of information available in the literature. The second step was to analyze these mechanisms under a loading condition that is representative of a fall, meaning at a higher strain rate, that are much lesser known and understood regarding the literature. The large set of samples and the inter-locations aspect was an important strength of the current study. The 300 samples used allowed a non-negligible support for the results found during this work. The inter-locations aspect had a great interest in understanding fracture processes, as the different locations do show different fracture behavior and microstructure. Cortical bone microstructure was assessed using synchrotron radiation μCT imaging. This technique allows the investigation of relatively large volumes of interest in limited scanning time without inferring the resolution.

The main results of the current study are the following. Our results showed that radius significantly better resists crack propagation that femoral diaphysis, femoral neck or tibial diaphysis. More specifically radius undergoes more efficient non-linear mechanisms to slow

down the fracture process. The non-weight bearing aspect of the radius, contrary to the other studied locations, suggests that the microstructure may actually have an influence on cortical bone fracture mechanisms. But if these different anatomical locations present different toughness considering the quasi-static condition, no differences were observed under fall-like loading. Regarding these results, we can assume that femoral diaphysis, femoral neck, tibial and radial diaphysis behave as a same material in term of fracture mechanisms when loaded under fall-like condition.

Investigating human cortical bone microstructure using synchrotron radiation micro-CT imaging showed that femur had a significantly different architecture than the radius. The Haversian canals observed within femoral diaphysis and neck were larger than in the radius. At the cellular scale, the geometry of lacunae was found to be different in the femoral diaphysis and neck compare to the radius. These differences might traduce the different nature of the weight bearing femur and the non-weight bearing radius at the microscopic scale. As a consequence on crack propagation mechanisms, the amount of micro-cracks formed due to the external quasi-static loading was significantly higher on the radius than in the femoral diaphysis or neck. This result is in accordance with the higher capacity of the radius to resist crack propagation: by undergoing more micro-damages formation, a higher amount of mechanical energy is dissipated, thus more energy is needed to propagate the main crack. Moreover, this amount of micro-defects was significantly lower under fall-like loading condition, and no more difference was found between the different locations in this configuration. Regarding the differences concerning mechanical parameters and morphometric feature, we may assume that cortical bone microstructure play a major role in the fracture process. By assessing these microstructural features we were able to determine that under fall loading configuration, cortical bone crack propagation mechanisms are less efficient than under quasi-static condition in dissipating energy during loading.

The influence of collagen cross-links maturation on cortical bone toughness was also investigated in the current study. Results showed that the influence of the maturation of enzymatic cross-links on the bone capacity to develop a process zone on the femoral diaphysis and radial diaphysis is not as obvious as highlighted in the literature. This plastic mechanism is related to the accumulation of micro-damages possibly due to an irreversible movement between collagen fibers. The present work encourages to perform further work on the investigation of these complex non-linear crack propagation mechanisms.

The last chapter of this document makes a synthesis of the relationships between all previous results. By pooling all these results, we were able to identify the architectural features involved in crack propagation mechanisms both under quasi-static and fall-like loading conditions. Results suggest that under quasi-static loading, elastic and plastic contributions of the deformation do not imply the same mechanisms. During the elastic phase, collagen cross-links appear to play a significant role whereas considering the plastic contribution, microstructural parameters alone can be used to predict the mechanical parameter. As the elastic contribution accounts for only 5 % of the overall toughness under quasi-static loading, we can consider that facture mechanisms are mostly non-linear. It is well known that the Haversian system is involved in crack propagation mechanisms. However the influence of the three-dimensional lacunar network highlighted in the current study is a new result. The shape of the lacunae combined with canals diameter appear to affect the bone capacity to form micro-damages during the process zone development. Considering the propagation regime, it is the lacunar density that seems to be determinant. Results suggest that under fall-like condition, elastic mechanisms are also mainly governed by biochemical mechanisms, and accounts for almost 25 % of the global mechanical response of cortical bone. When considering the non-linear mechanisms, the prediction is relatively poor. The main result found here states that, under fall-like loading condition, microstructure has less influence on crack propagation than under quasi-static condition.

This study provides new information on human cortical bone crack propagation mechanisms under quasi-static and fall-like loading condition, on different paired anatomical locations. We saw that the elastic contribution in this fall-like loading condition is related to biochemical and density parameters, but no fitting was found for the non-linear mechanisms. When considering only femoral and radial diaphysis, we can see that the Haversian system might be involved (Annex 4). Further work has to be done on these mechanisms involving the development of a process zone near a defect and their relationships with the bone microstructure including a higher set of samples for each anatomical location

Perspectives

The current study brought new knowledge on human cortical bone fracture mechanisms comparing two different loading conditions and four anatomical locations. These results open new perspectives to improve the prediction of the fracture risk.

A first future work should be done on the evaluation of the precision of the mechanical experiments. This specific protocol has been drawn up during the current study, but no validation protocol has been performed. But considering the relatively small size of the samples and of the experimental set up, it is probable that the precision of the obtained results may be affected. Some uncertainties due to the different measurement protocols can be estimated in order to increase the confidence of the results found in the current study.

An important and interesting methodological work has to be done specifically on the μCT data. By making further analyses, other fracture mechanisms may be identified. The osteon, and more particularly the cement lines, are known to be a determinant for crack propagation within the tissue. Although visible from the images, their contrast is weak and specific methods have to be developed to allow the segmentation of these mechanical units of cortical bone. Additional work can also be done concerning the topology of the fracture surface of our bone samples. Results on fracture toughness can be obtained by measuring the roughness of the surface, for example (Ponson et al., 2013). A surface analysis may also provide information on the scale of crack propagation mechanisms, whether it is crack deflection at the osteonal scale, or at the lamellae scale (Figure 54). Fractal dimensions might by a relevant parameter for this further study.

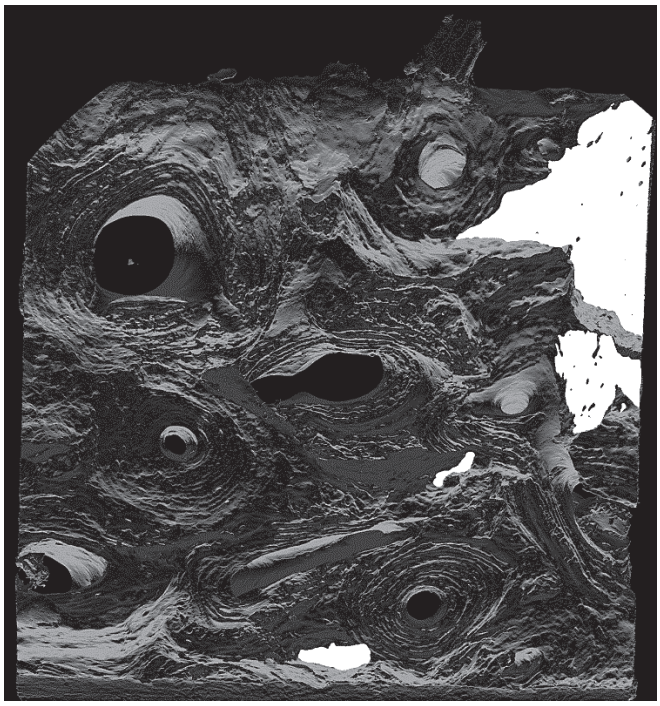

Figure 54 Fracture surface of human femoral diaphysis cortical bone samples loaded under quasi-static condition. Note the lamellae patterns around some haversian canals. The bottom of the image corresponds to the initial notch tip.

The clinical associated perspectives of this work first concern the relevance of the parameters analyzed in the current study compared to those assessable by clinicians. In images performed in this study, we investigate micro-cracks by using SR-µCT imaging at submicrometric spatial resolution with a pixel size of 0.7 µm. The High Resolution peripheral Quantitative Micro-Tomography (HR-pQCT) that could soon translate to clinics may produces images at a voxel size resolution up to nearly 60 µm, allowing thus the observation of less details than with SR-µCT. However, the use of contrast agent could open perspectives to detect cracked regions. Concerning collagen cross-links, an interesting work would be to compare the values found on cortical tissue with those that can be measured in urine. An interesting work could be to compare (and be able to compare) collagen cross-links obtained on cortical tissue with biological marker obtain in patient as CTX (a blood or urinary serum biomarker that can be measured to assess bone turnover), P1NP (bone formation markers).

A parallel study to the current one aimed at investigating fracture load of complete radius in fall loading conditions with prior HR-pQCT and DXA analyses (Zapata, 2015). The radius used in this previous study is the contro-lateral ones of those analyzed in the current study. A perspective work would then be to compare our results with those found in this previous study. In Zapata et al., results showed that under a fall configuration of loading, some radius

broke and some other did not. The question remains: " Are we able to determine whether or not a bone would fracture during a first critical loading with regards to our toughness parameters?".

Figure 55 presents the measured failure load of the contro-lateral radius depending on the fracture parameter $J_{el} + J_{process}$ under fall-like loading condition (corresponds to the total energy stored within the tissue before the actual initiation and propagation of a major crack). We can notice a significant positive correlation between these two mechanical parameters. No correlation was found with the other toughness parameters. Here we can assume that a tougher bone, in terms of elastic and process zone development, can handle a higher mechanical loading before breaking, the propagation regime may not operate in the fracture process of a real case of fracture. This result makes sense as the failure loads are considered as the maximum load during mechanical experiments that might be considered as equivalent of our ($J_{el} + J_{process}$) toughness measurement. This consolidates the hypothesis stating that human cortical bone toughness analyses can be further used for the improvement of the prediction of the risk of fracture. In further study, toughness parameters should be weighted by some geometrical parameters to consider the different shapes of the radii.

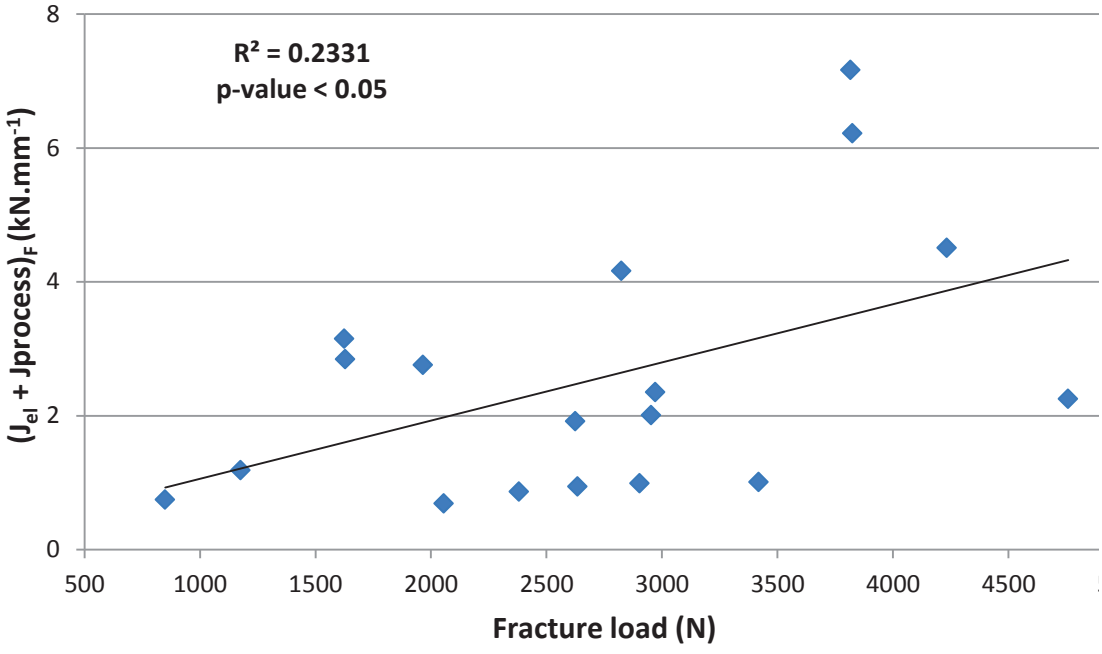

Figure 55 Fracture load measured on the left radius in function of ($J_{el} + J_{process}$) measured on the right radius under fall-like loading condition

This knowledge should be considered in further studies to improve finite element model aiming at the predicting fracture risk.

List of publications

Publications:

- First author

R.Gauthier, H.Follet, M.Langer, S.Meille, J.Chevalier, F.Peyrin, D.Mitton, 2017, Strain rate influence on human cortical bone toughness: a comparative study on four paired anatomical sites, JMBBM,

Congress:

- First author

R.Gauthier, H.Follet, M.Langer, E.Gineyts, F.Rongiéras, F.Peyrin, D.Mitton, 2017, Is there a relationship between human cortical bone toughness and collagen enzymatic cross-links?, 23rd congress of the European Society of Biomechanics, Sevilla, Spain

R.Gauthier, M.Langer, H.Follet, C.Olivier, F.Rongiéras, D.Mitton, F.Peyrin, 2017, Three-dimensional imaging of crack propagation mechanisms in human cortical bone on three paired anatomical locations, 21st International Bone Densitometry Workshow, Banz, Germany

R.Gauthier, R.Aubonnet, Y.Bala, Q.Vallet, N.Bochud, J-G.Minonzio, F.Rongiéras, H.Follet, P.Laugier, D.Mitton, 2016, Human tibial cortical thickness can predict its strength, 22d congress of the European Society of Biomechanics, Lyon, France

R.Gauthier, H.Follet, M.Langer, S.Meille, J.Chevalier, F.Peyrin, D.Mitton, 2016, Human cortical bone toughness at two strain rates on three paired anatomical locations, 22d congress of the European Society of Biomechanics, Lyon, France

R.Gauthier, H.Follet, D.Mitton, 2015, Effect of strain rate on the toughness of human tibial cortical bone, 40ème édition du congrès de la Société de Biomécanique, Paris, France

R.Gauthier, H.Follet, D.Mitton, 2015, Effet de la vitesse de déformation sur la ténacité de tibias humains, 22ème édition du Congrès Français de Mécanique, Lyon, France

R.Gauthier, H.Follet, D.Mitton, 2015, Strain rate influence on the toughness of human cortical bone, 21st congress of the European Congress of Biomechanics, Prague, Czech Republi

Bibliography

A.Rosenfeld, A.Kak, 1982. Digital Picture Processing. Elsevier.

Abraham, A.C., Agarwalla, A., Yadavalli, A., McAndrew, C., Liu, J.Y., Tang, S.Y., 2015. Multiscale Predictors of Femoral Neck *in situ* Strength in Aging Women: Contributions of BMD, Cortical Porosity, Reference Point Indentation, and Nonenzymatic Glycation. J. Bone Miner. Res. n/a-n/a. doi:10.1002/jbmr.2568

Akkus, O., Jepsen, K.J., Rimnac, C.M., 2000. Microstructural aspects of the fracture process in human cortical bone. Differences 5, 6065–6074.

Akkus, O., Rimnac, C.M., 2001. Cortical bone tissue resists fatigue fracture by deceleration and arrest of microcrack growth. J. Biomech. 34, 757–764. doi:10.1016/S0021-9290(01)00025-2

Ammann, P., Rizzoli, R., 2003. Bone strength and its determinants. Osteoporos. Int. 14 Suppl 3, S13–S18. doi:10.1007/s00198-002-1345-4

An, B., Liu, Y., Arola, D., Zhang, D., 2011. Fracture toughening mechanism of cortical bone: An experimental and numerical approach. J. Mech. Behav. Biomed. Mater. 4, 983–992. doi:10.1016/j.jmbbm.2011.02.012

Ascenzi, a, Bonucci, E., 1967. The Tensile Properties of Single Osteons. Anat. Rec. 158, 375–386. doi:10.1002/ar.1091580403

Ascenzi, a, Fabry, C., 1959. Technique for dissection and measurement of refractive index of osteones. J. Biophys. Biochem. Cytol. 6, 139–142. doi:10.1083/jcb.6.1.139

ASTM International, 2003. Standard Test Method for Measurement of Fracture Toughness. ASTM Stand.

Augat, P., Schorlemmer, S., 2006. The role of cortical bone and its microstructure in bone strength. Age Ageing 35, 27–31. doi:10.1093/ageing/afl081

Bailey, A.J., 2001. Molecular mechanisms of ageing in connective tissues. Mech. Ageing Dev. 122, 735–755. doi:10.1016/S0047-6374(01)00225-1

Bailey, A.J., Paul, R.G., Knott, L., 1998. Mechanisms of maturation and ageing of collagen. Mech. Ageing Dev. 106, 1–56. doi:10.1016/S0047-6374(98)00119-5

Bala, Y., Depalle, B., Douillard, T., Meille, S., Clément, P., Follet, H., Chevalier, J., Boivin, G., 2011. Respective roles of organic and mineral components of human cortical bone matrix in micromechanical behavior: An instrumented indentation study. J. Mech. Behav. Biomed. Mater. 4, 1473–1482. doi:10.1016/j.jmbbm.2011.05.017

Bala, Y., Depalle, B., Farlay, D., Douillard, T., Meille, S., Follet, H., Chapurlat, R., Chevalier, J., Boivin, G., 2012. Bone micromechanical properties are compromised during long-term

alendronate therapy independently of mineralization. J. Bone Miner. Res. 27, 825–834. doi:10.1002/jbmr.1501

Bala, Y., Lefevre, E., Roux, J.P., Baron, C., Lasaygues, P., Pithioux, M., Kaftandjian, V., Follet, H., 2016. Pore network microarchitecture influences human cortical bone elasticity during growth and aging. J. Mech. Behav. Biomed. Mater. 63, 164–173. doi:10.1016/j.jmbbm.2016.05.018

Bala, Y., Seeman, E., 2015. Bone's Material Constituents and their Contribution to Bone Strength in Health, Disease, and Treatment. Calcif. Tissue Int. 1–19. doi:10.1007/s00223-015-9971-y

Bala, Y., Zebaze, R., Seeman, E., 2015. Role of cortical bone in bone fragility. Curr. Opin. Rheumatol. 27, 406–413. doi:10.1097/BOR.0000000000000183

Barth, H.D., Launey, M.E., MacDowell, A. a., Ager, J.W., Ritchie, R.O., 2010. On the effect of X-ray irradiation on the deformation and fracture behavior of human cortical bone. Bone 46, 1475–1485. doi:10.1016/j.bone.2010.02.025

Beck, J.S., Nordin, B.E.C., 1960. Histological assessment of osteoporosis by iliac crest biopsy. J. Pathol. Bacteriol. 80, 391–397. doi:10.1002/path.1700800223

Behiri, J., 1990. Lakes, RS, Nakamura, S., Behiri, JC and Bonfield, W.," Fracture mechanics of bone with short cracks", Journal of Biomechanics, 23, 967-975 (1990). Silver.Neep.Wisc.Edu 975, 967–975.

Behiri, J.C., Bonfield, W., 1984. Fracture mechanics of bone--the effects of density, specimen thickness and crack velocity on longitudinal fracture. J. Biomech. 17, 25–34. doi:10.1016/0021-9290(84)90076-9

Bergland, A., Wyller, T.B., 2004. Risk factors for serious fall related injury in elderly women living at home. Inj. Prev. 10, 308–13. doi:10.1136/ip.2003.004721

Bergmann, K., Sypniewska, G., 2016. The influence of sample freezing at -80°C for 2-12 weeks on glycated haemoglobin (HbA1c) concentration assayed by HPLC method on Bio-Rad D-10© auto-analyzer. Biochem. Medica 421, 346–352. doi:10.11613/BM.2016.038

Berteau, J.-P., Gineyts, E., Pithioux, M., Baron, C., Boivin, G., Lasaygues, P., Chabrand, P., Follet, H., 2015. Ratio between mature and immature enzymatic cross-links correlates with post-yield cortical bone behavior: An insight into greenstick fractures of the child fibula. Bone 79, 190–195. doi:10.1016/j.bone.2015.05.045

Blue, M.E., Boskey, A.L., Doty, S.B., Fedarko, N.S., Hossain, M.A., Shapiro, J.R., 2015. Osteoblast function and bone histomorphometry in a murine model of Rett syndrome. Bone 76, 23–30. doi:10.1016/j.bone.2015.01.024

Bonewald, L.F., 2011. The amazing osteocyte. J. Bone Miner. Res. 26, 229–238. doi:10.1002/jbmr.320

Bonewald, L.F., Johnson, M.L., 2008. Osteocytes, mechanosensing and Wnt signaling. Bone 42,

606–615. doi:10.1016/j.bone.2007.12.224

Bonfield, W., 1987. Advances in the fracture mechanics of cortical bone. J. Biomech., F. {Gaynor} {Evans} {Anniversary} {Issue} on {Bone} {Biomechanics} 20, 1071–1081. doi:10.1016/0021-9290(87)90025-X

Bonfield, W., Datta, P.K., 1976. Fracture toughness of compact bone. J. Biomech. 9, 131–134. doi:10.1016/0021-9290(76)90151-2

Borchers, R.E., Gibson, L.J., Burchardt, H., Hayes, W.C., 1995. Effects of selected thermal variables on the mechanical properties of trabecular bone. Biomaterials 16, 545–551. doi:10.1016/0142-9612(95)91128-L

Bordier, P.J., Chot, S.T., 1972. Quantitative histology of metabolic bone disease. Clin. Endocrinol. Metab. 1, 197–215. doi:10.1016/S0300-595X(72)80057-4

Brown, C.U., Yeni, Y.N., Norman, T.L., 2000. Fracture toughness is dependent on bone location--a study of the femoral neck, femoral shaft, and the tibial shaft. J. Biomed. Mater. Res. 49, 380–389.

Buehler, M.J., 2007. Molecular nanomechanics of nascent bone: fibrillar toughening by mineralization. Nanotechnology 295102. doi:10.1088/0957-4484/18/29/295102

Buenzli, P.R., Sims, N. a., 2015. Quantifying the osteocyte network in the human skeleton. Bone 75, 144–150. doi:10.1016/j.bone.2015.02.016

Burr, D.B., Martin, R.B., Schaffler, M.B., Radin, E.L., 1985. Bone remodeling in response to in vivo fatigue microdamage. J. Biomech. 18, 189–200. doi:10.1016/0021-9290(85)90204-0

Burr, D.B., Schaffler, M.B., Frederickson, R.G., 1988. Composition of the cement line and its possible mechanical role as a local interface in human compact bone. J. Biomech. 21, 939–945. doi:10.1016/0021-9290(88)90132-7

Carriero, A., Zimmermann, E.A., Shefelbine, S.J., Ritchie, R.O., 2014. A methodology for the investigation of toughness and crack propagation in mouse bone. J. Mech. Behav. Biomed. Mater. 39, 38–47. doi:10.1016/j.jmbbm.2014.06.017

Chamay, a, Tschantz, P., 1972. Mechanical influences in bone remodeling. Experimental research on Wolff's law. J. Biomech. 5, 173–180. doi:10.1016/0021-9290(72)90053-X

Chappard, C., Basillais, A., Benhamou, L., Bonassie, A., Brunet-Imbault, B., Bonnet, N., Peyrin, F., 2006. Comparison of synchrotron radiation and conventional x-ray microcomputed tomography for assessing trabecular bone microarchitecture of human femoral heads. Med. Phys. 33, 3568–3577. doi:10.1118/1.2256069

Chappard, C., Bensalah, S., Olivier, C., Gouttenoire, P.J., Marchadier, a., Benhamou, C., Peyrin, F., 2013. 3D characterization of pores in the cortical bone of human femur in the elderly at different locations as determined by synchrotron micro-computed tomography images.

Osteoporos. Int. 24, 1023–1033. doi:10.1007/s00198-012-2044-4

Chen, H., Zhou, X., Shoumura, S., Emura, S., Bunai, Y., 2010. Age- And gender-dependent changes in three-dimensional microstructure of cortical and trabecular bone at the human femoral neck. Osteoporos. Int. 21, 627–636. doi:10.1007/s00198-009-0993-z

Cohen, A., Dempster, D.W., Müller, R., Guo, X.E., Nickolas, T.L., Liu, X.S., Zhang, X.H., Wirth, A.J., Van Lenthe, G.H., Kohler, T., McMahon, D.J., Zhou, H., Rubin, M.R., Bilezikian, J.P., Lappe, J.M., Recker, R.R., Shane, E., 2010. Assessment of trabecular and cortical architecture and mechanical competence of bone by high-resolution peripheral computed tomography: comparison with transiliac bone biopsy. Osteoporos. Int. 21, 263–273. doi:10.1007/s00198-009-0945-7

Cook, R.B., Curwen, C., Tasker, T., Zioupos, P., 2010. Fracture toughness and compressive properties of cancellous bone at the head of the femur and relationships to non-invasive skeletal assessment measurements. Med. Eng. Phys. 32, 991–997. doi:10.1016/j.medengphy.2010.06.014

Cooper, C., Atkinson, E.J., Jacobsen, S.J., O'Fallon, W.M., Melton, L.J., 1993. Population-Based Study of Survival after Osteoporotic Fractures. Am. J. Epidemiol. 137, 1001–1005. doi:10.1093/oxfordjournals.aje.a116756

Cooper, D.M.L., Thomas, C.D.L., Clement, J.G., Turinsky, A.L., Sensen, C.W., Hallgrímsson, B., 2007. Age-dependent change in the 3D structure of cortical porosity at the human femoral midshaft. Bone 40, 957–965. doi:10.1016/j.bone.2006.11.011

Court-Brown, C.M., Caesar, B., 2006. Epidemiology of adult fractures: A review. Injury 37, 691–697. doi:10.1016/j.injury.2006.04.130

Currey, J.D., 2001. Sacrificial bonds heal bone. Nature 414, 699. doi:10.1038/414699a

Currey, J.D., 1979. Mechanical properties of bone tissues with greatly differing functions. J. Biomech. 12, 313–319. doi:10.1016/0021-9290(79)90073-3

Danova, N.A., Colopy, S.A., Radtke, C.L., Kalscheur, V.L., Markel, M.D., Vanderby, R., McCabe, R.P., Escarcega, A.J., Muir, P., 2003. Degradation of bone structural properties by accumulation and coalescence of microcracks. Bone 33, 197–205. doi:10.1016/S8756-3282(03)00155-8

de Vernejoul, M.C., Kuntz, D., Miravet, L., Goutallier, D., Ryckewaert, A., 1981. Bone histomorphometric reproducibility in normal patients. Calcif. Tissue Int. 33, 369–374. doi:10.1007/BF02409458

Dempster, D.W., Compston, J.E., Drezner, M.K., Glorieux, F.H., Kanis, J.A., Malluche, H., Meunier, P.J., Ott, S.M., Recker, R.R., Parfitt, A.M., 2013. Standardized nomenclature, symbols, and units for bone histomorphometry: A 2012 update of the report of the ASBMR

Histomorphometry Nomenclature Committee. J. Bone Miner. Res. 28, 2–17. doi:10.1002/jbmr.1805

Depalle, B., Qin, Z., Shefelbine, S.J., Buehler, M.J., 2015. Influence of cross-link structure, density and mechanical properties in the mesoscale deformation mechanisms of collagen fibrils. J. Mech. Behav. Biomed. Mater. 52, 1–13. doi:10.1016/j.jmbbm.2014.07.008

Diab, T., Vashishth, D., 2005. Effects of damage morphology on cortical bone fragility. Bone 37, 96–102. doi:10.1016/j.bone.2005.03.014

Di Zenzo, S., Cinque, L., Levialdi, S., 1996. Run-based algorithms for binary image analysis and processing. IEEE Trans. Pattern Anal. Mach. Intell. 18, 83–89. doi:10.1109/34.476016

Diez-Perez, A., Güerri, R., Nogues, X., Cáceres, E., Peña, M.J., Mellibovsky, L., Randall, C., Bridges, D., Weaver, J.C., Proctor, A., Brimer, D., Koester, K.J., Ritchie, R.O., Hansma, P.K., 2010. Microindentation for in vivo measurement of bone tissue mechanical properties in humans. J. Bone Miner. Res. 25, 1877–1885. doi:10.1002/jbmr.73

Dong, P., Haupert, S., Hesse, B., Langer, M., Gouttenoire, P.J., Bousson, V., Peyrin, F., 2014. 3D osteocyte lacunar morphometric properties and distributions in human femoral cortical bone using synchrotron radiation micro-CT images. Bone 60, 172–185. doi:10.1016/j.bone.2013.12.008

Dong, X.N., Guo, X.E., 2004. The dependence of transversely isotropic elasticity of human femoral cortical bone on porosity. J. Biomech. 37, 1281–1287. doi:10.1016/j.jbiomech.2003.12.011

Dooley, C., Tisbo, P., Lee, T.C., Taylor, D., 2012. Rupture of osteocyte processes across microcracks: The effect of crack length and stress. Biomech. Model. Mechanobiol. 11, 759–766. doi:10.1007/s10237-011-0349-4

Dresselhaus, M.S., 1966. Solid State Physics Part II: Optical Properties of Solids. Proceedins Int. Sch. Phys. 198.

Duboeuf, F., Burt-Pichat, B., Farlay, D., Suy, P., Truy, E., Boivin, G., 2015. Bone quality and biomechanical function: A lesson from human ossicles. Bone 73, 105–110. doi:10.1016/j.bone.2014.12.009

Dubousset, J., 2014. la prévention des chutes est-elle possible ? Bull. Acad. Natl. Med. 198, 1055–1066.

Duchemin, L., Bousson, V., Raossanaly, C., Bergot, C., Laredo, J.D., Skalli, W., Mitton, D., 2008. Prediction of mechanical properties of cortical bone by quantitative computed tomography. Med. Eng. Phys. 30, 321–328. doi:10.1016/j.medengphy.2007.04.008

Ebacher, V., Guy, P., Oxland, T.R., Wang, R., 2012. Sub-lamellar microcracking and roles of canaliculi in human cortical bone. Acta Biomater. 8, 1093–1100. doi:10.1016/j.actbio.2011.11.013

Elder, F.R., Gurewitsch, A.M., Langmuir, R. V., Pollock, H.C., 1947. Radiation from Electrons in a Synchrotron. Phys. Rev. 71, 829–830. doi:10.1103/PhysRev.71.829.5

Evans, F.G., 1973. Mechanical Properties of Bone. Thomas, Spring.

Evans, F.G., Bang, S., 1967. Differences and Relationships Between the Physical Properties and the Microscopic Structure of Human Femoral, Tibial and Fibular Cortical Bone. Am. J. Anat. 120, 79–88. doi:10.1002/aja.1001200107

Eyre, D.R., Weis, M.A., Wu, J.J., 2010. Maturation of collagen ketoimine cross-links by an alternative mechanism to pyridinoline formation in cartilage. J. Biol. Chem. 285, 16675–16682. doi:10.1074/jbc.M110.111534

Fantner, G.E., Hassenkam, T., Kindt, J.H., Weaver, J.C., Birkedal, H., Pechenik, L., Cutroni, J. a, Cidade, G. a G., Stucky, G.D., Morse, D.E., Hansma, P.K., 2005. Sacrificial bonds and hidden length dissipate energy as mineralized fibrils separate during bone fracture. Nat. Mater. 4, 612–616. doi:10.1038/nmat1428

Farlay, D., Armas, L.A.G., Gineyts, E., Akhter, M.P., Recker, R.R., Boivin, G., 2016. Nonenzymatic Glycation and Degree of Mineralization Are Higher in Bone from Fractured Patients with Type 1 Diabetes Mellitus. J. Bone Miner. Res. 31, 190–195. doi:10.1002/jbmr.2607

Farlay, D., Boivin, G., 2012. Bone mineral quality. Osteoporosis 953–978. doi:10.5772/29091

Fleischmajer, R., Timpl, R., Tuderman, L., Raisher, L., Wiestner, M., Perlish, J.S., Graves, P.N., 1981. Ultrastructural identification of extension aminopropeptides of type I and III collagens in human skin. Proc. Natl. Acad. Sci. U. S. A. 78, 7360–4.

Foldhazy, Z., 2005. Exercise-induced strain and strain rate in the distal radius. J. Bone Jt. Surg. - Br. Vol. 87–B, 261–266. doi:10.1302/0301-620X.87B2.14857

Follet, H., Viguet-Carrin, S., Burt-Pichat, B., Dépalle, B., Bala, Y., Gineyts, E., Munoz, F., Arlot, M., Boivin, G., Chapurlat, R.D., Delmas, P.D., Bouxsein, M.L., 2011. Effects of preexisting microdamage, collagen cross-links, degree of mineralization, age, and architecture on compressive mechanical properties of elderly human vertebral trabecular bone. J. Orthop. Res. 29, 481–488. doi:10.1002/jor.21275

Gauthier, R., Follet, H., Langer, M., Meille, S., Chevalier, J., Rongiéras, F., Peyrin, F., Mitton, D., 2017. Strain rate influence on human cortical bone toughness: A comparative study of four paired anatomical sites. J. Mech. Behav. Biomed. Mater. 71, 223–230. doi:10.1016/j.jmbbm.2017.03.015

Genant, H.K., Cooper, C., Poor, G., Reid, I., Ehrlich, G., Kanis, J., Nordin, B.E., Barrett-Connor, E., Black, D., Bonjour, J.P., Dawson-Hughes, B., Delmas, P.D., Dequeker, J., Ragi Eis, S., Gennari, C., Johnell, O., Johnston, C.C., Lau, E.M., Liberman, U.A., Lindsay, R., Martin, T.J.,

Masri, B., Mautalen, C.A., Meunier, P.J., Khaltaev, N., 1999. Interim report and recommendations of the World Health Organization Task-Force for Osteoporosis. Osteoporos. Int. 10, 259–64. doi:10.1007/s001980050224

Genant, H.K., Engelke, K., Fuerst, T., Glüer, C.C., Grampp, S., Harris, S.T., Jergas, M., Lang, T., Lu, Y., Majumdar, S., Mathur, a, Takada, M., 1996. Noninvasive assessment of bone mineral and structure: state of the art. J. Bone Miner. Res. 11, 707–730. doi:10.1002/jbmr.5650110602

Gineyts, E., Borel, O., Chapurlat, R., Garnero, P., 2010. Quantification of immature and mature collagen crosslinks by liquid chromatography-electrospray ionization mass spectrometry in connective tissues. J. Chromatogr. B Anal. Technol. Biomed. Life Sci. 878, 1449–1454. doi:10.1016/j.jchromb.2010.03.039

Giraud-Guille, M.M., 1988. Twisted plywood architecture of collagen fibrils in human compact bone osteons. Calcif. Tissue Int. 42, 167–180. doi:10.1007/BF02556330

González-Agüero, a., Vicente-Rodríguez, G., Gómez-Cabello, a., Casajús, J. a., 2013. Cortical and trabecular bone at the radius and tibia in male and female adolescents with Down syndrome: A peripheral quantitative computed tomography (pQCT) study. Osteoporos. Int. 24, 1035–1044. doi:10.1007/s00198-012-2041-7

Granke, M., Grimal, Q., Saïed, A., Nauleau, P., Peyrin, F., Laugier, P., 2011. Change in porosity is the major determinant of the variation of cortical bone elasticity at the millimeter scale in aged women. Bone 49, 1020–1026. doi:10.1016/j.bone.2011.08.002

Granke, M., Makowski, A.J., Uppuganti, S., Does, M.D., Nyman, J.S., 2015. Identifying novel clinical surrogates to assess human bone fracture toughness. J. Bone Miner. Res. n/a-n/a. doi:10.1002/jbmr.2452

Granke, M., Makowski, A.J., Uppuganti, S., Nyman, J.S., 2016. Prevalent role of porosity and osteonal area over mineralization heterogeneity in the fracture toughness of human cortical bone. J. Biomech. 49, 2748–2755. doi:10.1016/j.jbiomech.2016.06.009

Gray, H., 1918. Anatomy of the human body, Lea & Febi. ed. Philadeplhia.

Griffith, a. a., 1921. The Phenomena of Rupture and Flow in Solids. Philos. Trans. R. Soc. A Math. Phys. Eng. Sci. 221, 163–198. doi:10.1098/rsta.1921.0006

Griffith, J.F., Engelke, K., Genant, H.K., 2010. Looking beyond bone mineral density: Imaging assessment of bone quality. Ann. N. Y. Acad. Sci. 1192, 45–56. doi:10.1111/j.1749-6632.2009.05378.x

Gryfe, C.I., Amies, A., Ashley, M.J., 1977. A longitudinal study of falls in an elderly population: I. Incidence and morbidity. Age Ageing 6, 201–210. doi:10.1093/ageing/6.4.201

Gupta, H.S., Krauss, S., Kerschnitzki, M., Karunaratne, a., Dunlop, J.W.C., Barber, a. H., Boesecke, P., Funari, S.S., Fratzl, P., 2013. Intrafibrillar plasticity through mineral/collagen

sliding is the dominant mechanism for the extreme toughness of antler bone. J. Mech. Behav. Biomed. Mater. 28, 366–382. doi:10.1016/j.jmbbm.2013.03.020

Gupta, H.S., Seto, J., Wagermaier, W., Zaslansky, P., Boesecke, P., Fratzl, P., 2006. Cooperative deformation of mineral and collagen in bone at the nanoscale. Proc. Natl. Acad. Sci. U. S. A. 103, 17741–17746. doi:10.1073/pnas.0604237103

Gupta, H.S., Wagermaier, W., Zickler, G. a., Aroush, D.R. Ben, Funari, S.S., Roschger, P., Wagner, H.D., Fratzl, P., 2005. Nanoscale deformation mechanisms in bone. Nano Lett. 5, 2108–2111. doi:10.1021/nl051584b

Hadjidakis, D.J., Androulakis, I.I., 2006. Bone remodeling. Ann. N. Y. Acad. Sci. 1092, 385–396. doi:10.1196/annals.1365.035

Hannah, K.M., Thomas, C.D.L., Clement, J.G., De Carlo, F., Peele, A.G., 2010. Bimodal distribution of osteocyte lacunar size in the human femoral cortex as revealed by micro-CT. Bone 47, 866–871. doi:10.1016/j.bone.2010.07.025

Hansen, U., Zioupos, P., Simpson, R., Currey, J.D., Hynd, D., 2008. The effect of strain rate on the mechanical properties of human cortical bone. J. Biomech. Eng. 130, 11011. doi:10.1115/1.2838032

Hansma, P.K., Fantner, G.E., Kindt, J.H., Thurner, P.J., Schitter, G., Turner, P.J., Udwin, S.F., Finch, M.M., 2005. Sacrificial bonds in the interfibrillar matrix of bone. J. Musculoskelet. Neuronal Interact. 5, 313–315.

Haupert, S., Guérard, S., Peyrin, F., Mitton, D., Laugier, P., 2014. Non destructive characterization of cortical bone micro-damage by nonlinear resonant ultrasound spectroscopy. PLoS One 9. doi:10.1371/journal.pone.0083599

Hayes, W.C., Piazza, S.J., Zysset, P.K., 1991. Biomechanics of fracture risk prediction of the hip and spine by quantitative computed tomography. Radiol. Clin. North Am. 29, 1–18.

Hazenberg, J.G., Taylor, D., Clive Lee, T., 2006. Mechanisms of short crack growth at constant stress in bone. Biomaterials 27, 2114–2122. doi:10.1016/j.biomaterials.2005.09.039

He, M.-Y., Hutchinson, J.W., 1989. Kinking of a Crack Out of an Interface. J. Appl. Mech. 56, 270. doi:10.1115/1.3176078

Herman, G.T., 1980. Filtered Backprojection for Parallel Beams, Academic P. ed, Fundamentals of Computerized Tomography, Advances in Pattern Recognition. Springer London, New York. doi:10.1007/978-1-84628-723-7

Hernlund, E., Svedbom, A., Ivergård, M., Compston, J., Cooper, C., Stenmark, J., McCloskey, E. V., Jönsson, B., Kanis, J.A., 2013. Osteoporosis in the European Union: Medical management, epidemiology and economic burden: A report prepared in collaboration with the International Osteoporosis Foundation (IOF) and the European Federation of Pharmaceutical Industry

Associations (EFPIA). Arch. Osteoporos. 8. doi:10.1007/s11657-013-0136-1

Hesse, B., Varga, P., Langer, M., Pacureanu, A., Schrof, S., Männicke, N., Suhonen, H., Maurer, P., Cloetens, P., Peyrin, F., Raum, K., 2015. Canalicular Network Morphology Is the Major Determinant of the Spatial Distribution of Mass Density in Human Bone Tissue: Evidence by Means of Synchrotron Radiation Phase-Contrast nano-CT. J. Bone Miner. Res. 30, 346–356. doi:10.1002/jbmr.2324

Hildebrand, T., Rüegsegger, P., 1997. Quantification of Bone Microarchitecture with the Structure Model Index. Comput. Methods Biomech. Biomed. Engin. 1, 15–23. doi:10.1080/01495739708936692

Holzer, G., von Skrbensky, G., Holzer, L. a, Pichl, W., 2009. Hip fractures and the contribution of cortical versus trabecular bone to femoral neck strength. J. Bone Miner. Res. 24, 468–474. doi:10.1359/JBMR.081108

Hounsfield, G.N., 1973. Computerized transverse axial scanning (tomography): Part 1. Description of system. Br. J. Radiol. 46, 1016–1022. doi:10.1259/0007-1285-46-552-1016

Irwin, G.R., 1960. Plastic zone near a crack and fracture toughness, in: 7th Sagamore Ordnance Materials Research Conference. p. IV. 63-78.

Irwin, G.R., 1957. Analysis of stresses and strains near the end of cracking traversing a plate. J. Appl. Mech. 24, 361–364.

Itoman, M., Nakamura, S., 1991. Experimental study on allogenic bone grafts. Int. Orthop. 15, 161–165. doi:10.1007/BF00179718

Johnell, O., Kanis, J. a., 2006. An estimate of the worldwide prevalence, mortality and disability associated with hip fracture. Osteoporos. Int. 15, 897–902. doi:10.1007/s00198-004-1627-0

Johnson, T.P.M., Socrate, S., Boyce, M.C., 2010. A viscoelastic, viscoplastic model of cortical bone valid at low and high strain rates. Acta Biomater. 6, 4073–4080. doi:10.1016/j.actbio.2010.04.017

Jones, a. C., Sheppard, a. P., Sok, R.M., Arns, C.H., Limaye, a., Averdunk, H., Brandwood, a., Sakellariou, a., Senden, T.J., Milthorpe, B.K., Knackstedt, M. a., 2004. Three-dimensional analysis of cortical bone structure using X-ray micro-computed tomography. Phys. A Stat. Mech. its Appl., Proceedings of the {International} {Conference} {New} {Materials} and {Complexity} 339, 125–130. doi:10.1016/j.physa.2004.03.046

Jowsey, J., 1966. Studies of Haversian systems in man and some animals. J. Anat. 100, 857–64. doi:10.1002/ajpa

Jowsey, J., Owen, M., Vaughan, J., 1953. Microradiographs and autoradiographs of cortical bone from monkeys injected with 90Sr. Br. J. Exp. Pathol. 34, 661–7.

Kanis, J. a., Oden, A., Johnell, O., Jonsson, B., De Laet, C., Dawson, A., 2001. The burden of

osteoporotic fractures: A method for setting intervention thresholds. Osteoporos. Int. 12, 417–427. doi:10.1007/s001980170112

Karim, L., Tang, S.Y., Sroga, G.E., Vashishth, D., 2013. Differences in non-enzymatic glycation and collagen cross-links between human cortical and cancellous bone. Osteoporos. Int. 24, 2441–2447. doi:10.1007/s00198-013-2319-4

Kasapi, M. a, Gosline, J.M., 1996. Strain-rate-dependent mechanical properties of the equine hoof wall. J. Exp. Biol. 199, 1133–1146.

Katsamenis, O.L., Chong, H.M.H., Andriotis, O.G., Thurner, P.J., 2012. Load-bearing in cortical bone microstructure: Selective stiffening and heterogeneous strain distribution at the lamellar level. J. Mech. Behav. Biomed. Mater. 17, 152–165. doi:10.1016/j.jmbbm.2012.08.016

Katsamenis, O.L., Jenkins, T., Quinci, F., Michopoulou, S., Sinclair, I., Thurner, P.J., 2013. A Novel Videography Method for Generating Crack-Extension Resistance Curves in Small Bone Samples. PLoS One 8, e55641. doi:10.1371/journal.pone.0055641

Katsamenis, O.L., Jenkins, T., Thurner, P.J., 2015. Toughness and damage susceptibility in human cortical bone is proportional to mechanical inhomogeneity at the osteonal-level. Bone 76, 158–168. doi:10.1016/j.bone.2015.03.020

Kazanci, M., Wagner, H.D., Manjubala, N.I., Gupta, H.S., Paschalis, E., Roschger, P., Fratzl, P., 2007. Raman imaging of two orthogonal planes within cortical bone. Bone 41, 456–461. doi:10.1016/j.bone.2007.04.200

Keaveny, T.M., Wachtel, E.F., Hayes, W.C., Dana, C.A., 1994. Differences Between the Tensile and Compressive Strengths of Bovine Tibial Trabecular Bone Depend on Modulus 27.

Kilappa, V., Moilanen, P., Xu, L., Nicholson, P.H.F., Timonen, J., Cheng, S., 2011. Low-frequency axial ultrasound velocity correlates with bone mineral density and cortical thickness in the radius and tibia in pre- and postmenopausal women. Osteoporos. Int. 22, 1103–1113. doi:10.1007/s00198-010-1273-7

Kimmel, D.B., Recker, R.R., Gallagher, J.C., Vaswani, a. S., Aloia, J.F., 1990. A comparison of iliac bone histomorphometric data in post-menopausal osteoporotic and normal subjects. Bone Miner. 11, 217–235. doi:10.1016/0169-6009(90)90061-J

Koester, K.J., Ager, J.W., Ritchie, R.O., 2008. The true toughness of human cortical bone measured with realistically short cracks. Nat. Mater. 7, 672–677. doi:10.1557/mrs2008.195

Koester, K.J., Barth, H.D., Ritchie, R.O., 2011. Effect of aging on the transverse toughness of human cortical bone: Evaluation by R-curves. J. Mech. Behav. Biomed. Mater. 4, 1504–1513. doi:10.1016/j.jmbbm.2011.05.020

Kulin, R.M., Jiang, F., Vecchio, K.S., 2011a. Loading rate effects on the R-curve behavior of cortical bone. Acta Biomater. 7, 724–732. doi:10.1016/j.actbio.2010.09.027

Kulin, R.M., Jiang, F., Vecchio, K.S., 2011b. Effects of age and loading rate on equine cortical bone failure. J. Mech. Behav. Biomed. Mater. 4, 57–75. doi:10.1016/j.jmbbm.2010.09.006

Lai, X., Price, C., Modla, S., Thompson, W.R., Caplan, J., Kirn-Safran, C.B., Wang, L., 2015. The dependences of osteocyte network on bone compartment, age, and disease. Bone Res. 3, 15009. doi:10.1038/boneres.2015.9

Langer, M., Pacureanu, A., Suhonen, H., Grimal, Q., Cloetens, P., Peyrin, F., 2012. X-Ray Phase Nanotomography Resolves the 3D Human Bone Ultrastructure. PLoS One 7. doi:10.1371/journal.pone.0035691

Langer, M., Peyrin, F., 2015. 3D X-ray ultra-microscopy of bone tissue. Osteoporos. Int. doi:10.1007/s00198-015-3257-0

Lanyon, L.E., Goodship, A.E., Pye, C.J., MacFie, J.H., 1982. Mechanically adaptive bone remodelling. J. Biomech. 15, 141–145. doi:10.1016/0021-9290(82)90246-9

Larrue, A., Rattner, A., Peter, Z.A., Olivier, C., Laroche, N., Vico, L., Peyrin, F., 2011. Synchrotron radiation micro-CT at the Micrometer scale for the analysis of the three-dimensional morphology of microcracks in human trabecular bone. PLoS One 6, e21297. doi:10.1371/journal.pone.0021297

Launey, M.E., Buehler, M.J., Ritchie, R.O., 2010. On the Mechanistic Origins of Toughness in Bone. Annu. Rev. Mater. Res. 40, 25–53. doi:10.1146/annurev-matsci-070909-104427

Lawn, B., 1993. Fracture of brittle solids. Cambridge.

Lee, T.C., Mohsin, S., Taylor, D., Parkesh, R., Gunnlaugsson, T., O'Brien, F.J., Giehl, M., Gowin, W., 2003. Detecting microdamage in bone. J. Anat. 203, 161–172. doi:10.1046/j.1469-7580.2003.00211.x

Lee, T.C., Staines, a., Taylor, D., 2002. Bone adaptation to load: Microdamage as a stimulus for bone remodelling. J. Anat. 201, 437–446. doi:10.1046/j.1469-7580.2002.00123.x

LeGeros, R.Z., Piliero, J.A., Pentel, L., 1983. Comparative Properties of Deciduous and Permanent (Young and Old) Human Enamel1. Gerodontology 2, 1–8. doi:10.1111/j.1741-2358.1983.tb00341.x

Leibson, C.L., Tosteson, A.N.A., Gabriel, S.E., Ransom, J.E., Melton, L.J., 2002. Mortality, Disability, and Nursing Home Use for Persons with and without Hip Fracture: A Population-Based Study. J. Am. Geriatr. Soc. 50, 1644–1650. doi:10.1046/j.1532-5415.2002.50455.x

Lieou, C.K.C., Elbanna, A.E., Carlson, J.M., 2013. Sacrificial bonds and hidden length in biomaterials: A kinetic constitutive description of strength and toughness in bone. Phys. Rev. E - Stat. Nonlinear, Soft Matter Phys. 88, 1–10. doi:10.1103/PhysRevE.88.012703

Lips, P., Courpron, P., Meunier, P.J., 1978. Mean wall thickness of trabecular bone packets in the human iliac crest: Changes with age. Calcif. Tissue Res. 26, 13–17. doi:10.1007/BF02013227

Lotz, J.C., Cheal, E.J., Hayes, W.C., 1995. Stress distributions within the proximal femur during gait and falls: Implications for osteoporotic fracture. Osteoporos. Int. 5, 252–261. doi:10.1007/BF01774015

Louis, O., Boulpaep, F., Willnecker, J., Van den Winkel, P., Osteaux, M., 1995. Cortical mineral content of the radius assessed by peripheral QCT predicts compressive strength on biomechanical testing. Bone 16, 375–379. doi:10.1016/8756-3282(94)00050-6

Lucksanasombool, P., Higgs, W. a J., Higgs, R.J.E.D., Swain, M. V., 2001. Fracture toughness of bovine bone: Influence of orientation and storage media. Biomaterials 22, 3127–3132. doi:10.1016/S0142-9612(01)00062-X

Manske, S.L., Liu-Ambrose, T., Cooper, D.M.L., Kontulainen, S., Guy, P., Forster, B.B., McKay, H.A., 2009. Cortical and trabecular bone in the femoral neck both contribute to proximal femur failure load prediction. Osteoporos. Int. 20, 445–453. doi:10.1007/s00198-008-0675-2

Marotti, G., 1979. Osteocyte orientation in human lamellar bone and its relevance to the morphometry of periosteocytic lacunae. Metab. Bone Dis. Relat. Res. 1, 325–333. doi:10.1016/0221-8747(79)90027-4

Martín-Badosa, E., Elmoutaouakkil, A., Nuzzo, S., Amblard, D., Vico, L., Peyrin, F., 2003. A method for the automatic characterization of bone architecture in 3D mice microtomographic images. Comput. Med. Imaging Graph. 27, 447–458. doi:10.1016/S0895-6111(03)00031-4

McCormack, J., Stover, S.M., Gibeling, J.C., Fyhrie, D.P., 2012. Effects of mineral content on the fracture properties of equine cortical bone in double-notched beams. Bone 50, 1275–1280. doi:10.1016/j.bone.2012.02.018

McNerny, E.M., Gong, B., Morris, M.D., Kohn, D.H., 2015. Bone Fracture Toughness and Strength Correlate With Collagen Cross-Link Maturity in a Dose-Controlled Lathyrism Mouse Model. J. Bone Miner. Res. 30, 455–464. doi:10.1002/jbmr.2356

Melvin, J.W., Evans, F.G., 1973. crack propagation in bone, in: ASME Biomaterials Symposium. American Society of Mechanical Engineers, Detroit, MI.

Meunier, P.J., Coindre, J.M., Edouard, C.M., Arlot, M.E., 1980. Bone histomorphometry in pacet's disease quantitative and dynamic analysis of pagetic and nonpagetic bone tissue. Arthritis Rheum. 23, 1095–1103. doi:10.1002/art.1780231005

Milovanovic, P., Zimmermann, E.A., Riedel, C., Scheidt, A. Vom, Herzog, L., Krause, M., Djonic, D., Djuric, M., Püschel, K., Amling, M., Ritchie, R.O., Busse, B., 2015. Multi-level characterization of human femoral cortices and their underlying osteocyte network reveal trends in quality of young, aged, osteoporotic and antiresorptive-treated bone. Biomaterials 45, 46–55. doi:10.1016/j.biomaterials.2014.12.024

Mischinski, S., Ural, A., 2011. Interaction of microstructure and microcrack growth in cortical

bone: a finite element study. Comput. Methods Biomech. Biomed. Engin. 1–14. doi:10.1080/10255842.2011.607444

Mobilio, S., Boscherini, F., Meneghini, C., 2015. Synchrotron radiation: Basics, methods and applications. Synchrotron Radiat. Basics, Methods Appl. 1–799. doi:10.1007/978-3-642-55315-8

Mohsin, S., O'Brien, F.J., Lee, T.C., 2006. Microcracks in compact bone: A three-dimensional view. J. Anat. 209, 119–124. doi:10.1111/j.1469-7580.2006.00554.x

Moreno, J., Forriol, F., 2002. Effects of preservation on the mechanical strength and chemical composition of cortical bone: An experimental study in sheep femora. Biomaterials 23, 2615–2619. doi:10.1016/S0142-9612(01)00402-1

Mullins, L.P., Bruzzi, M.S., McHugh, P.E., 2007. Measurement of the microstructural fracture toughness of cortical bone using indentation fracture. J. Biomech. 40, 3285–3288. doi:10.1016/j.jbiomech.2007.04.020

Myllyharju, J., Kivirikko, K.I., 2004. Collagens, modifying enzymes and their mutations in humans, flies and worms. Trends Genet. 20, 33–43. doi:10.1016/j.tig.2003.11.004

Nalla, R.K., Kruzic, J.J., Kinney, J.H., Balooch, M., Ager, J.W., Ritchie, R.O., 2006. Role of microstructure in the aging-related deterioration of the toughness of human cortical bone. Mater. Sci. Eng. C 26, 1251–1260. doi:10.1016/j.msec.2005.08.021

Nalla, R.K., Kruzic, J.J., Kinney, J.H., Ritchie, R.O., 2005a. Mechanistic aspects of fracture and R-curve behavior in human cortical bone. Biomaterials 26, 217–231. doi:10.1016/j.biomaterials.2004.02.017

Nalla, R.K., Kruzic, J.J., Kinney, J.H., Ritchie, R.O., 2004a. Effect of aging on the toughness of human cortical bone: Evaluation by R-curves. Bone 35, 1240–1246. doi:10.1016/j.bone.2004.07.016

Nalla, R.K., Kruzic, J.J., Ritchie, R.O., 2004b. On the origin of the toughness of mineralized tissue: Microcracking or crack bridging? Bone 34, 790–798. doi:10.1016/j.bone.2004.02.001

Nalla, R.K., Stölken, J.S., Kinney, J.H., Ritchie, R.O., 2005b. Fracture in human cortical bone: Local fracture criteria and toughening mechanisms. J. Biomech. 38, 1517–1525. doi:10.1016/j.jbiomech.2004.07.010

Nanes, M.S., Kallen, C.B., 2014. Osteoporosis. Semin. Nucl. Med. 44, 439–450. doi:10.1053/j.semnuclmed.2014.06.006

Nankaku, M., Kanzaki, H., Tsuboyama, T., Nakamura, T., 2005. Evaluation of hip fracture risk in relation to fall direction. Osteoporos. Int. 16, 1315–1320. doi:10.1007/s00198-005-1843-2

Nazarian, A., Hermannsson, B.J., Muller, J., Zurakowski, D., Snyder, B.D., 2009. Effects of tissue preservation on murine bone mechanical properties. J. Biomech. 42, 82–86.

doi:10.1016/j.jbiomech.2008.09.037

Nishida, T., Hanaki, T., Pezzotti, G., 1994. Effect of root notch radius on the fracture toughness of a fine-grained alumina. J. Am. Ceram. Soc. 77, 606–608.

Norman, T.L., Wang, Z., 1997. Microdamage of human cortical bone: Incidence and morphology in long bones. Bone 20, 375–379. doi:http://dx.doi.org/10.1016/S8756-3282(97)00004-5

Nuzzo, S., Lafage-Proust, M.H., Martin-Badosa, E., Boivin, G., Thomas, T., Alexandre, C., Peyrin, F., 2002. Synchrotron Radiation Microtomography Allows the Analysis of Three-Dimensional Microarchitecture and Degree of Mineralization of Human Iliac Crest Biopsy Specimens: Effects of Etidronate Treatment. J. Bone Miner. Res. 17, 1372–1382. doi:10.1359/jbmr.2002.17.8.1372

O'Brien, F.J., Taylor, D., Dickson, G.R., Lee, T.C., 2000. Visualisation of three-dimensional microcracks in compact bone. J. Anat. 197 Pt 3, 413–420. doi:10.1046/j.1469-7580.2000.19730413.x

O'Brien, F.J., Taylor, D., Lee, T.C., 2005a. The effect of bone microstructure on the initiaton and growth of microcracks. J. Orthop. Res. 23, 475–480.

O'Brien, F.J., Taylor, D., Lee, T.C., 2005b. The effect of bone microstructure on the initiation and growth of microcracks, J. Orthop. Res. doi:10.1016/j.orthres.2004.08.005

Olvera, D., Zimmermann, E.A., Ritchie, R.O., 2012. Mixed-mode toughness of human cortical bone containing a longitudinal crack in far-field compression. Bone 50, 331–336. doi:10.1016/j.bone.2011.11.004

Oxlund, H., Barckman, M., Ørtoft, G., Andreassen, T.T., 1995. Reduced concentrations of collagen cross-links are associated with reduced strength of bone. Bone 17, 365–371. doi:10.1016/8756-3282(95)00328-B

Pacureanu, A., Langer, M., Boller, E., Tafforeau, P., Peyrin, F., 2012. Nanoscale imaging of the bone cell network with synchrotron X-ray tomography: optimization of acquisition setup. Med. Phys. 39, 2229. doi:10.1118/1.3697525

Paganin, D., Mayo, S.C., Gureyev, T.E., Miller, P.R., Wilkins, S.W., 2002. Simultaneous phase and amplitude extraction from a single defocused image of a homogeneous object. J. Microsc. 206, 33–40. doi:10.1046/j.1365-2818.2002.01010.x

Panjabi, M.M., Krag, M., Summers, D., Videman, T., 1985. Biomechanical time???tolerance of fresh cadaveric human spine specimens. J. Orthop. Res. 3, 292–300. doi:10.1002/jor.1100030305

Parfitt, M.A., Drezner, M.K., Glorieux, F.H., Kanis, J. a, Malluche, H., Meunier, P.J., Ott, S.M., Recker, R.R., 1987. Bone Histomorphometry : Standardization of Nomenclature, Symbols, and Units 2, 595–610.

Parnell, W.J., Grimal, Q., 2009. The influence of mesoscale porosity on cortical bone anisotropy. Investigations via asymptotic homogenization. J. R. Soc. Interface 6, 97–109. doi:10.1098/rsif.2008.0255

Paschalis, E.P., Verdelis, K., Doty, S.B., Boskey, a L., Mendelsohn, R., Yamauchi, M., 2001. Spectroscopic characterization of collagen cross-links in bone. J. Bone Miner. Res. 16, 1821–1828. doi:10.1359/jbmr.2001.16.10.1821

Pelker, R.R., Friedlaender, G.E., Markham, T.C., Panjabi, M.M., Moen, C.J., 1984. Effects of freezing and freeze-drying on the biomechanical properties of rat bone. J. Orthop. Res. 1, 405–11. doi:10.1002/jor.1100010409

Perilli, E., Bala, Y., Zebaze, R., Reynolds, K.J., Seeman, E., 2015. Regional Heterogeneity in the Configuration of the Intracortical Canals of the Femoral Shaft. Calcif. Tissue Int. doi:10.1007/s00223-015-0014-5

Peyrin, F., Engelke, K., 2012. CT Imaging: Basics and New Trends. Handb. Part. Detect. Imaging 883–915. doi:10.1007/978-3-642-13271-1_37

Phelps, J.B., Hubbard, G.B., Wang, X., Agrawal, C.M., 2000. Microstructural heterogeneity and the fracture toughness of bone. J. Biomed. Mater. Res. 51, 735–741. doi:10.1002/1097-4636(20000915)51:4<735::AID-JBM23>3.0.CO;2-G

Pistoia, W., van Rietbergen, B., Lochmüller, E.-M., Lill, C. a, Eckstein, F., Rüegsegger, P., 2002. Estimation of distal radius failure load with micro-finite element analysis models based on three-dimensional peripheral quantitative computed tomography images. Bone 30, 842–848. doi:10.1016/S8756-3282(02)00736-6

Pistoia, W., Van Rietbergen, B., Rüegsegger, P., 2003. Mechanical consequences of different scenarios for simulated bone atrophy and recovery in the distal radius. Bone 33, 937–945. doi:10.1016/j.bone.2003.06.003

Ponson, L., Srivastava, A., Osovski, S., Bouchaud, E., Tvergaard, V., Needleman, A., 2013. Correlating toughness and roughness in ductile fracture 1–5.

Poole, K.E.S., Treece, G.M., Mayhew, P.M., Vaculík, J., Dungl, P., Horák, M., Štěpán, J.J., Gee, A.H., 2012. Cortical thickness mapping to identify focal osteoporosis in patients with hip fracture. PLoS One 7, 1–8. doi:10.1371/journal.pone.0038466

Pope, M.H., Outwater, J.O., 1972. The fracture characteristics of bone substance. J. Biomech. 5, 457–465. doi:10.1016/0021-9290(72)90004-8

Poundarik, A. a, Wu, P.-C., Evis, Z., Sroga, G.E., Ural, A., Rubin, M., Vashishth, D., 2015. A direct role of collagen glycation in bone fracture. J. Mech. Behav. Biomed. Mater. 50, 82–92. doi:10.1016/j.jmbbm.2015.05.025

Qiu, S., Sudhaker Rao, D., Fyhrie, D.P., Palnitkar, S., Parfitt, A.M., 2005. The morphological

association between microcracks and osteocyte lacunae in human cortical bone. Bone 37, 10–15. doi:10.1016/j.bone.2005.01.023

Radon, J., 1917. Über die Bestimmung von Funktionen durch ihre Integralwerte l ängs gewisse Mannigfaltigkeiten. Berichte Sächsische Gesellschaft der Wissenschaften 69, 262–277.

Rath Bonivtch, A., Bonewald, L.F., Nicolella, D.P., 2007. Tissue strain amplification at the osteocyte lacuna: A microstructural finite element analysis. J. Biomech. 40, 2199–2206. doi:10.1016/j.jbiomech.2006.10.040

Reilly, D.T., Burstein, a H., 1975. The elastic and ultimate properties of compact bone tissue. J. Biomech. 8, 393–405. doi:10.1016/0021-9290(75)90075-5

Revell, P. a, 1983. Histomorphometry of bone. J. Clin. Pathol. 36, 1323–1331. doi:10.1136/jcp.37.6.713-b

Reznikov, N., Shahar, R., Weiner, S., 2014. Three-dimensional structure of human lamellar bone: The presence of two different materials and new insights into the hierarchical organization. Bone 59, 93–104. doi:10.1016/j.bone.2013.10.023

Rho, J.Y., Kuhn-Spearing, L., Zioupos, P., 1998. Mechanical properties and the hierarchical structure of bone. Med. Eng. Phys. 20, 92–102. doi:10.1016/S1350-4533(98)00007-1

Rice, J.R., 1968. A Path Independent Integral and the Approximate Analysis of Strain Concentration by Notches and Cracks. J. Appl. Mech. 35, 379. doi:10.1115/1.3601206

Ritchie, R.O., 1999. Mechanisms of Fatigue-Crack Propagation in Ductile and Brittle Solids. Int. J. Fract. 100, 55–83. doi:10.1023/A:1018655917051

Ritchie, R.O., 1988. Mechanisms of fatigue crack propagation in metals, ceramics and composites: Role of crack tip shielding. Mater. Sci. Eng. A 103, 15–28. doi:10.1016/0025-5416(88)90547-2

Ritchie, R.O., Buehler, M.J., Hansma, P., 2009. Plasticity and toughness in bone. Phys. Today 62, 41–47. doi:10.1063/1.3156332

Ritchie, R.O., Koester, K.J., Ionova, S., Yao, W., Lane, N.E., Ager, J.W., 2008. Measurement of the toughness of bone: A tutorial with special reference to small animal studies. Bone 43, 798–812. doi:10.1016/j.bone.2008.04.027

Ritchie, R.O., Nalla, R.K., Kruzic, J.J., Ager, J.W., Balooch, G., Kinney, J.H., 2006. Fracture and ageing in bone: Toughness and structural characterization. Strain 42, 225–232. doi:DOI 10.1111/j.1475-1305.2006.00282.x

Robertson, D.M., Barrett, C.R., 1978. Fracture toughness, critical crack length and plastic zone size in bone. J. Biomech. 11, 359–364. doi:10.1016/0021-9290(78)90070-2

Robinovitch, S.N., Hayes, W.C., McMahon, T. a, 1991. Prediction of femoral impact forces in falls on the hip. J. Biomech. Eng. 113, 366–374. doi:10.1115/1.2895414

Rubinacci, a., Tresoldi, D., Scalco, E., Villa, I., Adorni, F., Moro, G.L., Fraschini, G.F., Rizzo, G., 2012. Comparative high-resolution pQCT analysis of femoral neck indicates different bone mass distribution in osteoporosis and osteoarthritis. Osteoporos. Int. 23, 1967–1975. doi:10.1007/s00198-011-1795-7

Saito, M., Fujii, K., Soshi, S., Tanaka, T., 2006. Reductions in degree of mineralization and enzymatic collagen cross-links and increases in glycation-induced pentosidine in the femoral neck cortex in cases of femoral neck fracture. Osteoporos. Int. 17, 986–995. doi:10.1007/s00198-006-0087-0

Saito, M., Marumo, K., 2010. Collagen cross-links as a determinant of bone quality: A possible explanation for bone fragility in aging, osteoporosis, and diabetes mellitus. Osteoporos. Int. 21, 195–214. doi:10.1007/s00198-009-1066-z

Saito, M., Marumo, K., Fujii, K., Ishioka, N., 1997. Single-Column High-Performance Liquid Chromatographic–Fluorescence Detection of Immature, Mature, and Senescent Cross-Links of Collagen. Anal. Biochem. 253, 26–32. doi:10.1006/abio.1997.2350

Salomé, M., Peyrin, F., Cloetens, P., Odet, C., Laval-Jeantet, a M., Baruchel, J., Spanne, P., 1999. A synchrotron radiation microtomography system for the analysis of trabecular bone samples. Med. Phys. 26, 2194–2204. doi:10.1118/1.598736

Sanborn, B., Gunnarsson, C.A., Foster, M., Weerasooriya, T., 2016. Quantitative Visualization of Human Cortical Bone Mechanical Response: Studies on the Anisotropic Compressive Response and Fracture Behavior as a Function of Loading Rate. Exp. Mech. 81–95. doi:10.1007/s11340-015-0060-y

Schladitz, K., Ohser, J., Nagel, W., 2006. Measuring Intrinsic Volumes in Digital 3d Images. Discret. Geom. Comput. Imag. 4245, 247–258. doi:10.1007/11907350_21

Schneider, P., Meier, M., Wepf, R., Müller, R., 2011. Serial FIB/SEM imaging for quantitative 3D assessment of the osteocyte lacuno-canalicular network. Bone 49, 304–311. doi:10.1016/j.bone.2011.04.005

Schrof, S., Varga, P., Galvis, L., Raum, K., Masic, A., 2014. 3D Raman mapping of the collagen fibril orientation in human osteonal lamellae. J. Struct. Biol. 187, 266–275. doi:10.1016/j.jsb.2014.07.001

Sedlin, E.D., Hirsch, C., 1966. Factors affecting the determination of the physical properties of femoral cortical bone. Acta Orthop. Scand. 37, 29–48. doi:10.3109/17453676608989401

Seeman, E., Delmas, P.D., 2006. Bone quality--the material and structural basis of bone strength and fragility. N. Engl. J. Med. 354, 2250–2261. doi:10.1056/NEJMra053077

Shannahan, L., Weerasooriya, T., Gunnarsson, A., Sanborn, B., Lamberson, L., Shannahan, L., Lamberson, L., Weerasooriya, T., Gunnarsson, A., 2015. Rate-dependent fracture modes in

human femoral cortical bone. Int. J. Fract. 194, 81–92. doi:10.1007/s10704-015-0035-0

Shapiro, J.R., Boskey, A.L., Doty, S.B., Lukashova, L., Blue, M.E., 2017. Zoledronic acid improves bone histomorphometry in a murine model of Rett syndrome. Bone 99, 1–7. doi:10.1016/j.bone.2017.03.040

Sherman, V.R., Yang, W., Meyers, M. a., 2015. The materials science of collagen. J. Mech. Behav. Biomed. Mater. 1–29. doi:10.1016/j.jmbbm.2015.05.023

Shier, D., Butler, J., Lewis, R., 1974. Skeletal system, in: Hol's Human Anatomy and Physiology. pp. 132–177. doi:10.1016/B978-0-7020-2782-6.50015-6

Silver, F.H., Christiansen, D.L., Snowhill, P.B., Chen, Y., 2001. Transition from viscous to elastic-based dependency of mechanical properties of self-assembled type I collagen fibers. J. Appl. Polym. Sci. 79, 134–142. doi:10.1002/1097-4628(20010103)79:1<134::AID-APP160>3.0.CO;2-E

Siris, E.S., Adler, R., Bilezikian, J., Bolognese, M., Dawson-Hughes, B., Favus, M.J., Harris, S.T., Jan De Beur, S.M., Khosla, S., Lane, N.E., Lindsay, R., Nana, a. D., Orwoll, E.S., Saag, K., Silverman, S., Watts, N.B., 2014. The clinical diagnosis of osteoporosis: A position statement from the National Bone Health Alliance Working Group. Osteoporos. Int. 25, 1439–1443. doi:10.1007/s00198-014-2655-z

Siris, E.S., Chen, Y.-T., Abbott, T. a, Barrett-Connor, E., Miller, P.D., Wehren, L.E., Berger, M.L., 2004. Bone mineral density thresholds for pharmacological intervention to prevent fractures. Arch. Intern. Med. 164, 1108–1112. doi:10.1001/archinte.164.10.1108

Slyfield, C.R., Tkachenko, E. V, Wilson, D.L., J, H.C., 2012. Three-dimensional dynamic bone histomorphometry. J. Bone Miner. Res. 27, 486–495. doi:10.1097/MCO.0b013e32831cef61.Inflammatory

Sobelman, O.S., Gibeling, J.C., Stover, S.M., Hazelwood, S.J., Yeh, O.C., Shelton, D.R., Martin, R.B., 2004. Do microcracks decrease or increase fatigue resistance in cortical bone? J. Biomech. 37, 1295–1303. doi:10.1016/j.jbiomech.2003.12.034

Spadaro, J.A., Werner, F.W., Brenner, R.A., Fortino, M.D., Fay, L.A., Edwards, W.T., 1994. Cortical and trabecular bone contribute strength to the osteopenic distal radius. J. Orthop. Res. 12, 211–218. doi:10.1002/jor.1100120210

Sroga, G.E., Siddula, A., Vashishth, D., 2015. Glycation of human cortical and cancellous bone captures differences in the formation of maillard reaction products between glucose and ribose. PLoS One 10, 1–19. doi:10.1371/journal.pone.0117240

Stankeiwicz, P.J., Metz, K.R., Sassani, J.W., Briggs, R.W., 1989. Nuclear magnetic resonance study of free and bound water fractions in normal lenses. Invest. Ophthalmol. Vis. Sci. 30, 2361–2369.

Stevens, A., Lowe, J., 2006. Appareil Musculosquelettique, in: Elsevier, Masson (Eds.), Histologie Humaine. pp. 265–278.

Sumi, Y., Nemat-Nasser, S., Keer, L.M., 1983. On crack branching and curving in a finite body. Int. J. Fract. 21, 67–79. doi:10.1007/BF01134200

Swain, M. V, 1989. R-Curve Behavior. J. Am. Ceram. Soc.

Tan, J.S., Eng, J.J., Robinovitch, S.N., Warnick, B., 2006. Wrist impact velocities are smaller in forward falls than backward falls from standing. J. Biomech. 39, 1804–1811. doi:10.1016/j.jbiomech.2005.05.016

Tang, S.Y., Allen, M.R., Phipps, R., Burr, D.B., Vashishth, D., 2009. Changes in non-enzymatic glycation and its association with altered mechanical properties following 1-year treatment with risedronate or alendronate. Osteoporos. Int. 20, 887–894. doi:10.1007/s00198-008-0754-4

Tang, S.Y., Vashishth, D., 2011. The relative contributions of non-enzymatic glycation and cortical porosity on the fracture toughness of aging bone. J. Biomech. 44, 330–336. doi:10.1016/j.jbiomech.2010.10.016

Tang, S.Y., Vashishth, D., 2010. Non-enzymatic glycation alters microdamage formation in human cancellous bone. Bone 46, 148–154. doi:10.1016/j.bone.2009.09.003

Taylor, D., 2006. The fracture mechanics of bone. An. Mec. ma Fract. I, 7–11.

Taylor, D., Kasiri, S., Brazel, E., 2009. Fatigue of Bone. Frat. ed Integrità Strutt. 10, 12–20. doi:10.3221/IGF-ESIS.10.02

The American Society of Mechanical Engineers (ASME), 2006. E 1820-01: Standard Test Method for Measurement of Fracture Toughness. … . Philadelphia PA Am. Soc. Test. … 46.

Thurner, P.J., Chen, C.G., Ionova-Martin, S., Sun, L., Harman, A., Porter, A., Ager, J.W., Ritchie, R.O., Alliston, T., 2010. Osteopontin deficiency increases bone fragility but preserves bone mass. Bone 46, 1564–1573. doi:10.1016/j.bone.2010.02.014

Thurner, P.J., Erickson, B., Jungmann, R., Schriock, Z., Weaver, J.C., Fantner, G.E., Schitter, G., Morse, D.E., Hansma, P.K., 2007. High-speed photography of compressed human trabecular bone correlates whitening to microscopic damage. Eng. Fract. Mech. 74, 1928–1941. doi:10.1016/j.engfracmech.2006.05.024

Treece, G.M., Gee, a. H., Mayhew, P.M., Poole, K.E.S., 2010. High resolution cortical bone thickness measurement from clinical CT data. Med. Image Anal. 14, 276–290. doi:10.1016/j.media.2010.01.003

Treece, G.M., Poole, K.E.S., Gee, a. H., 2012. Imaging the femoral cortex: Thickness, density and mass from clinical CT. Med. Image Anal. 16, 952–965. doi:10.1016/j.media.2012.02.008

Turnbull, T.L., Baumann, A.P., Roeder, R.K., 2014. Fatigue microcracks that initiate fracture are

located near elevated intracortical porosity but not elevated mineralization. J. Biomech. 47, 3135–3142. doi:10.1016/j.jbiomech.2014.06.022

Ural, A., Vashishth, D., 2014. Hierarchical perspective of bone toughness – from molecules to fracture. Int. Mater. Rev. 59, 245–263. doi:10.1179/1743280414Y.0000000031

Ural, A., Zioupos, P., Buchanan, D., Vashishth, D., 2011. The effect of strain rate on fracture toughness of human cortical bone: A finite element study. J. Mech. Behav. Biomed. Mater. 4, 1021–1032. doi:10.1016/j.jmbbm.2011.03.011

Ushiki, T., 2002. Collagen fibers, reticular fibers and elastic fibers. A comprehensive understanding from a morphological viewpoint. Arch. Histol. Cytol. doi:10.1679/aohc.65.109

van der Rest, M., Garrone, R., 1991. Collagen family of proteins. FASEB J. 5, 2814–23.

Van Haaren, E.H., Van Der Zwaard, B.C., Van Der Veen, A.J., Heyligers, I.C., Wuisman, P.I., Smit, T.H., 2008. Effect of long-term preservation on the mechanical properties of cortical bone in goats. Acta Orthop. 79, 708–716. doi:10.1080/17453670810016759

van Hove, R.P., Nolte, P.A., Vatsa, A., Semeins, C.M., Salmon, P.L., Smit, T.H., Klein-Nulend, J., 2009. Osteocyte morphology in human tibiae of different bone pathologies with different bone mineral density - Is there a role for mechanosensing? Bone 45, 321–329. doi:10.1016/j.bone.2009.04.238

Van Lenthe, G.H., Müller, R., 2008. CT-Based Visualization and Quantification of Bone Microstructure In Vivo. IBMS Bonekey 5, 410–425. doi:10.1138/20080348

van Oers, R.F.M., Wang, H., Bacabac, R.G., 2015. Osteocyte Shape and Mechanical Loading. Curr. Osteoporos. Rep. 13, 61–66. doi:10.1007/s11914-015-0256-1

van Rietbergen, B., Ito, K., 2015. A survey of micro-finite element analysis for clinical assessment of bone strength: The first decade. J. Biomech. 48, 832–841. doi:10.1016/j.jbiomech.2014.12.024

Varga, P., Baumbach, S., Pahr, D., Zysset, P.K., 2009. Validation of an anatomy specific finite element model of Colles' fracture. J. Biomech. 42, 1726–1731. doi:10.1016/j.jbiomech.2009.04.017

Varga, P., Hesse, B., Langer, M., Schrof, S., Männicke, N., Suhonen, H., Pacureanu, A., Pahr, D., Peyrin, F., Raum, K., 2014. Synchrotron X-ray phase nano-tomography-based analysis of the lacunar-canalicular network morphology and its relation to the strains experienced by osteocytes in situ as predicted by case-specific finite element analysis. Biomech. Model. Mechanobiol. doi:10.1007/s10237-014-0601-9

Varga, P., Pacureanu, A., Langer, M., Suhonen, H., Hesse, B., Grimal, Q., Cloetens, P., Raum, K., Peyrin, F., 2013. Investigation of the three-dimensional orientation of mineralized collagen fibrils in human lamellar bone using synchrotron X-ray phase nano-tomography. Acta

Biomater. 9, 8118–8127. doi:10.1016/j.actbio.2013.05.015

Vashishth, D., 2007. Hierarchy of bone microdamage at multiple length scales. Int. J. Fatigue 29, 1024–1033. doi:10.1016/j.ijfatigue.2006.09.010

Vashishth, D., 2007. The role of the collagen matrix in skeletal fragility. Curr. Osteoporos. Rep. 5, 62–66. doi:10.1007/s11914-007-0004-2

Vashishth, D., 2004. Rising crack-growth-resistance behavior in cortical bone: Implications for toughness measurements. J. Biomech. 37, 943–946. doi:10.1016/j.jbiomech.2003.11.003

Vashishth, D., Behiri, J.C., Bonfield, W., 1997. Crack growth resistance in cortical bone: Concept of microcrack toughening. J. Biomech. 30, 763–769. doi:10.1016/S0021-9290(97)00029-8

Vashishth, D., Gibson, G.J., Fyhrie, D.P., 2005. Sexual dimorphism and age dependence of osteocyte lacunar density for human vertebral cancellous bone. Anat. Rec. - Part A Discov. Mol. Cell. Evol. Biol. 282, 157–162. doi:10.1002/ar.a.20146

Vashishth, D., Gibson, G.J., Khoury, J.I., Schaffler, M.B., Kimura, J., Fyhrie, D.P., 2001. Influence of nonenzymatic glycation on biomechanical properties of cortical bone. Bone 28, 195–201. doi:10.1016/S8756-3282(00)00434-8

Vatsa, A., Breuls, R.G., Semeins, C.M., Salmon, P.L., Smit, T.H., Klein-Nulend, J., 2008. Osteocyte morphology in fibula and calvaria - Is there a role for mechanosensing? Bone 43, 452–458. doi:10.1016/j.bone.2008.01.030

Verborgt, O., Gibson, G.J., Schaffler, M.B., 2000. Loss of osteocyte integrity in association with microdamage and bone remodeling after fatigue in vivo. J. Bone Miner. Res. 15, 60–67. doi:10.1359/jbmr.2000.15.1.60

Verbruggen, S.W., Vaughan, T.J., McNamara, L.M., 2012. Strain amplification in bone mechanobiology: a computational investigation of the in vivo mechanics of osteocytes. J. R. Soc. Interface 9, 2735–2744. doi:10.1098/rsif.2012.0286

Verhulp, E., van Rietbergen, B., Huiskes, R., 2008. Load distribution in the healthy and osteoporotic human proximal femur during a fall to the side. Bone 42, 30–35. doi:10.1016/j.bone.2007.08.039

Viguet-Carrin, S., Garnero, P., Delmas, P.D., 2006. The role of collagen in bone strength. Osteoporos. Int. 17, 319–336. doi:10.1007/s00198-005-2035-9

Viguet-Carrin, S., Gineyts, E., Bertholon, C., Delmas, P.D., 2009. Simple and sensitive method for quantification of fluorescent enzymatic mature and senescent crosslinks of collagen in bone hydrolysate using single-column high performance liquid chromatography. J. Chromatogr. B 877, 1–7. doi:10.1016/j.jchromb.2008.10.043

Voide, R., Schneider, P., Stauber, M., Wyss, P., Stampanoni, M., Sennhauser, U., Van Lenthe, G.H., Müller, R., 2009. Time-lapsed assessment of microcrack initiation and propagation in

murine cortical bone at submicrometer resolution. Bone 45, 164–173. doi:10.1016/j.bone.2009.04.248

Wachter, N.J., Augat, P., Krischak, G.D., Mentzel, M., Kinzl, L., Claes, L., 2001. Prediction of cortical bone porosity in vitro by microcomputed tomography. Calcif. Tissue Int. 68, 38–42. doi:10.1007/s002230001182

Wachter, N.J., Augat, P., Krischak, G.D., Sarkar, M.R., Mentzel, M., Kinzl, L., Claes, L., 2001. Prediction of strength of cortical bone in vitro by microcomputed tomography. Clin. Biomech. 16, 252–256. doi:10.1016/S0268-0033(00)00092-9

Wagermaier, W., Klaushofer, K., Fratzl, P., 2015. Fragility of Bone Material Controlled by Internal Interfaces. Calcif. Tissue Int. doi:10.1007/s00223-015-9978-4

Wakamatsu, E., Sissions, H.A., 1969. The cancellous bone of the iliac crest. Calcif. Tissue Int. 4, 147–161.

Walker, R.P., 1992. Synchrotron Radiation. Cern Accel. Sch. Course Gen. Accel. Phys. 437–459.

Wallach, S., Feinblatt, J.D., Carstens, J.H., Avioli, L. V., 1992. The bone quality problem. Calcif. Tissue Int. 51, 169–172. doi:10.1007/BF00334542

Wang, L., Wang, Y., Han, Y., Henderson, S.C., Majeska, R.J., Weinbaum, S., Schaffler, M.B., 2005. In situ measurement of solute transport in the bone lacunar-canalicular system. Proc. Natl. Acad. Sci. U. S. A. 102, 11911–11916. doi:10.1073/pnas.0505193102

Wang, W., Elbanna, A., 2014. Crack propagation in bone on the scale of mineralized collagen fibrils: Role of polymers with sacrificial bonds and hidden length. Bone 68, 20–31. doi:10.1016/j.bone.2014.07.035

Weinbaum, S., Cowin, S.C., Zeng, Y., 1994. A model for the excitation of osteocytes by mechanical loading-induced bone fluid shear stresses. J. Biomech. 27, 339–360. doi:10.1016/0021-9290(94)90010-8

Willett, T.L., Sutty, S., Gaspar, A., Avery, N., Grynpas, M., 2013. In vitro non-enzymatic ribation reduces post-yield strain accommodation in cortical bone. Bone 52, 611–622. doi:10.1016/j.bone.2012.11.014

Wolff, J., 1892. The Law of Bone Remodelling. Berlin, Heidelberg.

Wolfram, U., Schwiedrzik, J.J., Mirzaali, M.J., Bürki, A., Varga, P., Olivier, C., Peyrin, F., Zysset, P.K., 2016. Characterizing microcrack orientation distribution functions in osteonal bone samples. J. Microsc. 0, 1–14. doi:10.1111/jmi.12440

Woodside, M., Willett, T.L., 2016. Elastic-plastic fracture toughness and rising JR-curve behavior of cortical bone is partially protected from irradiation-sterilization-induced degradation by ribose protectant. J. Mech. Behav. Biomed. Mater. 64, 53–64. doi:10.1016/j.jmbbm.2016.07.001

Woodyard, J.R., 1948. High-energy particle accelerators. Electr. Eng. 67, 759–767. doi:10.1109/EE.1948.6444266

World Health Organization, 2007. WHO Global Report on Falls Prevention in Older Age., Community Health. doi:978 92 4 156353 6

Yamaguchi, H., Kikugawa, H., Asaka, T., Kasuya, H., Kuninori, M., 2011. Measurement of Cortical Bone Strain Distribution by Image Correlation Techniques and from Fracture Toughness. Mater. Trans. 52, 1026–1032. doi:10.2320/matertrans.M2010426

Yamauchi, M., Woodley, D.T., Mechanic, G.L., 1988. Aging and cross-linking of skin collagen. Biochem. Biophys. Res. Commun. 152, 898–903. doi:10.1016/S0006-291X(88)80124-4

Yan, J., 2005. Elasti-Plastic fracutre mechanics of compact bone.

Yan, J., Mecholsky, J.J., Clifton, K.B., 2007. How tough is bone? Application of elastic-plastic fracture mechanics to bone. Bone 40, 479–484. doi:10.1016/j.bone.2006.08.013

Yang, Q.D., Cox, B.N., Nalla, R.K., Ritchie, R.O., 2006a. Fracture length scales in human cortical bone: The necessity of nonlinear fracture models. Biomaterials 27, 2095–2113. doi:10.1016/j.biomaterials.2005.09.040

Yang, Q.D., Cox, B.N., Nalla, R.K., Ritchie, R.O., 2006b. Re-evaluating the toughness of human cortical bone. Bone 38, 878–887. doi:10.1016/j.bone.2005.10.014

Yeni, Y.N., Brown, C.U., Wang, Z., Norman, T.L., 1997. The influence of bone morphology on fracture toughness of the human femur and tibia. Bone 21, 453–459. doi:10.1016/S8756-3282(97)00173-7

Yeni, Y.N., Fyhrie, D.P., 2002. Fatigue damage-fracture mechanics interaction in cortical bone. Bone 30, 509–514. doi:10.1016/S8756-3282(01)00696-2

Yeni, Y.N., Norman, T.L., 2000a. Calculation of porosity and osteonal cement line effects on the effective fracture toughness of cortical bone in longitudinal crack growth. J. Biomed. Mater. Res. 51, 504–509. doi:10.1002/1097-4636(20000905)51:3<504::AID-JBM27>3.0.CO;2-I

Yeni, Y.N., Norman, T.L., 2000b. Fracture toughness of human femoral neck: Effect of microstructure, composition, and age. Bone 26, 499–504. doi:10.1016/S8756-3282(00)00258-1

Zapata, E., 2015. Bone strength of the human distal radius under fall loading conditions : an experimental and numerical study.

Zebaze, R., Ghasem-Zadeh, A., Bohte, A., Iuliano-Burns, S., Mirams, M., Price, R.I., Mackie, E.J., Seeman, E., 2010. Intracortical remodelling and porosity in the distal radius and post-mortem femurs of women: a cross-sectional study. Lancet 375, 1729–1736. doi:10.1016/S0140-6736(10)60320-0

Zimmermann, E.A., Gludovatz, B., Schaible, E., Busse, B., Ritchie, R.O., 2014. Fracture resistance

of human cortical bone across multiple length-scales at physiological strain rates. Biomaterials 35, 5472–5481. doi:10.1016/j.biomaterials.2014.03.066

Zimmermann, E.A., Launey, M.E., Barth, H.D., Ritchie, R.O., 2009. Mixed-mode fracture of human cortical bone. Biomaterials 30, 5877–5884. doi:10.1016/j.biomaterials.2009.06.017

Zimmermann, E.A., Ritchie, R.O., 2015. Bone as a Structural Material. Adv. Healthc. Mater. 4, 1287–1304. doi:10.1002/adhm.201500070

Zimmermann, E.A., Schaible, E., Bale, H., Barth, H.D., Tang, S.Y., Reichert, P., Busse, B., Alliston, T., Ager, J.W., Ritchie, R.O., 2011. Age-related changes in the plasticity and toughness of human cortical bone at multiple length scales. Proc. Natl. Acad. Sci. U. S. A. 108, 14416–14421. doi:10.1073/pnas.1107966108

Zimmermann, E.A., Schaible, E., Bale, H., Barth, H.D., Tang, S.Y., Reichert, P., Busse, B., Alliston, T., Ager, J.W., Ritchie, R.O., Schaible, E., Bale, H., Barth, H.D., Tang, S.Y., Reichert, P., 2012. Age-related changes in the plasticity and toughness of human cortical bone at multiple length scales. Proc. Natl. Acad. Sci. 109, 11890–11890. doi:10.1073/pnas.1209596109

Zimmermann, E.A., Schaible, E., Gludovatz, B., Schmidt, F.N., Riedel, C., Krause, M., Vettorazzi, E., Acevedo, C., Hahn, M., Püschel, K., Tang, S., Amling, M., Ritchie, R.O., Busse, B., 2016. Intrinsic mechanical behavior of femoral cortical bone in young , osteoporotic and bisphosphonate- treated individuals in low- and high energy fracture conditions. Nat. Publ. Gr. 1–12. doi:10.1038/srep21072

Zioupos, P., 1998. Recent developments in the study of failure of solid biomaterials and bone: “Fracture” and “pre-fracture” toughness. Mater. Sci. Eng. C 6, 33–40. doi:10.1016/S0928-4931(98)00033-2

Zioupos, P., Currey, J.D., Hamer, a. J., 1999. The role of collagen in the declining mechanical properties of aging human cortical bone. J. Biomed. Mater. Res. 45, 108–116. doi:10.1002/(SICI)1097-4636(199905)45:2<108::AID-JBM5>3.0.CO;2-A

Zioupos, P., Hansen, U., Currey, J.D., 2008. Microcracking damage and the fracture process in relation to strain rate in human cortical bone tensile failure. J. Biomech. 41, 2932–2939. doi:10.1016/j.jbiomech.2008.07.025

Annex

Annex 1 Spearman correlation coefficient matrix between the volume fractions and the coefficient of absorption n the three anatomical locations

Femoral diaphysis

	μ	Ca.V/BV	Ca.Th	SD Ca.Th	Lc.V/BV	μCr.V/BV	$\mu Cr.V/BV_{QS}$	$TotCr.V/BV_{QS}$	$\mu Cr.V/BV_F$	$TotCr.V/BV_F$
μ	1	ns	ns	ns	ns	ns	ns	ns	ns	ns
Ca.V/BV		1	0.91*	0.98*	ns	ns	ns	ns	ns	ns
Ca.Th			1	0.93*	ns	ns	ns	ns	ns	ns
SD Ca.Th				1	ns	ns	ns	ns	ns	ns
Lc.V/BV					1	ns	0.86*	ns	ns	ns
μCr.V/BV						1	ns	ns	ns	ns
$\mu Cr.V/BV_{QS}$							1	0.79*	ns	ns
$TotCr.V/BV_{QS}$								1	ns	ns
$\mu Cr.V/BV_F$									1	0.76*
$TotCr.V/B_F$										1

Femoral neck

	μ	Ca.V/BV	Ca.Th	SD Ca.Th	Lc.V/BV	μCr.V/BV	$\mu Cr.V/BV_{QS}$	$TotCr.V/BV_{QS}$	$\mu Cr.V/BV_F$	$TotCr.V/BV_F$
μ	1	-0.83*	ns	-0.83*	ns	ns	ns	ns	ns	ns
Ca.V/BV		1	0.79*	0.95*	ns	ns	ns	ns	ns	ns
Ca.Th			1	0.79*	ns	ns	ns	ns	ns	ns
SD Ca.Th				1	-0.76*	ns	ns	ns	ns	ns
Lc.V/BV					1	ns	ns	ns	ns	ns
μCr.V/BV						1	0.79*	ns	ns	ns
$\mu Cr.V/BV_{QS}$							1	0.86*	ns	ns
$TotCr.V/BV_{QS}$								1	ns	ns
$\mu Cr.V/BV_F$									1	ns
$TotCr.V/B_F$										1

Radial diaphysis

	μ	Ca.V/BV	Ca.Th	SD Ca.Th	Lc.V/BV	μCr.V/BV	$\mu Cr.V/BV_{QS}$	$TotCr.V/BV_{QS}$	$\mu Cr.V/BV_F$	$TotCr.V/BV_F$
μ	1	-0.86*	-0.91*	-0.76*	ns	ns	ns	-0.64*	ns	ns
Ca.V/BV		1	0.88*	0.83*	ns	ns	0.76*	ns	ns	ns
Ca.Th			1	0.74*	ns	ns	0.81*	ns	ns	0.74*
SD Ca.Th				1	ns	ns	0.88*	ns	ns	ns
Lc.V/BV					1	ns	ns	ns	ns	ns
μCr.V/BV						1	ns	ns	ns	ns
$\mu Cr.V/BV_{QS}$							1	ns	ns	ns
$TotCr.V/BV_{QS}$								1	ns	ns
$\mu Cr.V/BV_F$									1	ns
$TotCr.V/B_F$										1

$_{QS}$ Quasi-static, $_F$ Fall, non-indication means control
***p < 0.05, ns non-significant**

Annex 2 Mature, immature, CX and PEN inter-correlation matrix between the four anatomical locations (Pearson coefficient r is given when p-value < 0.05)

Immature = [HLNL + DHLNL]				
r	**Femoral lateral diaphysis**	**Femoral medial diaphysis**	**Femoral neck**	**Radial diaphysis**
Femoral lateral diaphysis	1	0.85***	0.79***	ns
Femoral medial diaphysis		1	0.81**	ns
Femoral neck			1	ns
Radial diaphysis				1
Mature = [PYP + DPD]				
r	**Femoral lateral diaphysis**	**Femoral medial diaphysis**	**Femoral neck**	**Radial diaphysis**
Femoral lateral diaphysis	1	0.68***	ns	0.43*
Femoral medial diaphysis		1	ns	ns
Femoral neck			1	0.72***
Radial diaphysis				1
CX =[HLNL + DHLNL] / [PYD + DPD]				
r	**Femoral lateral diaphysis**	**Femoral medial diaphysis**	**Femoral neck**	**Radial diaphysis**
Femoral lateral diaphysis	1	0.92***	0.77***	ns
Femoral medial diaphysis		1	0.64**	ns
Femoral neck			1	ns
Radial diaphysis				1
PEN				
r	**Femoral lateral diaphysis**	**Femoral medial diaphysis**	**Femoral neck**	**Radial diaphysis**
Femoral lateral diaphysis	1	0.81***	ns	ns
Femoral medial diaphysis		1	0.44*	0.44*
Femoral neck			1	ns
Radial diaphysis				1

*** p-value < 0.0001; ** p-value < 0.01; * p-value < 0.05; ns: non-significant

Annex 3 Pearson's coefficient matrix between all different parameters investigated in the current study on the four anatomical locations (* p-value < 0.05; ** p-value < 0.01; *** p-value < 0.0001; ns: non-significant; QS: Quasi-Static; F: Fall)

Femoral lateral diaphysis

r	J_{el} (QS)	J_{el} (F)	J_{pl} (QS)	J_{pl} (F)	$J_{process}$ (QS)	$J_{process}$ (F)	J_{prop} (QS)	J_{prop} (F)	CX	PEN	Age
J_{el} (QS)	1	ns	ns	ns	ns	ns	ns	ns	ns	ns	ns
J_{el} (F)		1	ns	ns	ns	ns	ns	ns	ns	- 0.59**	ns
J_{pl} (QS)			1	0.64**	ns	ns	0.95***	ns	ns	ns	ns
J_{pl} (F)				1	0.68**	0.70***	ns	0.76***	ns	ns	ns
$J_{process}$ (QS)					1	ns	ns	0.58**	ns	ns	ns
$J_{process}$ (F)						1	ns	ns	ns	ns	ns
J_{prop} (QS)							1	ns	ns	ns	ns
J_{prop} (F)								1	0.67**	- 0.54**	ns
CX									1	- 0.67**	ns
PEN										1	0.51**
Age											1

Femoral medial diaphysis

r	J_{el} (QS)	J_{el} (F)	J_{pl} (QS)	J_{pl} (F)	$J_{process}$ (QS)	$J_{process}$ (F)	J_{prop} (QS)	J_{prop} (F)	CX	PEN	Age
J_{el} (QS)	1	ns	ns	ns	ns	ns	ns	ns	ns	ns	ns
J_{el} (F)		1	ns	ns	ns	ns	ns	ns	ns	ns	ns
J_{pl} (QS)			1	0.61**	ns	ns	0.97***	ns	ns	ns	ns
J_{pl} (F)				1	ns *	0.76***	0.53**	0.76***	ns	ns	ns
$J_{process}$ (QS)					1	ns	ns	ns	ns	ns	ns
$J_{process}$ (F)						1	ns	ns	ns	ns	ns
J_{prop} (QS)							1	ns	ns	ns	ns
J_{prop} (F)								1	ns	ns	ns
CX									1	- 0.63**	ns
PEN										1	0.64**
Age											1

Femoral neck

r	J_{el} (QS)	J_{el} (F)	J_{pl} (QS)	J_{pl} (F)	$J_{process}$ (QS)	$J_{process}$ (F)	J_{prop} (QS)	J_{prop} (F)	CX	PEN	Age
J_{el} (QS)	1	ns	ns	ns	ns	ns	ns	ns	ns	ns	0.49**
J_{el} (F)		1	0.53**	ns	ns	ns	ns	ns	ns	ns	ns
J_{pl} (QS)			1	ns	0.73***	ns	0.93***	ns	ns	ns	ns
J_{pl} (F)				1	ns	ns	ns	0.78***	ns	ns	ns
$J_{process}$ (QS)					1	ns	0.61**	ns	ns	ns	ns
$J_{process}$ (F)						1	ns	ns	ns	ns	ns
J_{prop} (QS)							1	ns	ns	ns	ns
J_{prop} (F)								1	ns	ns	ns
CX									1	- 0.76***	ns
PEN										1	ns
Age											1

Radial diaphysis

r	J_{el} (QS)	J_{el} (F)	J_{pl} (QS)	J_{pl} (F)	$J_{process}$ (QS)	$J_{process}$ (F)	J_{prop} (QS)	J_{prop} (F)	CX	PEN	Age
J_{el} (QS)	1	ns	ns	ns	ns	ns	ns	ns	ns	ns	ns
J_{el} (F)		1	ns	ns	ns	ns	ns	ns	ns	ns	ns
J_{pl} (QS)			1	0.48*	0.64**	ns	0.94***	ns	ns	ns	- 0.61***
J_{pl} (F)				1	ns	0.54**	ns	0.71***	ns	ns	ns
$J_{process}$ (QS)					1	ns	ns	ns	ns	ns	ns
$J_{process}$ (F)						1	ns	ns	ns	ns	ns
J_{prop} (QS)							1	ns	ns	ns	0.56**
J_{prop} (F)								1	ns	ns	ns
CX									1	ns	- 0.50**
PEN										1	0.67***
Age											1

Annex 4 Spearman's coefficient between biomechanical and biochemical or morphometric parameters for each anatomical location

Femoral diaphysis

Biomechanical parameter	Rate	Immature	Mature	μ	Ca.Dm	Lc.N/BV	Lc.ρ_1
J_{el}	Quasi-static:	0.10	0.00	0.21	0.05	0.43	0.17
	Fall:	**0.91***	0.24	-0.05	-0.10	-0.17	-0.55
$J_{process}$	Quasi-static:	0.59	-0.24	0.14	-0.56	-0.41	-0.51
	Fall:	-0.09	-0.50	0.61	**-1***	**-0.79***	**-0.89***
$J_{el} + J_{process}$	Quasi-static:	0.62	-0.21	0.12	-0.24	-0.53	-0.52
	Fall:	-0.04	-0.50	0.61	**-1***	**-0.79***	**-0.89***
J	Quasi-static:	0.31	-0.31	0.24	-0.41	**-0.83***	-0.60
	Fall:	0.02	-0.31	0.02	-0.43	**-0.91***	-0.48

Femoral Neck

Biomechanical parameter	Rate	Immature	Mature	μ	Ca.Dm	Lc.N/BV	Lc.ρ_1
J_{el}	Quasi-static:	0.43	0.54	0.19	-0.21	0.00	-0.52
	Fall:	0.37	0.66	-0.10	-0.07	0.24	-0.12
$J_{process}$	Quasi-static:	-0.09	0.66	0.05	**-0.79***	0.55	0.05
	Fall:	-0.60	0.43	0.52	-0.14	-0.21	-0.02
$J_{el} + J_{process}$	Quasi-static:	0.03	**0.89***	0.19	**-0.88***	0.62	0.07
	Fall:	-0.60	0.43	0.50	-0.19	-0.31	0.05
J	Quasi-static:	0.54	0.54	-0.10	-0.38	0.31	-0.29
	Fall:	0.83	0.43	-0.50	0.33	-0.38	**-0.79***

Radial diaphysis

Biomechanical parameter	Rate	Immature	Mature	μ	Ca.Dm	Lc.N/BV	Lc.ρ_1
J_{el}	Quasi-static:	0.12	0.69	0.71	-0.43	-0.54	-0.64
	Fall:	0.50	0.36	**0.76***	-0.62	-0.50	-0.43
$J_{process}$	Quasi-static:	-0.07	0.62	0.43	-0.14	-0.30	-0.60
	Fall:	0.57	0.48	0.55	-0.21	-0.10	-0.50
$J_{el} + J_{process}$	Quasi-static:	-0.07	0.62	0.43	-0.14	-0.29	-0.60
	Fall:	0.69	0.48	**0.74***	**-0.91***	-0.38	-0.64
J	Quasi-static:	0.41	0.33	0.31	-0.21	-0.14	-0.24
	Fall:	0.74	0.29	0.62	-0.57	-0.43	-0.36

** p-value ≤ 0.05; ** p-value ≤ 0.01; ns: non-significant

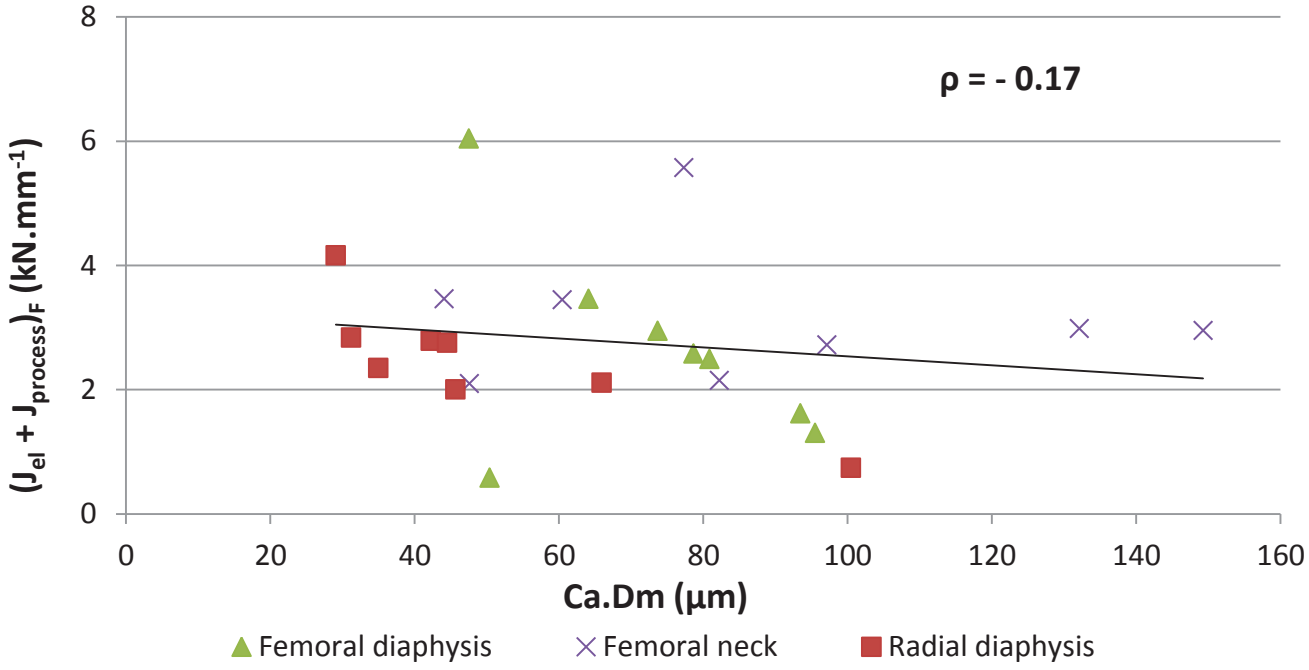

Annex 5 Jel + Jprocess under fall-like loading condition in function of Ca.Dm. Note that for femoral and radial diaphysis, the relation is almost linear.

Appendix 1 French summary

L'ostéoporose demeure aujourd'hui un problème majeur de santé publique. Des estimation montrent qu'une fracture osseuse se produit toutes les 3 secondes à travers le monde, avec comme conséquence un risque accru d'invalidité ou même de mortalité, ainsi qu'un poids économique non négligeable (Cooper et al., 1993; Hernlund et al., 2013; Johnell and Kanis, 2006; Leibson et al., 2002). En clinique l'ostéoporose est diagnostiquée en évaluant la densité du tissu osseux à l'aide de la technique de DXA (Dual X-ray Absoptiometry, (Genant et al., 1996)). Cette technique utilisée aujourd'hui en clinique, présente cependant certaines limites quant à la prédiction du risque de fracture. Environ 50 % des patients diagnostiqués comme n'étant pas à risque ont tout de même souffert d'une fracture osseuse après l'examen clinique (Siris et al., 2004). Si la densité permet une prédiction fiable de la résistance osseuse dans des conditions de chargement standard (Louis et al., 1995), les fractures osseuses *in vivo* impliquent des chargements complexes (Robinovitch et al., 1991; Verhulp et al., 2008). En 1991, Hayes *et al.* ont défini le risque de fracture comme étant le ratio entre l'effort appliqué à l'os et sa charge à la rupture (Hayes et al., 1991). Avec les récentes évolutions des techniques d'imagerie à haute résolution exploitables en clinique, des modèles numériques permettant de mieux estimer ce risque de fracture osseuse sont en voie de développement (Pistoia et al., 2002; Varga et al., 2009). Les fractures osseuses se produisent généralement à la suite d'une chute due à une perte d'équilibre, impliquant donc des vitesses de chargement élevées (Dubousset, 2014; Foldhazy, 2005; World Health Organization, 2007). Pour prédire le risque de fracture de façon précise, il semble ainsi nécessaire de considérer des chargements représentatifs d'une chute. Dans la majeure partie des cas, les modèles jusqu'alors développés pour prédire le risque de fracture, ne sont pas représentatifs de ce qu'il se produit dans un cas réel de chute (van Rietbergen and Ito, 2015).

A l'échelle macroscopique, l'os est constitué de deux matériaux différents : l'os trabéculaire qui présente une porosité importante et se situe au centre de l'organe ; et l'os cortical qui est compact et périphérique. Si l'implication de ces deux types de matériaux dans les mécanismes de fractures osseuses est avérée, l'implication de l'os cortical a été montré comme étant plus déterminant lorsqu'on considère les fractures diaphysaires ((Bala et al., 2015; Holzer et al., 2009). Le processus de fracture au sein de l'os cortical est un problème complexe qui implique l'organisation du tissu dans sa globalité (Seeman and Delmas, 2006). La ténacité semble être un paramètre intéressant étant donné qu'elle nous informe sur l'énergie qu'il est nécessaire d'apporter au matériau pour propager une fissure au travers de sa microstructure (Ritchie, 1988). De nombreux mécanismes de

propagation de fissure ont été étudiés dans le passé, mettant en avant les propriétés multi-échelles du tissu cortical quant à ces mécanismes (Zimmermann and Ritchie, 2015). Ces mécanismes de durcissement sont connus dans des conditions de chargement standard, peu étudient leur rôle dans des conditions de chargement représentatif d'une chute. Il a cependant été montré que la vitesse de chargement avait une influence significative sur la ténacité osseuse (Shannahan et al., 2015; Zimmermann et al., 2014). L'influence de la localisation anatomique sur ces mécanismes est elle aussi peu renseignée alors que l'arrangement microstructural peut différer d'un site à l'autre (Brown et al., 2000; Wolff, 1892).

Dans ce contexte, l'objectif de cette étude est d'évaluer la ténacité de l'os cortical humain au niveau de diaphyses fémorales, cols fémoraux, diaphyses tibiales et diaphyses radiales appariés, en considérant à la fois des conditions de chargement quasi-statique standard et de chargements représentatifs d'une chute. Des analyses morphométriques ont été menées pour évaluer les paramètres microstructuraux de l'os à différentes échelles avant et après la propagation d'une fissure à l'aide de micro-tomographie par rayonnement synchrotron. Des mesures biochimiques ont aussi été réalisées afin de quantifier le vieillissement du collagène. Les mécanismes de fracture ont alors été caractérisés dans leur globalité et fourniront à la communauté biomécanique de nouvelles connaissances concernant les mécanismes de propagation de fissure de l'os cortical humain dans des conditions de chute.

Les principaux résultats qui ressortent de cette étude concernent les expérimentations biomécaniques. A notre connaissance, cette étude est la première à donner des résultats concernant la ténacité au niveau du radius. Les résultats obtenus montrent que le radius résiste mieux à une propagation de fissure que les autres sites étudiés quand il est sollicité dans des conditions quasi-statiques, notamment quand on s'intéresse aux mécanismes plastiques. Ces mécanismes non-linéaires qui se manifestent lors du chargement sont plus efficaces pour retarder la propagation de fissure au niveau du radius qu'au niveau du fémur ou du tibia. La nature non-porteuse du radius, contrairement au fémur ou au tibia qui supportent le poids du corps, nous permet d'émettre l'hypothèse que la morphologie de l'organe étudié peut influer sur les mécanismes de fracture. Mais, si les différents sites anatomiques étudiés présentent des comportements mécaniques différents dans des conditions quasi-statiques, elles n'existent plus lorsqu'on considère des conditions de type chute. Lors d'une chute, la diaphyse fémorale, le col fémoral, la diaphyse tibiale et la diaphyse radiale se comportent de la même façon face à une propagation de fissure.

L'analyse de la microstructure de l'os cortical humain à l'aide de l'imagerie en micro-tomographie par rayonnement synchrotron a montré que le fémur présente une architecture significativement

différente à celle du radius, à la fois au niveau du système de Havers qu'à l'échelle lacunaire. Ces différences peuvent confirmer que les organes porteurs et non porteurs présentent des microstructures différentes. Concernant les mécanismes de fracture, le volume de micro-fissures formées à la suite du chargement appliqué est plus important au niveau du radius que dans la diaphyse ou le col fémoral. Ce résultat est cohérent vis-à-vis des mesures biomécaniques : la formation de micro-fissure dissipe de l'énergie alors emmagasinée lors du chargement mécanique, d'avantage d'énergie devra alors être apportée pour propager la fissure principale. Dans le cas d'une chute, ce volume décroit de façon significative pour les sites étudiés. De plus la comparaison entre les différentes localisations anatomiques ne montre aucune différence. Au regard de ces résultats, nous pouvons confirmer que la microstructure joue un rôle primordiale dans les mécanismes de fractures de l'os cortical humain. Ces propriétés morphométriques semblent moins adaptées lorsque le matériau est sollicité dans des conditions représentatives d'une chute.

Basé sur de récentes études de la littérature, nous avons aussi évalué l'influence du vieillissement du cross-linking du collagène sur la ténacité osseuse. En accord avec la littérature, les résultats trouvés dans cette étude montrent que la maturation des cross-links enzymatiques a une influence sur la capacité de l'os cortical à manifester des mécanismes non-linéaires, et notamment sur sa capacité à développer sa zone de process. Ce mécanisme plastique est associé à l'accumulation de micro-endommagements au sein du tissu dans une zone limitée avant leur coalescence et la propagation d'une fissure principale. L'augmentation de la concentration en cross-links matures trivalents relativement à celle des cross-links immatures divalents limite cette capacité à manifester ces mécanismes non-linéaires dans des conditions de chargement quasi-statiques. L'hypothèse émise comme explication de ce phénomène, est que la nature trivalente des cross-links matures limite les mouvements inter-fibrilles qui ont été montré comme jouant un rôle dans les mécanismes de fracture de l'os cortical.

En regroupant ces différentes observations, nous sommes donc capables d'identifier les caractéristiques architecturales impliquées dans les mécanismes de fractures de l'os cortical humain, à la fois dans des conditions quasi-statiques standards ou représentatives d'une chute. Les résultats montrent que les mécanismes impliqués dans les contributions élastiques et plastiques de la déformation ne sont pas les mêmes. Dans des conditions de chargement quasi-statique, la contribution élastique est majoritairement gouvernée par le cross-linking du collagène et la densité du tissu. Les mécanismes non-linéaires sont, eux, associés à la morphométrie du tissu. Comme le régime élastique ne représentent que 5 % de la réponse mécanique de l'os cortical, il semble cohérent de considérer que les mécanismes de propagation de fissure dans des conditions de chargement quasi-statique sont principalement non-linéaires. Le rôle du système Haversien dans les

mécanismes de fractures de l'os cortical est déjà connu. L'influence du réseau lacunaire évoqué dans cette étude est un nouveau résultat. L'association entre la taille des canaux de Havers et la géométrie des lacunes semblent altérer la capacité de l'os à manifester la formation de micro-endommagements dans la zone de process. Lors de la phase de propagation, dèsque la zone de process a atteint sa taille maximale, le paramètre critique semble être la densité lacunaire. Dans des conditions représentatives d'une chute, les mécanismes élastiques sont aussi régis par le cross-linking du collagène et la densité du tissu. Dans ces conditions d'expérimentations, le régime élastique représente 25 % de la réponse globale du tissu. Les paramètres étudiés dans cette étude ne permettent pas de prédire de façon fiable le régime non-linéaire de la réponse de l'os cortical humain dans des conditions de chute. Le résultat principal de cette étude est que lors d'une chute, la microstructure du tissu intervient de façon moindre que lors d'un chargement quasi-statique.

Cette étude apporte de nouvelles connaissances sur les mécanismes de propagation de fissure de l'os cortical humain sur différents sites appariés ainsi que de l'influence de la vitesse de chargement sur ces mécanismes. Le parallèle qu'il existe entre la mesure de ténacité et le risque de fracture osseuse peut être fait avec le paramètre (J_{el} + $J_{process}$) mesuré dans des conditions de chargement représentatif d'une chute. L'étude montre que le régime élastique est associé à la biochimie et la densité du matériau. Les mécanismes plastiques sont en revanche plus difficiles à déterminer. En isolant les diaphyses fémorales et radiales, le système Haversian semble impliqué dans ces mécanismes. Mais en intégrant les résultats obtenus au niveau du col fémoral, le résultat est moins évident. Des travaux supplémentaires semblent nécessaires afin de déterminer de façon précise ces mécanismes de propagation de fissures lors d'une chute. L'approfondissement des analyses morphométriques sont d'un intérêt majeur pour définir précisément comment se manifestent les mécanismes de fracture au sein du tissu cortical. La qualité et l'importance de ces analyses en micro-tomographie méritent l'acquisition d'un plus grand nombre d'échantillons.

Abstract

A fracture is estimated every three seconds in the world, leading to an increased risk of impairment or even mortality. The biomechanical knowledge of bone fracture mechanisms in a fall configuration of loading is of great interest for the development of clinical method for the prediction of the risk of fracture. Toughness seems to be a good candidate to investigate this fracture process as it corresponds to the energy needed to propagate a crack through cortical bone complex microstructure. The aim of this study was thus to evaluate human cortical bone toughness parameter under both quasi-static and fall-like loading conditions on paired anatomical locations. Micro-computed tomography images using synchrotron radiation and collagen cross-links maturation measurements were performed to investigate the influence of the tissue microstructure on crack propagation. Results found showed that under quasi-static condition, the different anatomical locations present different mechanical behavior. Radius significantly better resist crack propagation than the other studied locations. Considering a fall-like loading condition, no more difference is observed between the locations but a significant decreased is measured compare to the quasi-static configuration. Human cortical bone has a better capacity to resist crack propagation under a quasi-static loading condition. By investigating the tissue microstructural and biochemical parameters, we observed different organization from a location to another that explains the mechanical differences. The microstructural features appear to be determinant for crack propagation mechanisms under quasi-static condition, but they play a lesser role under fall-like condition. These results imply that the tissue microstructure is not a determinant when dealing with the prediction of the risk of fracture. Further work has to be done to reach out which parameters are more determinants under a specific fall-like loading condition.

Keywords: Human cortical bone toughness, fall-like condition, paired anatomical locations, three-dimensional microstructure, collagen cross-links

Résumé

Il est estimé qu'une fracture se produit toutes les trois secondes dans le monde, accompagné par un risque élevé d'invalidité ou même de mortalité. La connaissance des mécanismes de fractures dans une configuration de chargement représentatif d'une chute semble être d'un intérêt majeur pour le développement de méthodes dédiées à la prédiction du risque de fracture. La ténacité est un paramètre approprié lorsqu'on s'intéresse à ces mécanismes de fracture, elle détermine l'énergie nécessaire pour propager une fissure à travers l'architecture du tissu. L'objectif de cette thèse est d'évaluer la ténacité de l'os cortical humain, considérant à la fois des conditions chargement quasi-statique et représentatif d'une chute sur sites anatomiques appariés. L'acquisition d'images en micro-tomographie ainsi qu'une mesure des cross-links ont été réalisées afin d'évaluer leur influence sur les mécanismes fracture osseuse. Les résultats ont montré que dans des conditions quasi-statiques, les différents sites anatomiques présentent des propriétés mécaniques différentes : le radius résiste mieux à une propagation de fissure. Dans des conditions de chute, il n'y a plus de différences entre ces sites, mais la ténacité décroit de façon significative par rapport au chargement quasi-statique. L'os cortical résiste mieux à une propagation de fissure dans des conditions quasi-statiques. Les analyses microstructurales et biochimiques ont montré des différences entre les sites anatomiques qui expliquent les différences mécaniques. Les caractéristiques architecturales du tissu sont déterminantes vis-à-vis des mécanismes de fracture dans des conditions quasi-statiques. Mais leur rôle lors d'une chute est moins évident. Ces résultats impliquent que la microstructure de l'os cortical n'est pas un déterminant majeur vis-à-vis du risque de fracture. De futures études doivent être réalisées afin de déterminer les paramètres essentiels dans des conditions représentatives d'une chute.

Mots clés : Ténacité de l'os cortical humain, chute, sites anatomiques appariés, microstructure tridimensionnelle, cross-links